UNSTEADY FLOW PHENOMENA IN AN AXIAL FLOW COMPRESSOR

by

P.J. BOXHALL B.E. (HONS.)

Submitted in partial fulfilment of the requirements

for the degree of

Master of Engineering Science

UNIVERSITY OF TASMANIA

HOBART

December 1971

ABSTRACT

A broad investigation of the unsteady flow phenomena which occur in an axial flow compressor is presented. It is based on an analysis of hot wire measurements of the time variation in velocity at fixed points in the flow through a single stage machine with three blade rows. The study has been confined mainly to the "potential flow" unsteadiness due to the rotor movement and the effect of wakes from one blade row interacting with downstream rows. A general experimental investigation of the compressor blade wakes is included. The results are compared with velocity distributions calculated from existing potential flow models of the flow through a cascade, and a new model based on the approximations of thin aerofoil theory is developed by the author. Consideration is given to the development of a model of a blade wake and the author's potential flow model is extended to include a wake and boundary layer thickness effect. Also included is an account of a brief experimental investigation of the noise generated by the compressor due to blade row interaction effects.

CONTENTS

CONTENTS (Cont.)

PREFACE

This thesis presents an investigation of unsteady flow phenomena in an axial flow compressor, based on an experimental study performed in a single stage, low speed machine with three rows of blades (inlet guide vanes, rotor and stator). The study is virtually the start of a programme, being undertaken at the University of Tasmania, aimed at building up an accurate picture of the unsteady flow effects pertaining to the real flow through a machine, so that these might be taken into account in design procedures.

The variation in absolute velocity with time at fixed points in the flow through the compressor has been recorded by photographing oscilloscope traces from a hot wire anemometer. This work is devoted mainly to an analysis and discussion of these results.

The subject is introduced in Chapter One with a description of the main types of unsteady flows which occur in an axial flow machine, a brief review of previous investigations, and an outline of some practical unsteady flow problems which warrant investigation. In Chapter Two, details of the experimental equipment and techniques are given. A brief description of the research compressor is followed by an account of the construction and calibration of the hot wire probes. Problems of wire vibration and calibration drift are discussed.

Measurements of the "potential flow" variation in absolute velocity upstream of the rotor are presented and discussed in Chapter Three. It is found (for the particular flow conditions adopted) that the movement of the rotor causes a significant absolute velocity defect-equal to half the mean velocity 0.03 chord-lengths upstream of the leading edge, and still evident 0.7 chord-lengths upstream. The results are compared with a potential flow model of the flow through a cascade of thick aerofoils developed by Frith (Ref. 12). Good agreement is obtained - the measured and calculated velocity defects differ by only 5-6%. The interaction effect of the rotor blades cutting the inlet guide vane (I.G.V.) wakes is considered by examining a series of photographs depicting a hot wire traverse through the wake just upstream of the rotor. Surprisingly, there is no change in the "potential flow" velocity distribution, implying no change in blade circulation, as the I.G.V. wake is traversed by the rotor blades. This result is discussed in some detail. The chapter concludes with the development of a simple potential flow model based on a thin aerofoil approximation of the rotor blades, in which each profile is ultimately replaced with a row of vortices

and sources distributed along the circular arc camber-line. The development of this model shows that the upstream "potential flow" velocity defect can be thought of as consisting of separable circulation and thickness components.

In Chapter Four, measurements of the time variation in absolute flow velocity downstream of the rotor are analysed. The measured curves show the combined effect of the "potential flow" unsteadiness and the velocity defect of the rotor wakes. The velocity defect of the rotor wake in the absolute flow is observed to be only about 12% of the mean velocity and approximately constant with axial position from the trailing edge to 0.5 chord-lengths downstream. A sequence of photographs representing a traverse through the I.G.V. wake avenue just downstream of the trailing edge shows significant changes in the mean velocity distribution across the wake, in contrast to the situation upstream. The measurements indicate a drop in the overall velocity defect of possibly as much as 50% near the centre of the I.G.V. wake avenue. As the "potential flow" unsteadiness downstream of the rotor cannot be measured directly, this is examined by considering the Frith and vortex-source model flow approximations. It is inferred that the downstream velocity defects are only about 20% of the defects for corresponding positions upstream.

In Chapter Five, the vortex-source model is extended to include the added thickness effect of the rotor blade boundary layer and wake. An approximate displaced surface for a rotor blade is constructed by assuming the rotor wake in the relative flow to be the same as the stator wake - it is not possible to determine the relative velocity distribution in the rotor wake from the measured absolute velocity profiles. Hot wire measurements of the velocity distribution downstream of the stator are presented and discussed. It is shown that considerable difficulty arises in attempting to define a displacement thickness for a blade wake in the region of the trailing edge. Approximate δ^* values for the stator wake are calculated after making simplifying assumptions regarding the curved flow near the trailing edge. These are used to construct the effective rotor blade shape, which is then incorporated in a revised vortex-source model. The additional thickness effect is found to give increases of the order of 50% in the predicted downstream absolute velocity defects and significant shifts in the positions of the velocity minima. A discussion of vortex sheet models of a blade wake is also included in this chapter.

A brief investigation of the compressor noise generated as a result of blade row interaction effects is described in Chapter

Six. Sound pressure measurements recorded at a test station near the compressor intake screens show the change in interaction noise for

a. different axial clearances between the I.G.V. and rotor rows; and
b. different relative peripheral settings of the I.G.V. and stator rows.

It is shown that the interaction noise can be significantly reduced by suitably adjusting the relative peripheral positions of the I.G.V. and stator rows.

CHAPTER 1

INTRODUCTION

Present methods of axial flow machine design consider each blade row as a separate cascade, stationary in space, with the fluid approaching at the appropriate angle of incidence. The flow velocity and direction on each side of the row are assumed to be constant with time and position. This avoids the complexities of unsteady flow and, as far as machine performance is concerned, satisfactory results are obtained.

Clearly the movement of rotor blades which do work on the fluid and have finite thickness must produce unsteadiness relative to a stationary observer. Also the fluid velocity at any given axial station is not constant with peripheral position, but varies due to the effects of blade circulation and thickness. Under these conditions it is clear that, when a stationary blade row and a rotating row are situated close together (as space saving requirements usually demand), there will be significant blade row interaction effects, and the instantaneous flow conditions for each blade will depend on the relative positions of the two rows.

The "potential flow" unsteadiness arising from the movement of a rotor is, in fact, essential to the transfer of energy between the fluid and the moving blades. This is demonstrated by Dean (Ref. 1) and Horlock (Ref. 2) as follows. For an unsteady but reversible and adiabatic compressible flow,

$$-\frac{1}{\rho}\frac{\partial p}{\partial \xi} = \frac{\partial q}{\partial t} + q\frac{\partial q}{\partial \xi} \qquad \text{.....(1.1)}$$

where q is the velocity along a streamline ξ, and p is the pressure. Since the flow is isentropic,

$$-\frac{1}{\rho}\frac{\partial p}{\partial \xi} = -\frac{\partial h}{\partial \xi} \qquad \text{.....(1.2)}$$

where h and ρ are specific enthalpy and density respectively. From Eqs. (1.1) and (1.2),

$$\frac{\partial h_o}{\partial \xi} = \frac{\partial h}{\partial \xi} + q\frac{\partial q}{\partial \xi} = -\frac{\partial q}{\partial t} \qquad \text{.....(1.3)}$$

where h_o is the stagnation enthalpy.

Eq. (1.3) states that, for frictionless adiabatic flow, the spatial rate of change in the stagnation enthalpy (or head, in an incompressible flow) in the direction of the instantaneous velocity at a point is proportional to the instantaneous time rate of change of fluid velocity at that point. In other words, if the flow is steady ($\partial q/\partial t = o$), the stagnation enthalpy is constant along each

streamline and the shaft work must be zero.

Another significant cause of flow unsteadiness in an axial flow machine is the action of wakes shed from one blade row impinging on a following row. This may involve interaction either between two stators or between two rows having relative motion. The passage of the blade wakes through a machine is illustrated diagrammatically in Fig. 1.1. The section represents the situation at mid blade height in the research compressor and depicts the instantaneous position of the blade wakes for a particular position of the rotor relative to the two stationary rows. The wakes from the upstream stationary row are effectively chopped into segments by the rotating row. The action results from the speeding up of the wake fluid particles which travel over the suction surface of the rotor blade and the slowing down of particles which move over the pressure surface. The segments are reoriented - so that they do not become reunited at the outlet - and proceed along a fixed avenue. A similar effect occurs with the passage of the rotor wakes over the stator blades.

Other unsteady flows which may occur in an axial flow turbomachine are

a. Flow relative to a vibrating blade, and in particular self-induced vibration or flutter. (See Whitehead, Ref. 3).
b. A self-induced flow instability such as rotating stall - under certain conditions, it is possible for one or more single stall cells to form and move from blade to blade around a row. Axial symmetry is destroyed with part of the annulus containing stalled blades, while the other contains unstalled blades. A summary of analyses of rotating stall is given by Yeh (Ref. 4).
c. Unsteadiness due to variations in mass flow through a machine which may occur as a result of changing boundary conditions on pressure.

The consequences of unsteady flow in a turbomachine are most significant. The pressure fluctuations produced in unsteady flow can excite considerable vibration in the blades and other machine parts and so introduce major mechanical design problems. The generation of fluctuating pressures is, of course, also a mechanism of noise generation. There is currently a great need in the aircraft industry for research directed at compressor noise reduction, and an understanding of the associated unsteady flow phenomena is essential.

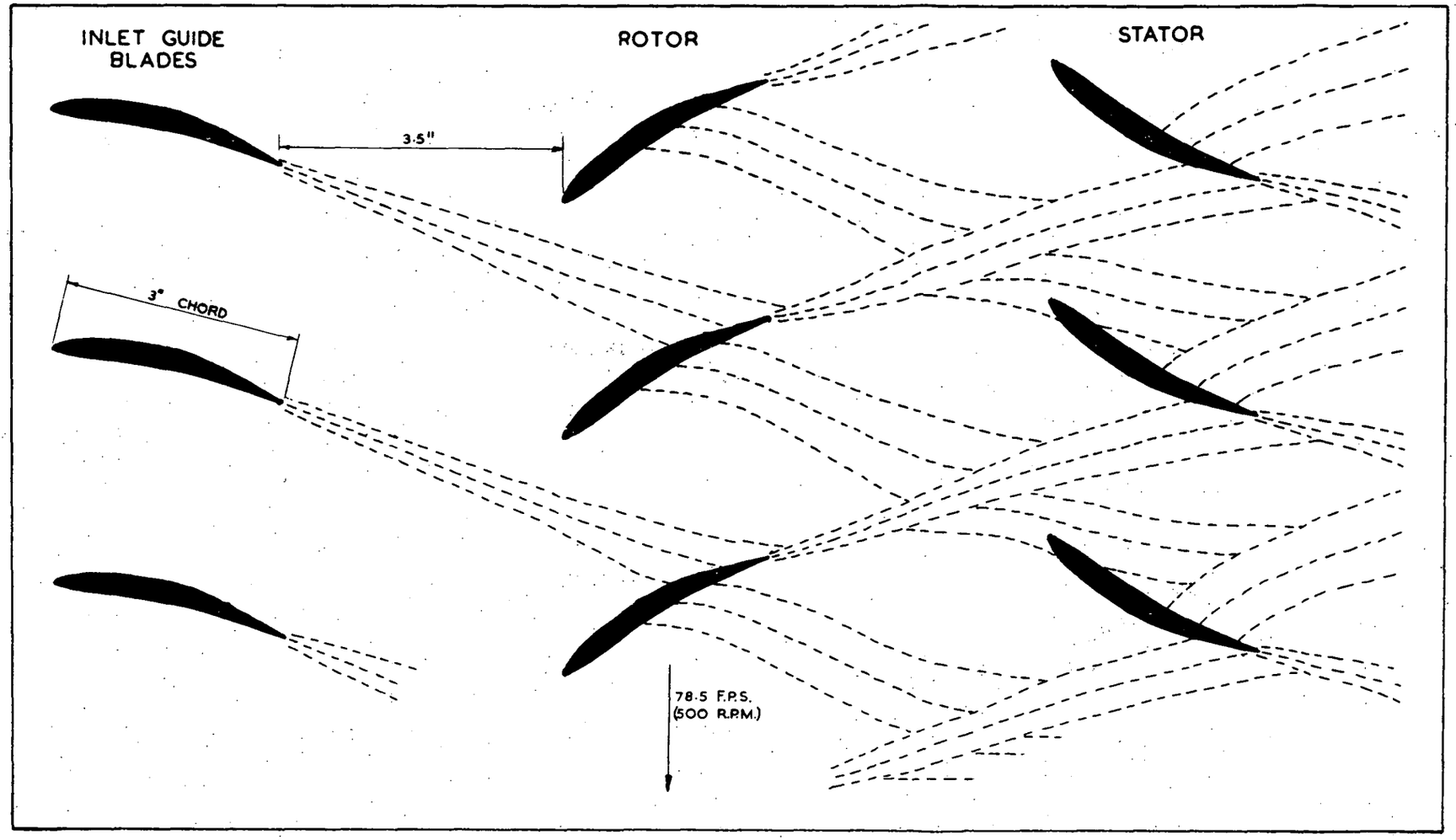

FIG. 1.1 SECTION SHOWING INSTANTANEOUS POSITION OF COMPRESSOR BLADE WAKES

The failure of the gas circulators at Hinkley Point Nuclear Power Station in 1963 (Ref. 5) provides an example of the magnitude of excitation possible as a result of unsteady flow effects. Metal fatigue failures occurred in some of the machine components as a result of abnormally high acoustic excitation. A later investigation showed that the excitation was due largely to aerodynamic interference between inlet guide vane and rotor rows.

The analysis of unsteady flow in turbomachines has been the subject of considerable theoretical treatment, but, oddly enough, very little actual measurement has been performed to test the theories which have been developed. Probably the earliest analytical treatment was published by Von Karman and Sears in 1938 (Ref. 6). These authors applied the theory of thin aerofoils to the case of an oscillating aerofoil and also to the problem of a plane aerofoil entering a sharp-edged gust and produced expressions for the unsteady lift and moment acting on the aerofoils in each case. Theoretical models describing a wide variety of unsteady flow problems associated with axial flow machines have since been developed. Most of these are based on thin aerofoil theory. A comprehensive review of these analyses is given by Horlock in Ref. 2.

To the author's knowledge, the only reported measurements of unsteady flow phenomena in axial flow compressors actually carried out within a machine are those of Smith (Ref. 7) and Parker (Ref. 8). Other workers have performed experimental studies of the flow in the vicinity of oscillating single aerofoils, but the results of such investigations are largely irrelevant to the real unsteady flow problems in a turbomachine. Smith (Ref. 7) considers the motion of a wake from a stationary blade row as it passes through a downstream rotating row and discusses the phenomenon of wake chopping described above. He presents sketches of hot-wire anemometer traces taken downstream of the first rotor in a four stage, low speed research compressor. These are velocity-time curves depicting rotor wake profiles, with fluid representing the inlet guide vane wake identifiable as turbulent fluctuations superimposed on the mean traces. (Similar measurements have been performed by the author downstream of the rotor in the Vortex Wind Tunnel and are presented in Chapter 4 of this thesis.)

Parker (Ref. 8) presents an experimental investigation of the pressure fluctuations on the surface of the inlet guide vanes (I.G.Vs.) in an axial flow compressor stage produced by the motion of the downstream rotor blades. The magnitude of the pressure fluctuations were recorded as sound pressure levels in dB for

different I.G.V./rotor arrangements. The investigation established that the potential flow interaction between blade rows was a significant source of generation of fluctuating pressures (and therefore of noise) and of blade vibration excitation.

There is a need for extensive measurement of the various unsteady flow phenomena which occur in a turbomachine in order to test existing flow models and provide empirical data so that unsteady flow effects might be taken into account in machine design. Once such data is available it will be possible to choose velocity triangles, blade profiles and axial spacings to minimize the flow fluctuations as far as performance and mechanical considerations will allow.

It is desirable to determine exactly how the fluid particles move through a machine under the influence of varying potential flow fields and varying velocity defects due to wakes etc. One can define many practical unsteady flow problems associated with an axial flow machine, for example:

(1) What is the variation in flow velocity with time at any point in the flow due to the movement of the rotor and what are the relative contributions of the rotor blade circulation and thickness to this variation?

(2) What is the relative flow pattern around a moving blade and does this vary significantly with time due, for example, to the effect of wakes from upstream rows? A question of particular interest is whether the Kutta-Joukowski condition will apply in unsteady flow.

(3) What effect does the movement of the rotor have on the wake from an upstream row?

(4) What happens when wakes from different blade rows interact - or when a wake and boundary layer interact?

(5) What effect do the different unsteady flow phenomena have on the performance of an axial flow machine and what is their relative importance?

(6) Which unsteady flow effects are most important in the generation of noise?

Measurements of some of the unsteady flow phenomena discussed above have been carried out in the Vortex Wind Tunnel at the University of Tasmania. This is essentially a single stage, low speed, axial flow machine with three rows of blades (inlet guide vanes, rotor and stator) and is described extensively in Chapter Two of this thesis. The study has been confined mainly to the "potential flow" disturbances due to the rotor movement and wake effects, and has included a general investigation of the compressor blade wakes.

Hot wire measurements have been taken both upstream and downstream of the rotor and also downstream of the stator. The investigations have been restricted to two-dimensional effects and all measurements have been carried out at mid blade height.

As part of the general investigation of unsteady flow phenomena, a brief study of noise generated by blade row interaction effects has also been carried out by measuring sound pressure levels in the vicinity of the working section of the compressor for different blade row configurations.

The following chapters consist essentially of the presentation and analysis of velocity - time curves corresponding to many different points in the flow through the compressor. To the author's knowledge the series of measurements represents the first experimental record of many important unsteady flow phenomena which occur in an axial flow machine. The results are compared with existing mathematical models of compressor flow and a new model based on the approximations of thin aerofoil theory is developed. Many different aspects of the problem are presented and the author has not attempted to investigate all in depth. One of the main objects of the investigation has been to determine the most important unsteady flow effects and to point out areas of need for detailed study.

CHAPTER 2

EXPERIMENTAL EQUIPMENT AND TECHNIQUES

2.1 Vortex Wind Tunnel

All measurements were carried out in the Department of Supply's Vortex Wind Tunnel at the University of Tasmania. This compressor is a single stage, low speed, axial flow machine comprising three rows of blades (inlet guide vanes, rotor and stator) and was designed and built at the Aeronautical Research Laboratories in Melbourne.

A longitudinal section of the tunnel is shown in Fig. 2.1. Air enters the machine nearly radially through an opening 7 ft. in diameter and 2 ft. wide, then is turned through 90 deg. into an annulus 45 in. outside diameter providing a contraction ratio of 7:1. The inlet is covered with a wire gauze which helps to give nearly uniform inlet conditions. The working section is made of aluminium and accommodates the three blade rows in a parallel section one diameter (45 in.) long. This is followed by a further parallel section about $1\frac{1}{4}$ diameters long made of plywood; then there is a diffusing section, also of plywood (approximately 4 diameters in length). The included whole angle of the diffuser is 7 deg. and it has a cylindrical core. At the end of the diffusing section the flow exits nearly radially through a flared outlet and returns through the room to the inlet. The outlet opening is controlled by a cylindrical throttle mounted on rails, giving continuous variation in throttle from zero to 30 ins.

The compressor is powered by a 40 H.P. motor with a Ward-Leonard control allowing continuous manual speed control between 150 r.p.m. and 750 r.p.m. This corresponds to a range of Reynolds number (based on blade chord and vector mean velocity) from 3×10^4 to 2×10^5. The shaft speed was measured by a stroboscope triggered at a basic frequency of 100 Hz from a crystal clock. This method enabled the speed to be kept constant to about 2 in 500.

The tunnel design includes the facility for splitting the machine casing either between the guide vane and rotor rows or between the rotor and stator rows. This is provided by bolted flanged annular rings that make up the machine casing in this region. The inlet section is mounted on rails and can be rolled away from the main body of the machine to provide access to the blades. Instrument slots are provided on the horizontal diameter and give access to the

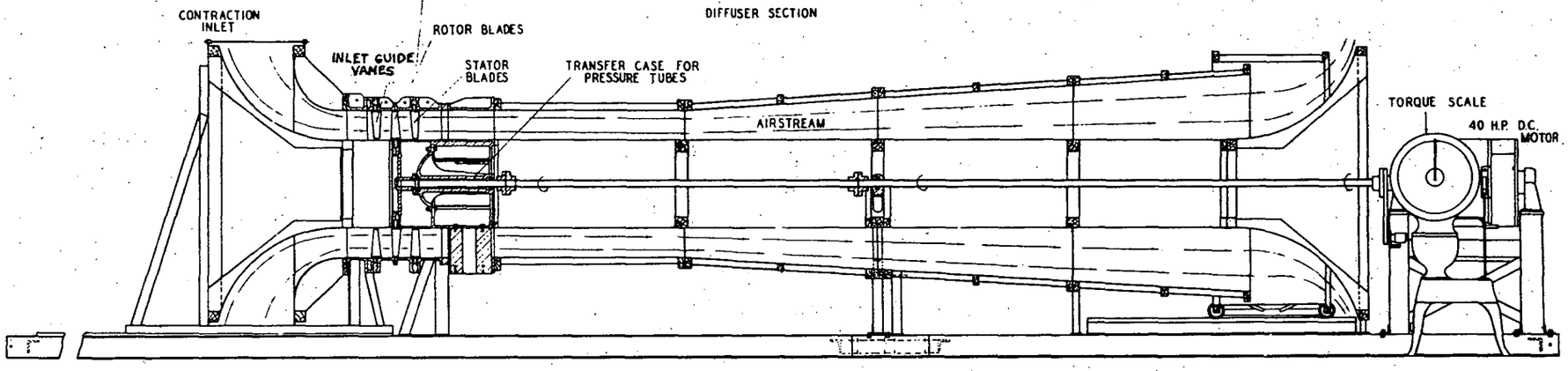

LONGITUDINAL SECTION OF TUNNEL

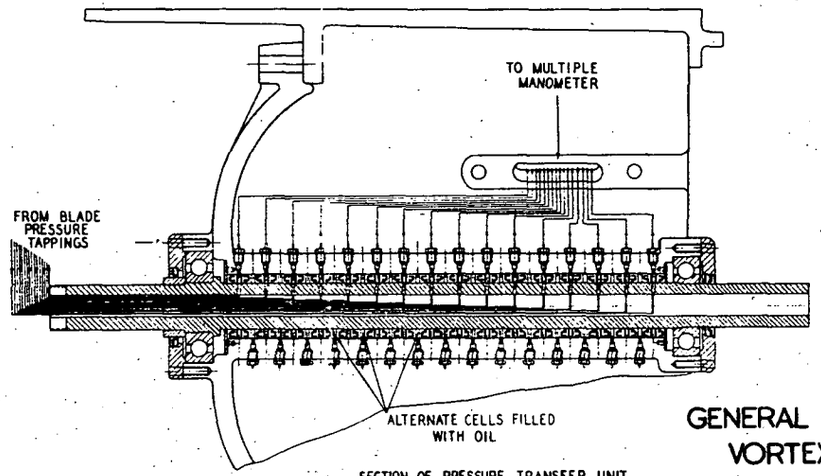

SECTION OF PRESSURE TRANSFER UNIT

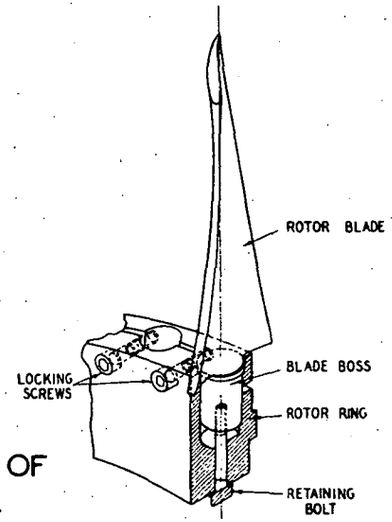

CROSS SECTION OF VARIABLE-STAGGER ROTOR BLADE ASSEMBLY

GENERAL ARRANGEMENT OF VORTEX WIND TUNNEL & PART SECTIONS

FIG. 2.1

spaces upstream and downstream of each blade row. Other openings in the casing accommodate thermometers for recording the ambient temperature at different stations in the flow and a pitot-static tube for flow measurement. Limited visualisation within themachine is provided by perspex windows inserted between the flanges in the machine casing.

Probes are mounted in a carriage fitted to the tunnel side allowing movement in the axial and radial directions and rotation of the instrument on its horizontal axis. The axial and radial positions are controlled by micrometer screws and can be set to an accuracy of 0.001 ins. The angular position of the probe is controlled by a micrometer drive, which permits the yaw angle to be set within 0.01 deg. The stationary blade rows are mounted on cylindrical rings which can be rotated so that the blades are traversed past the stationary measuring probe. The position of the blades is recorded by the zero of a vernier on a scale mounted outside the compressor giving readings to 0.001 ins. at mid blade height.

The blades are machined from aluminium to a tolerance of 0.001 ins. per inch of chord. The blades are 9 ins. long with a constant chord of 3 ins. along the entire blade height. There are 38 blades in the stationary rows and 37 in the rotor, giving mean space/chord ratios of 0.99 and 1.02 respectively. The axial distance between the centres of neighbouring blade rows is approximately two chord lengths, giving an axial clearance of a little over a chord length. There is, however, provision for decreasing the axial spacing between blade rows by 2 ins. (2/3 chord-length) - this is effected by changing the bolted annular rings in the machine casing of the working section.

The blade profile is a C4 section on a circular arc camber-line with a maximum thickness/chord ratio of 10% at 30% chord. The blades are twisted about a radial straight line through the middle of the camber line of all sections. The machine is designed on the basis of Howell's data to give nominally free vortex conditions at the design point ($\phi = 0.8$) with 50% reaction at mid-blade height and uniform work output along the blade.

A more detailed description of the wind tunnel and compressor is given by Oliver (Ref. 9). The major dimensions of the machine are listed in appendix A.

2.2 Hot Wire Anemometry

Measurements of flow velocity in the Vortex Wind Tunnel were obtained with a "DISA" Type 55A01 constant temperature anemometer used in conjunction with probes constructed at the University of Tasmania. The time variation of velocity at fixed points in the flow was recorded by photographing oscilloscope traces of the hot wire voltage. The oscilloscope time base was triggered externally by the voltage from a photocell circuit which was activated by light passing through a slit in a disc on the compressor drive shaft. All oscilloscope traces then represented the velocity in the vicinity of the same few rotor blades. Approximately 60 consecutive traces were recorded on each photograph, so that mean flow conditions could be determined. This was particularly necessary in cases where random fluctuations were not small compared with the variation in velocity due to the special unsteady flow effect being measured. An electronic linearizer was used in conjunction with the anemometer, so that velocity defects and turbulence levels could be read directly from the photographs with suitable scaling.

2.2.1 Design and Construction of Hot Wire Probes

The hot wire probes consisted of 0.0003 in. diameter tungsten wire spot welded to 0.020 in. diameter nickel prongs which had been tapered and flattened at the tips. The probes were fixed to 0.25 in. O.D. steel tube supports which housed the electrical leads connecting the prongs to a co-axial outlet socket. Details of the probe construction are shown in Fig. 2.2.

The average wire length used was about 0.12 ins. giving a length/diameter ratio of 400. This l/d value represented a satisfactory compromise. The shorter the wire, the smaller its thermal inertia and hence the greater its sensitivity to velocity fluctuations. A short wire also allows better spatial discrimination for measurements. However, if a wire is too short, the cooling effects of the supports prohibit any part of the wire from having a uniform temperature distribution along it. The reading is then influenced considerably by the end cooling effects and is very sensitive to the orientation of the supports in the flow. (See Hinze, Ref. 10). A longer wire is easier to line up against a blade or casing surface and gives more accurate mean velocity readings provided detailed spatial discrimination is not required.

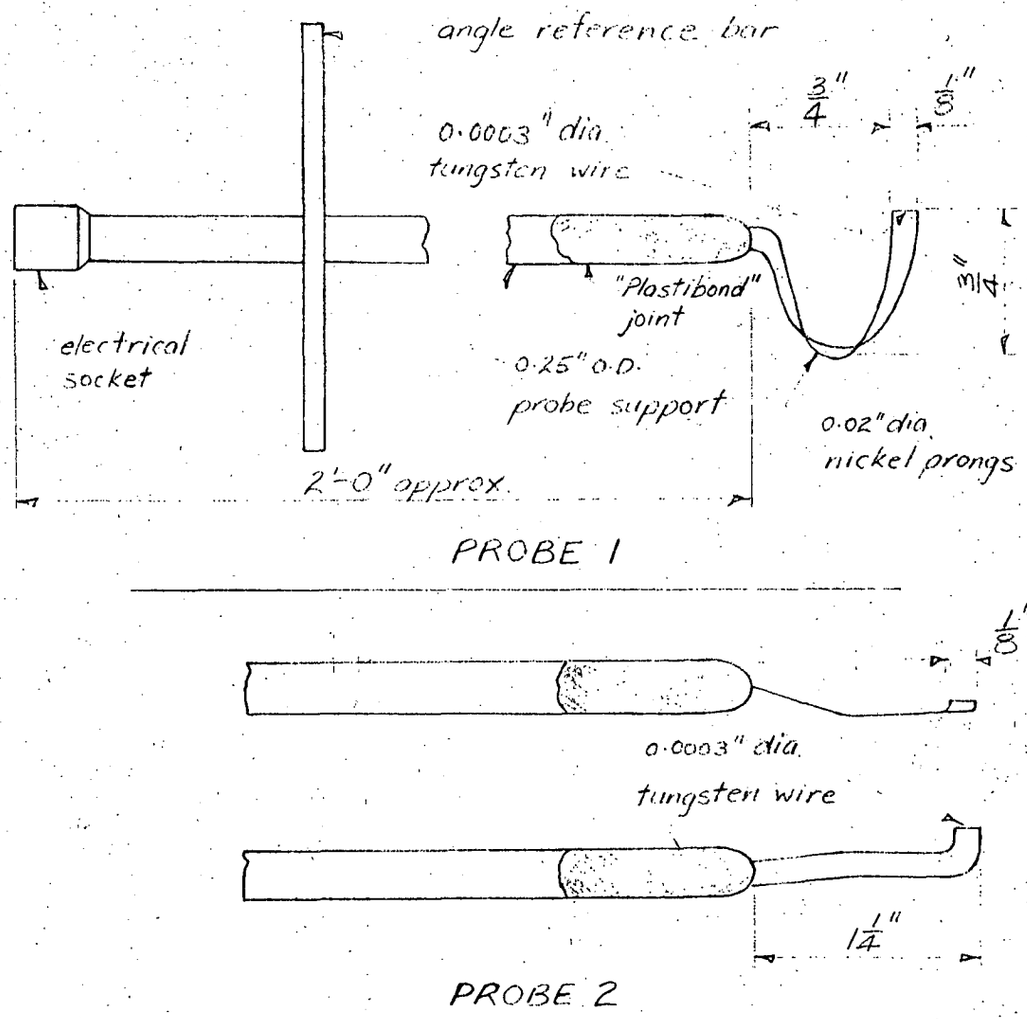

FIG. 2.2 HOT WIRE PROBES

Fig. 2.2 shows details of two probes used in the investigations. The orientation of the prongs was determined by the following factors:-

a. Positioning requirement - especially for measurements close to the rotor row.
b. The need to minimize distortion of flow at the measuring point due to the probe.
c. Rigidity to ensure negligible probe vibration.
d. Susceptibility to wire fracture when handling and positioning the probe.

Probe 1 was positioned with the plane of the prongs oriented in the direction of the absolute flow and, initially, was used for all measurements except those close to the rotor

leading edge, for which probe 2 was required. However, probe 2 was found to be very susceptible to wire fracture when mounting in the tunnel and later measurements near the rotor leading edge were performed with probe 1 positioned with the plane of the prongs at right angles to the flow direction (see Fig. 3.1). It was, of course, necessary to calibrate the same probe in each of the two positions.

2.2.2 Calibrations

The probes were calibrated in the 9 in. square working section of a recirculating tunnel over a speed range of 0 to 110 f.p.s. The tunnel provided a very uniform velocity distribution and a low level of free stream turbulence (maximum approximately 0.3% at 100 f.p.s.) Velocity heads from the pitot-static tube used as a standard were measured on a Betz micro-manometer. The anemometer voltages were recorded on a digital voltmeter which gave readings to 0.01 volt.

A wire for calibration was first cleaned by spraying with a solvent. (Good results were obtained using "Penetone M-26", an electrical equipment cleaner in aero-pack form). The probe was then mounted in the calibration tunnel and the wire checked for vibration by observing the voltage fluctuations on the oscilloscope screen as the air speed in the tunnel was slowly increased from zero to its maximum value. Any vibration, due to excessive tension in the wire, has the effect of producing an oscillatory variation in the flow velocity relative to the measuring element. This is observed as a very regular high frequency oscillation of relatively large amplitude, which occurs at certain critical speeds. Such vibrations are undesirable as they may be interpreted as turbulent fluctuations. In most cases, the vibration could be eliminated by carefully adjusting the prongs to release the tension in the wire, but at the same time leaving the wire fairly taut for good spatial discrimination. Very few workers have reported similar trouble with wire vibrations, and one wonders how many turbulence measurements presented in the literature have included wire vibration as a component.

A typical calibration curve is plotted in Fig. 2.3. The anemometer voltages were corrected for changes in ambient temperature using the following basic expression:

$$\Delta E = E \alpha Ra \, \Delta T / 2(Rw-Ra) \qquad \ldots\ldots(2.1)$$

where E = uncorrected anemometer voltage

ΔE = anemometer voltage correction

α = thermal coefficient of resistivity of the wire

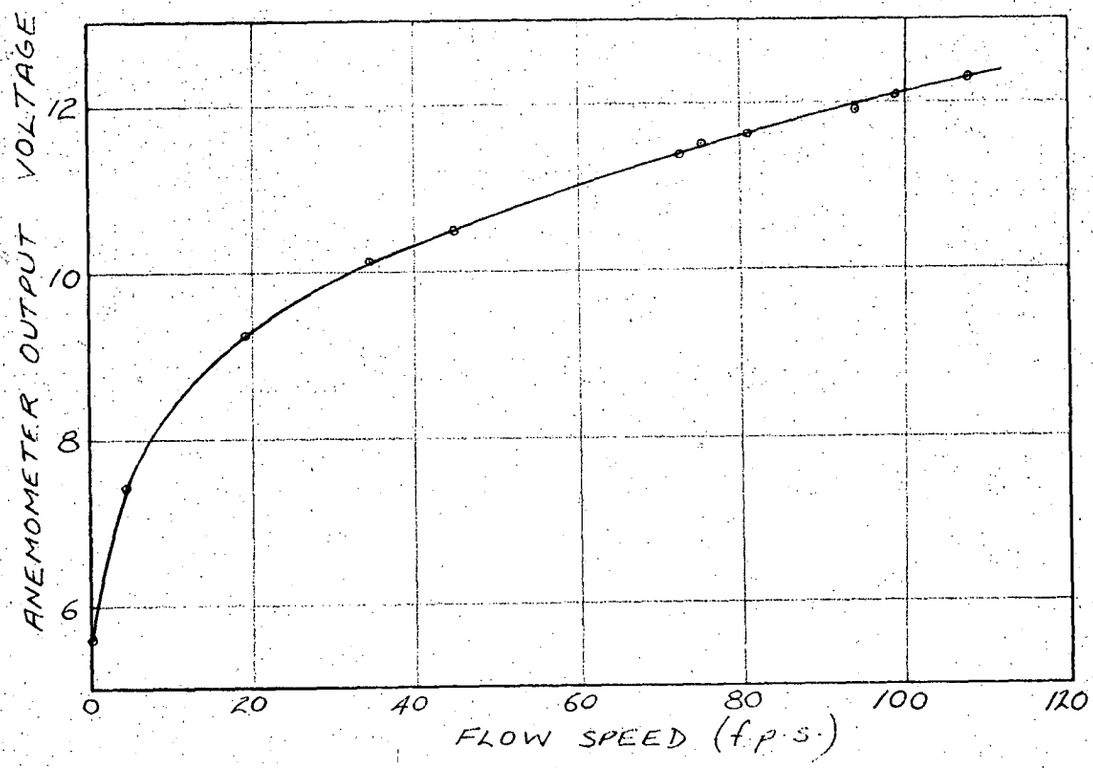

FIG. 2.3 HOT WIRE CALIBRATION

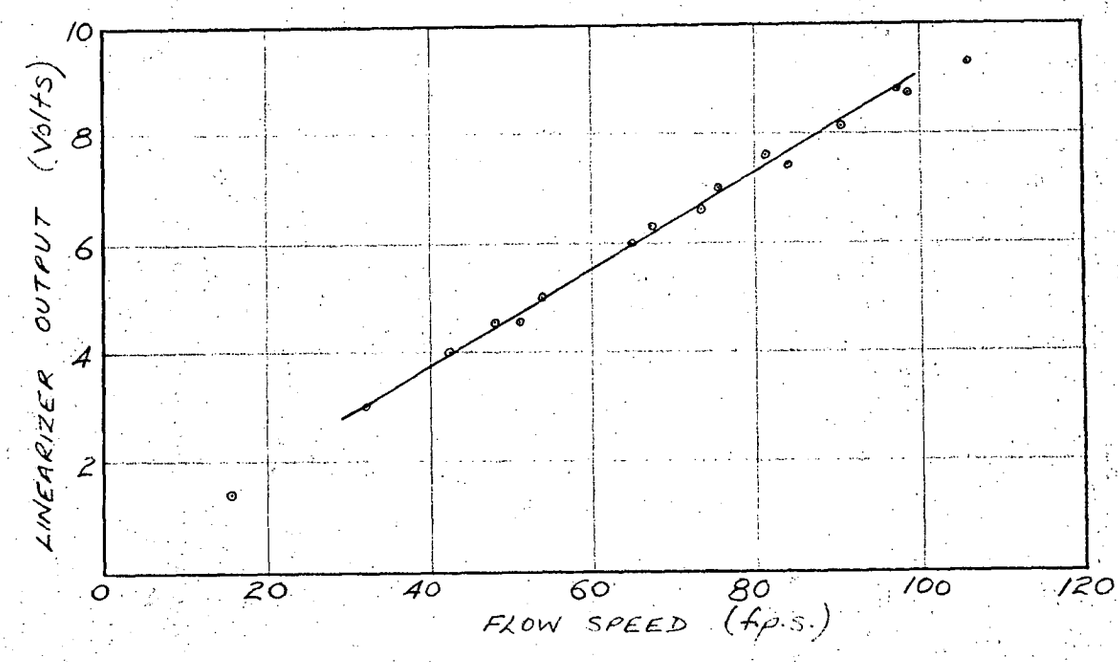

FIG. 2.4 CALIBRATION OF LINEARIZER OUTPUT

Ra = wire resistance at ambient temperature

ΔT = variation in air temperature from reference temperature

Rw = operating wire resistance.

It was found that the calibration curve could be represented by an equation of the form

$$E^2 = A + BV^n \qquad .....(2.2)$$

Where E is the anemometer output voltage

V the flow velocity

and A, B and n are constants

with n taking the value 0.445. (Compare this with a value of n = 0.5 used by King, Ref. 11).

Calibration of Linearized Voltages

Fig. 2.4 shows a calibration of the linearizer output voltage corresponding to the anemometer voltage of Fig. 2.3 as input. The linearizer transfer function is

$$Eout = K(Ein^2 - Eino^2)^m \qquad .....(2.3)$$

where K, Eino and m are constants.

Substituting Eq. (2.2) for the anemometer output voltage:

$$Eout = K(A + BV^n - Eino^2)^m \qquad .....(2.4)$$

Hence by setting $Eino^2 = A$ and $m = 1/n$, a linear relationship between Eout and V should be obtained. These linearizer settings were used to produce the calibration of Fig. 2.4.

Two sets of points are shown - one set obtained as the speed was increased from 0 to 110 f.p.s., and the other as the speed was decreased back to zero. It is thought that the scatter is due largely to changes in ambient temperature; the increase in air temperature from 0 to 110 f.p.s. during a calibration was usually about 3 deg. C. No temperature correction was used for the linearized voltages as there was no simple method corresponding to Eq. (2.1) for the anemometer voltages. There may also have been indeterminable changes with temperature in the transfer function of the linearizer. Eq. (3.3) indicates that any change in Vin (anemometer voltage) due to change in ambient temperature is amplified by the linearizer, the effect being greater for higher speeds because of the squaring of Vin. This could explain the observed tapering off of the linearizer output as the speed increased. However, it was possible to draw a straight line to fit the points well in the working range (30 to 90 f.p.s.).

The linearized calibration curve was used only to establish a scale on the oscilloscope traces of velocity fluctuations to enable direct reading of velocity defects and turbulence levels from the photographs. Values of mean flow velocity were determined using the calibration curve of the non-linearized anemometer voltage (Fig. 2.3).

2.2.3 Orientation of Probes in the Flow

It was necessary, of course, to calibrate the probes with the wire and prongs oriented in the same position relative to the flow direction as they would be during measurement in the compressor. The hot wire was always positioned perpendicular (approximately) to the flow direction with the ends of the prongs perpendicular to the wire and usually parallel to the flow direction.

When mounting the probe in the Vortex Wind Tunnel, the prongs could only be positioned roughly in the desired direction relative to the flow. During measurement, the probe was also subject to the angle variations associated with blade wakes and flow variations near the leading and trailing edges of blades. Such changes could be as large as 10 deg. on either side of the mean. For these reasons, a brief investigation was carried out to determine the effect on the anemometer voltage of different orientations of the probe in the flow.

This was performed for a probe of the second type (see Fig. 2.2) by rotating the instrument in the chuck of the recirculating tunnel during calibration. The hot wire, itself, was at all times perpendicular to the direction of flow. The investigations were performed at a low tunnel speed where the anemometer voltage was most sensitive to changes in flow velocity. It was found that the prongs could be rotated through an angle of 20 deg. either side of the mean position without any change at all in the reading. For angles greater than 20 deg. any change in the reading was small enough to be neglected without serious error. It was felt that this was sufficient justification for neglecting possible deviations from the calibration curve due to flow angle changes in wakes etc.

When the probe was rotated through an angle of 90 deg. so that the ends of the prongs were perpendicular to the direction of flow, a marked oscillation was observed on the oscilloscope trace. This was thought to be a probe vibration possibly induced as a result of vortex shedding from the prongs - the Reynolds number based on prong diameter was of the order of 200.

2.2.4 Calibration Drift

Prior to calibration, the hot wires were allowed to anneal for about 30 minutes at the normal temperature. A wire was usually calibrated two or three times to test repeatability, ensuring that there was no drift in calibration due to further changes in the physical state of the element with continued heating. During investigations in the Vortex Wind Tunnel, the calibration was checked regularly by making sure that any variation in the free stream anemometer voltage reading was due to corresponding changes in the ambient temperature and pitot-static tube readings. At the completion of each series of measurements the probe was removed and recalibrated, after first cleaning with "Penetone M-26".

Calibration drifts were encountered from time to time, and were found to be caused by particles of dust or other foreign matter accumulating on the hot wire. Such occurrences were usually evident as a very noticeable decrease in the peak to peak voltage on the oscilloscope trace. The impurities have the effect of changing the thermal conductivity of the element and the flow pattern around it. In many cases, excellent restoration could be obtained by spraying the wire with "Penetone M-26". Otherwise the wire was recalibrated (or completely replaced) and the series of measurements recommenced. Consequently, a policy of strict cleanliness was observed in the laboratory and the intake screens were freed from dust with a vacuum cleaner before commencing a series of measurements.

(In particular, trouble has been experienced with fumes from galvanised iron welding operations in an adjoining laboratory. The wire became coated with a film of ZnO. A similar effect was experienced with an acetate spray which was being used to prepare for a china clay visualization study in another part of the aerodynamics laboratory. In both these cases, restoration was obtained after cleaning with the "Penetone M-26".)

CHAPTER 3

INVESTIGATION OF UNSTEADY FLOW UPSTREAM OF THE ROTOR

3.1 Introduction

The initial investigations for this thesis were concerned with the basic "potential flow" variation in flow velocity with time arising from the movement of the rotor. It was desirable, in the first instance, to avoid the complication of blade wakes and so the first measurements were taken just upstream of the rotor leading edge.[1] Obviously, it was still necessary to account for the effect of wakes from the inlet guide vane row. There might also be other effects due to blade row interaction which would cause the velocity-time relationship to vary with the position of the probe relative to the adjacent guide vanes; however these are expected to be small because of the large clearance of over one chordlength between the I.G.V. and rotor rows.

3.2 Measurement of "Potential Flow" Velocity Variation

The variation in absolute flow velocity with time at different axial positions upstream of the rotor was measured at mid blade height by photographing oscilloscope traces of the linearized voltage from a hot wire probe (see Fig. 3.1).

FIG. 3.1 HOT WIRE SITUATED 1/2 IN. UPSTREAM OF ROTOR L.E.

---

1. For the purposes of this thesis, the rotor blade leading and trailing edges are defined by the points of intersection of the camber line with the blade surface.

a1. 0.08 INS. (2.7%C) U/S

Vert. Scale: 11.38 fps/div.
Horl. Scale: 1.0 msec/div.

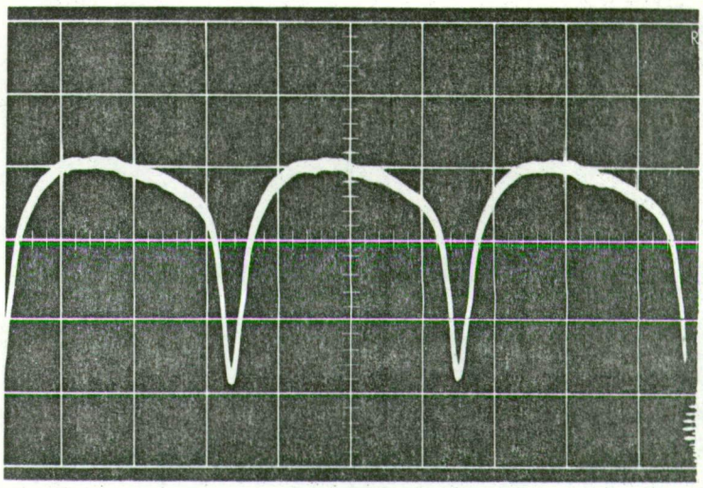

a2. 0.08 INS. (2.7%C) U/S

Vert. Scale: 5.69 fps/div.
Horl. Scale: 0.5 msec/div.

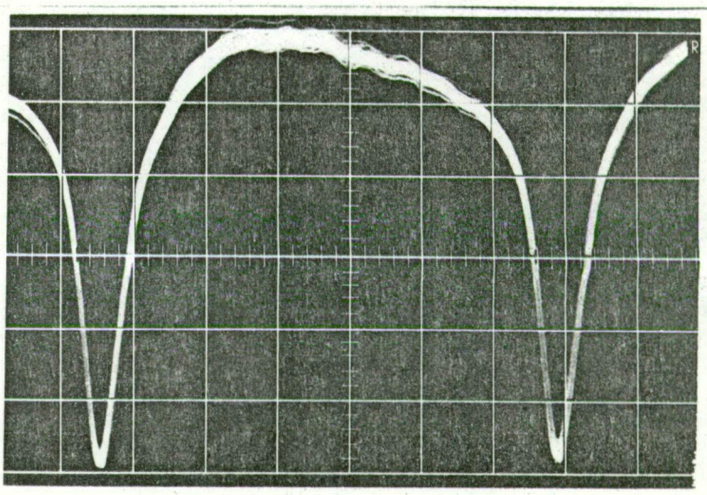

b. 0.26 INS. (8.7%C) U/S

Vert. Scale: 5.69 fps/div.
Horl. Scale: 0.5 msec/div.

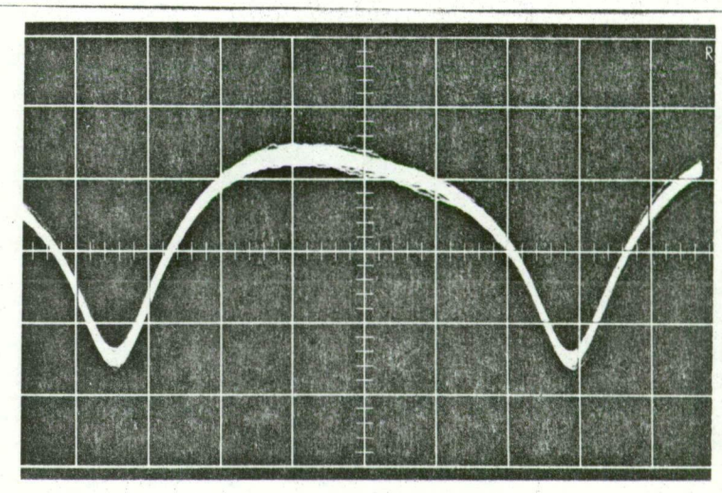

c. 0.73 INS. (24.4%C) U/S

Vert. Scale: 2.28 fps/div.
Horl. Scale: 0.5 msec/div.

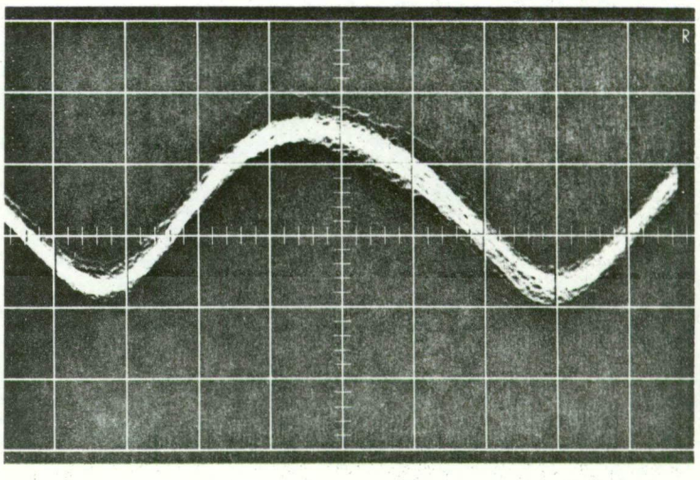

FIG. 3.2
VELOCITY-TIME PROFILES
UPSTREAM OF THE ROTOR

Mean Velocity = 66.5 fps

For the first series of measurements, the I.G.V. row was in each case rotated to position the hot wire clear of any blade wake region. Photographs for three of eight stations considered between 0 and 2.13 ins. (71%C) upstream of the rotor leading edge are shown in Fig. 3.2. The tunnel speed was 500 r.p.m. and the throttle opening was 8 ins. At mid blade height, this corresponds to the velocity diagram shown in Fig. 3.3, with relative flow angles of α_1 = 42.4 deg. and α_2 = 25.0 deg. and overall performance coefficients ϕ = 0.75 and ψ = 0.70. This is close to the blading design point (ϕ = 0.80, ψ = 0.64).

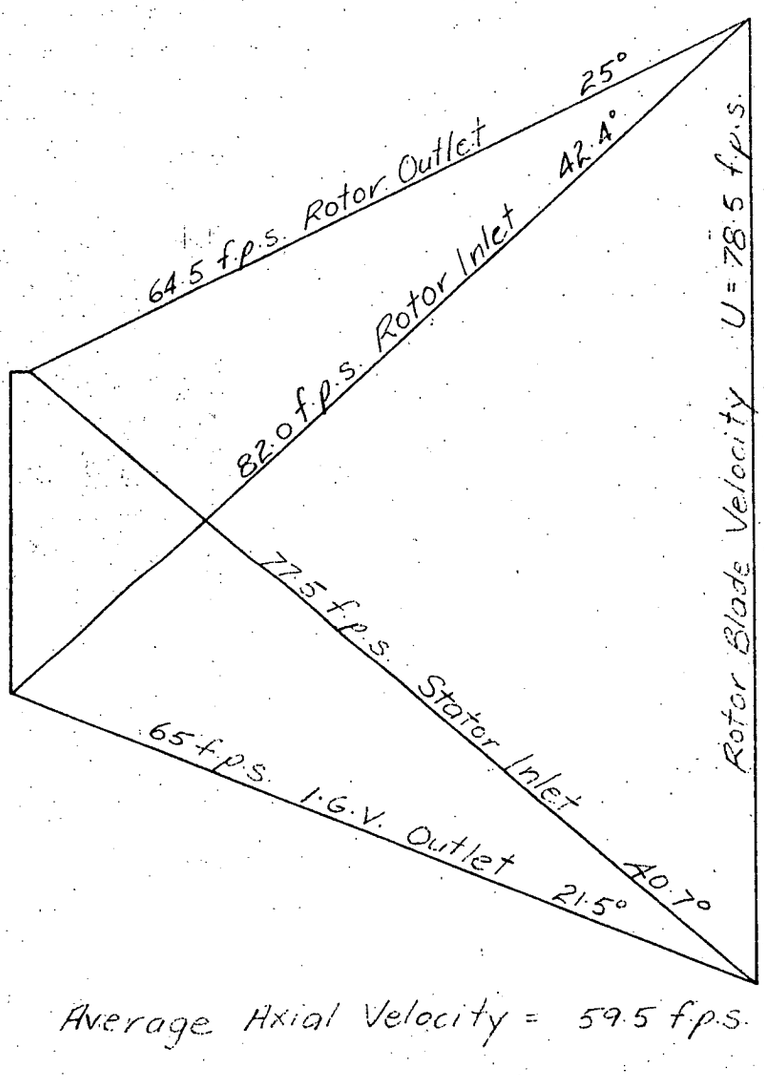

FIG. 3.3 VELOCITY DIAGRAM
(Mid Blade Height, 500 r.p.m., 8 in. Throttle)

N.B. a. Each photograph shows approximately 60 consecutive traces from the same group of blades.

b. Axial positions are quoted relative to the rotor leading edge (L.E.).

c. Photographs 3.2 a(2), 3.2 b and 3.2 c show the variation in velocity over a time 1.5 τ (approx.) and photograph 3.2 a(1) over a time 3.0 τ. (τ is the time taken for the rotor to move a distance equal to one blade spacing and equals 3.18 msec at 500 r.p.m.)

d. The velocity scale is not the same for all photographs.

e. The left hand side of the velocity dip corresponds to the pressure surface side of the rotor blade.

f. Unfortunately, there was no accurate means for determining the exact position of the rotor blade relative to the hot wire for each point on the trace.

3.3 Analysis of Photographs

Although the hot wire was always situated outside the I.G.V. wake, it must be realized that some large part of the rotor blade itself was always in the wake, regardless of the position of the rotor relative to the wire (See Fig. 1.1). In moving a distance equal to one blade spacing, a rotor blade made a complete traverse through the guide vane wake, so that each point on the trace was recorded with the rotor blade in a different position relative to the wake. Therefore, although the wire recorded no actual wake fluid particle velocities, the "potential flow" velocities that it did record were determined by the flow around the rotor blades - and this may have varied with the position of the rotor relative to the wake. However later investigations showed that the "potential flow" variation in velocity due to the rotor movement was actually independent of the position of the I.G.V. wake. This somewhat surprising result is discussed fully in Section 3.5.

The general shape of the velocity profiles is as would be expected from a consideration of the circulation around a compressor blade - a general decrease in flow velocity across a blade spacing from suction surface to pressure surface and a pronounced velocity defect due to the reverse circulation component of the velocity, as the nose of the blade passes the hot wire. Intuitively, one might also expect this large velocity dip to be due in part to a "flow stopping" effect of the "thick" rotor blade,

especially for measurements close to the leading edge of the rotor. This rotor blade thickness effect is discussed later in Section 3.6.

3.3.1 Velocity Defect

It is seen that, at a position 0.08 ins. (2.7%C) upstream of the leading edge, the passage of the rotor causes the flow velocity to drop by as much as 32 f.p.s., for a mean velocity of 66.5 f.p.s. The effect of the rotor blade circulation was found to be experienced by the fluid as far upstream as 2.0 ins. (67%C). A complete curve showing the decay of the velocity defect, $(V_{max}-V_{min})/\bar{V}$, with axial distance upstream of the rotor leading edge is presented in Fig. 3.4.

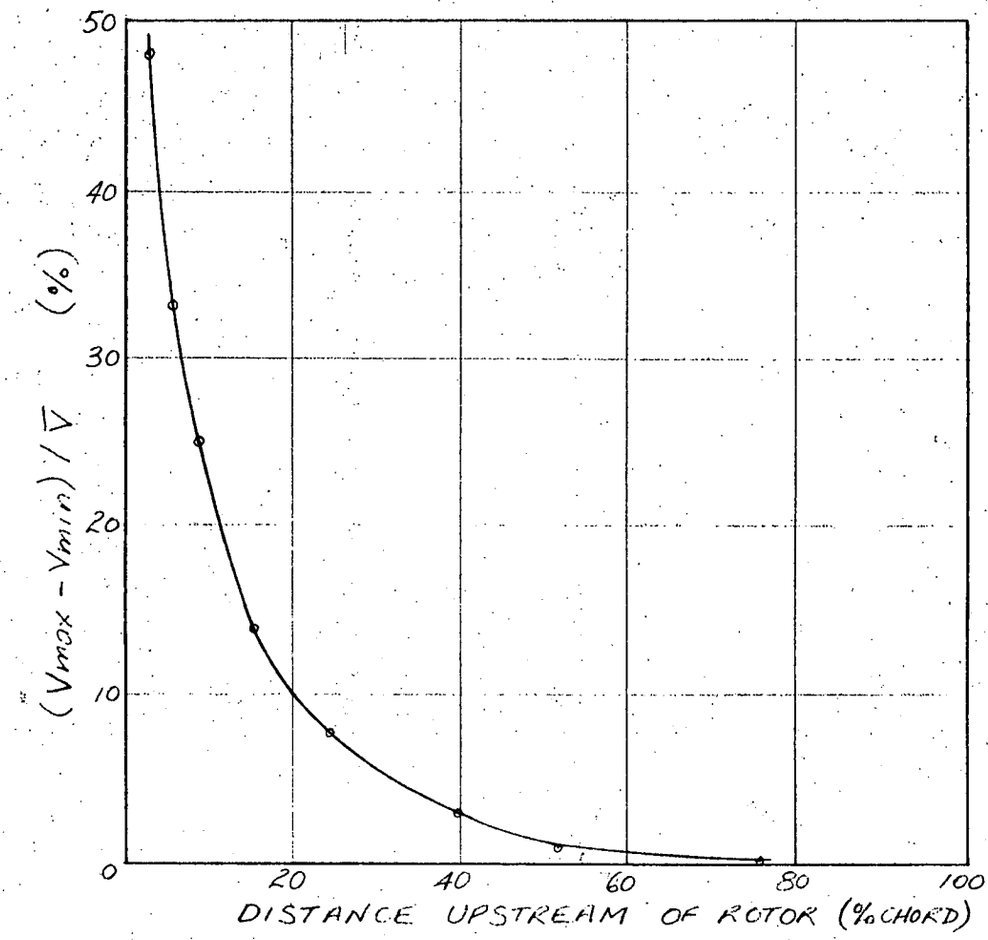

FIG. 3.4 DECAY OF VELOCITY DEFECT

3.3.2 Equivalence of Time and Distance Profiles

The upstream variation in absolute velocity due to the rotor movement is shown later to be independent of the position of the I.G.Vs. However, it cannot be concluded from this that the presence of the guide vane row and its wakes has no effect on the "potential flow" variation in the velocity upstream of the rotor. The flow around each rotor blade may include a mean component due to interaction effects from the guide vane row, and therefore be constant and not vary with the position of the rotor relative to the guide vanes. It was not possible to determine experimentally whether this was the case or not. This problem is discussed further in Section 3.5.

The author decided to assume, for the purpose of further analysis, that the "potential flow" pattern around the rotor was not influenced by guide vane interaction effects. Arguments based on this premise may prove useful, even though there is little justification for such an assumption at this time. Under these conditions, the curves of velocity against time shown in Fig. 3.2 are equivalent to instantaneous plots of absolute velocity against distance in the peripheral direction for a theoretical situation in which wakes and circulation effects from the I.G.V. row are not present. This is explained briefly as follows.
If there are no effects due to other blade rows, the instantaneous plot of absolute velocity against distance must be the same - relative to the rotor blades - at all times. Hence, the stationary hot wire records each consecutive point on the velocity-distance curve as the rotor moves past. There remains only to replace the time scale on the photographs with an equivalent peripheral distance scale and because the rotor moves at constant speed, this scale is linear.

3.3.3 Locus of Absolute Velocity Minima

The oscilloscope traces were triggered at the same rotor position for all photographs, thus making it possible to investigate movements of various parts of the equivalent velocity-distance profiles in the peripheral direction with changing axial position. It was found that the velocity minimum occurred at the same position for each axial location (as accurately as the photographs would allow) to at least as far upstream as 1.18 ins. (39%C). See photographs 3.2 a(2), 3.2 b and 3.2 c. This indicates that the locus of the velocity minima is oriented in the axial direction and does not follow the rotor relative stagnation streamline (rotor inlet angle 42.4 deg.) as might at first be expected. This apparent anomaly is

discussed further in Section 3.4.

3.3.4 Probe Vibration

An interesting feature of the measurements was the consistent ripple in the region of maximum velocity on the oscilloscope traces of photographs 3.2 a. This is observed to be roughly sinusoidal and corresponds to a frequency of about 4000 Hz. It was thought that this would be due to a vibration in the wire, prongs or probe support - or some combination of these - induced when the probe was situated very close to the passing rotor blades. (The reader is referred to the discussion of wire vibration in Section 2.2). As a check on this, some approximate natural frequencies were calculated:-

a. probe support as a cantilever: 190 Hz.
b. prong as a cantilever: 1700Hz.
c. hot wire as a beam built-in at both ends: 5000Hz.

These values suggest that the ripple is most likely due to either a wire vibration or a higher order prong vibration or both, but other possibilities cannot be ruled out. Similar vibrations of the same order of frequency were observed during some other flow measurements upstream of the rotor, and were found to be more noticeable at larger throttle openings. They were also more marked nearer the hub than at the tip. This showed that the exciting force, whatever its nature, was dependent on the flow and/or flow angles, as might be expected when it is considered that any induction of vibration in the probe must come from the air. There was no apparent change in the frequency of the vibration with the change in flow or flow angle.

This type of vibration has been encountered frequently during measurement close to the rotor, both upstream and downstream of it, and presents no real problem to flow studies, provided it can be recognized and is not confused with natural flow variations.

3.4 Comparison of Measurements with a Potential Flow Model

3.2.1 Thick Aerofoil Mapping Model

Assuming, as suggested above, that the "potential flow" pattern around the rotor was not influenced by guide vane row interaction effects, it was possible to compare the measurements (equivalent to velocity-distance curves) with results from a recently developed potential flow model of the flow through a cascade of aerofoils. The particular model considered was developed by Frith (Ref. 12) - a closed mapping function is used to transform the flow about a unit circle due to complex sources

and sinks in the ζ or circle plane to the flow through a cascade of thick, cambered aerofoils in the z or cascade plane. Further details of the method are given in Appendix B. Frith's model was incorporated in an Elliot 503 digital-computer programme developed by Oliver (Ref. 13) to calculate the co-ordinates and corresponding flow velocities (relative and absolute) and angles of streamlines for the relative flow through a cascade representing the rotor in the Vortex Wind Tunnel. Results were computed for mean flow conditions corresponding to the velocity diagram of Fig. 3.3. Clearly, in using this mapping model, it was only possible to approximate the actual blade shape. The agreement between the analytical and C4 sections is shown in Fig. 3.5. The absolute and relative flow velocities at a particular axial position were obtained from the programme results by interpolating between values on each streamline.

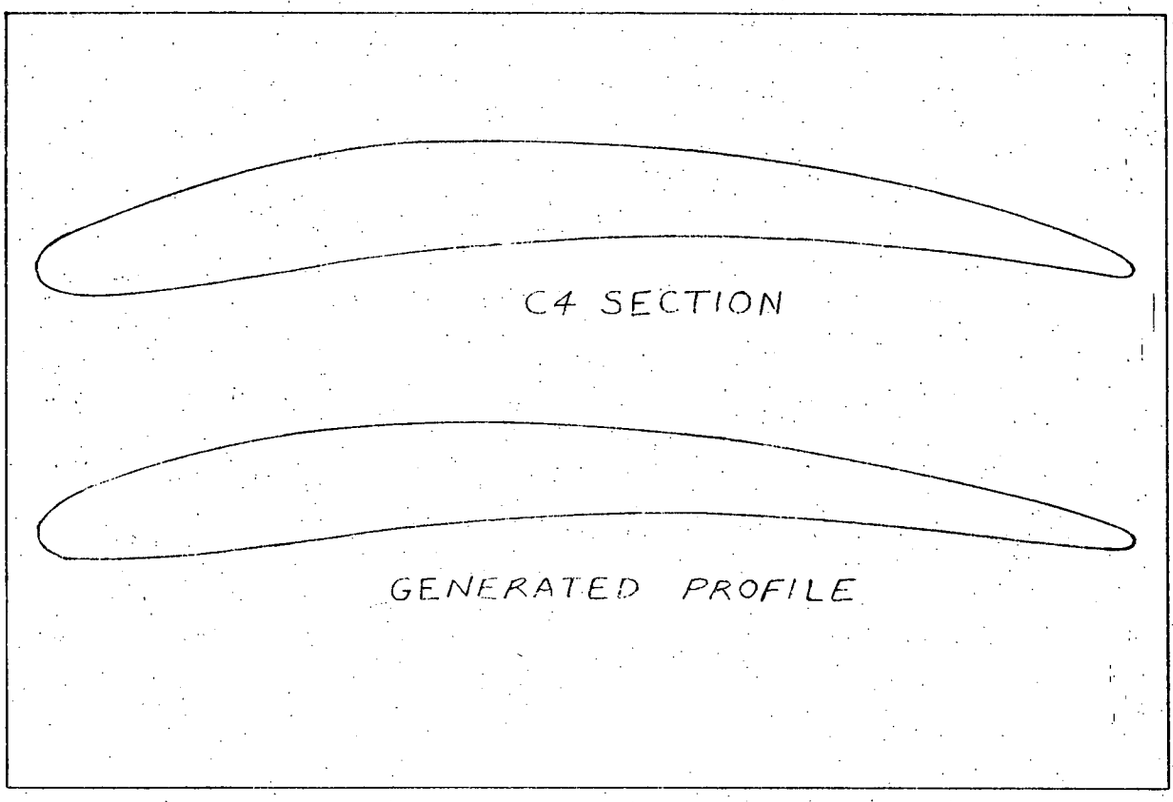

FIG. 3.5 COMPARISON BETWEEN GENERATED AND ACTUAL BLADE PROFILES

3.4.2 Comparison of Measured and Calculated Profiles

Graphs of absolute velocity against peripheral position were compared with mean profiles reproduced from the photographs of Fig. 3.2. Comparisons for two axial positions - 0.16 ins. (5.23%C) and 0.45 ins. (14.7%C) upstream of the rotor - are shown in Fig. 3.6. As explained above, the position of the rotor leading edge on the measured velocity-distance curves was not known. In Fig. 3.6, the measured and calculated mean velocities were first aligned and then the two sets of curves were moved relative to each other horizontally to give the best position of agreement. For the purposes of the comparison the measured velocities were non-dimensionalized by dividing by an axial velocity value which would make the experimental and calculated values of $(\frac{V}{Va})_{mean}$ equal at 1.076.[1] As exemplified in the figure there was very good agreement in both shape and dimensions between the mapping model and measured curves, the agreement improving with distance from the rotor. A comparison of the velocity defects for the curves of Fig. 3.6 is shown in the following table.

TABLE 3.1

Measured and Calculated Velocity Defects

POSITION UPSTREAM OF ROTOR (ins.)	$\frac{Vmax-Vmin}{Va}$ (MEASURED)	$\frac{Vmax-Vmin}{Va}$ (CALCULATED)	DIFFERENCE
0.16	0.356	0.334	6%
0.45	0.150	0.143	5%

The small differences in velocity defect values could almost be attributed to experimental error alone. As was observed for the measured profiles, the calculated absolute velocity minima occur at the same peripheral position for both axial stations considered in Fig. 3.6. This is seen to correspond to an axial line meeting the rotor blade very close to the leading edge. There were, however, significant differences in the shape of the measured and calculated curves, particularly for positions close to the leading edge. Apart from necessitating an approximate blade shape, the mapping model neglects the rotor blade boundary layer and wake,

---

1. It was difficult to accurately assess the real value of Va between the I.G.V. and rotor rows at the time of measurement. The Va used above was 61.5 f.p.s., compared with the nominal value of 60.5 f.p.s. for the velocity diagram of Fig. 3.3.

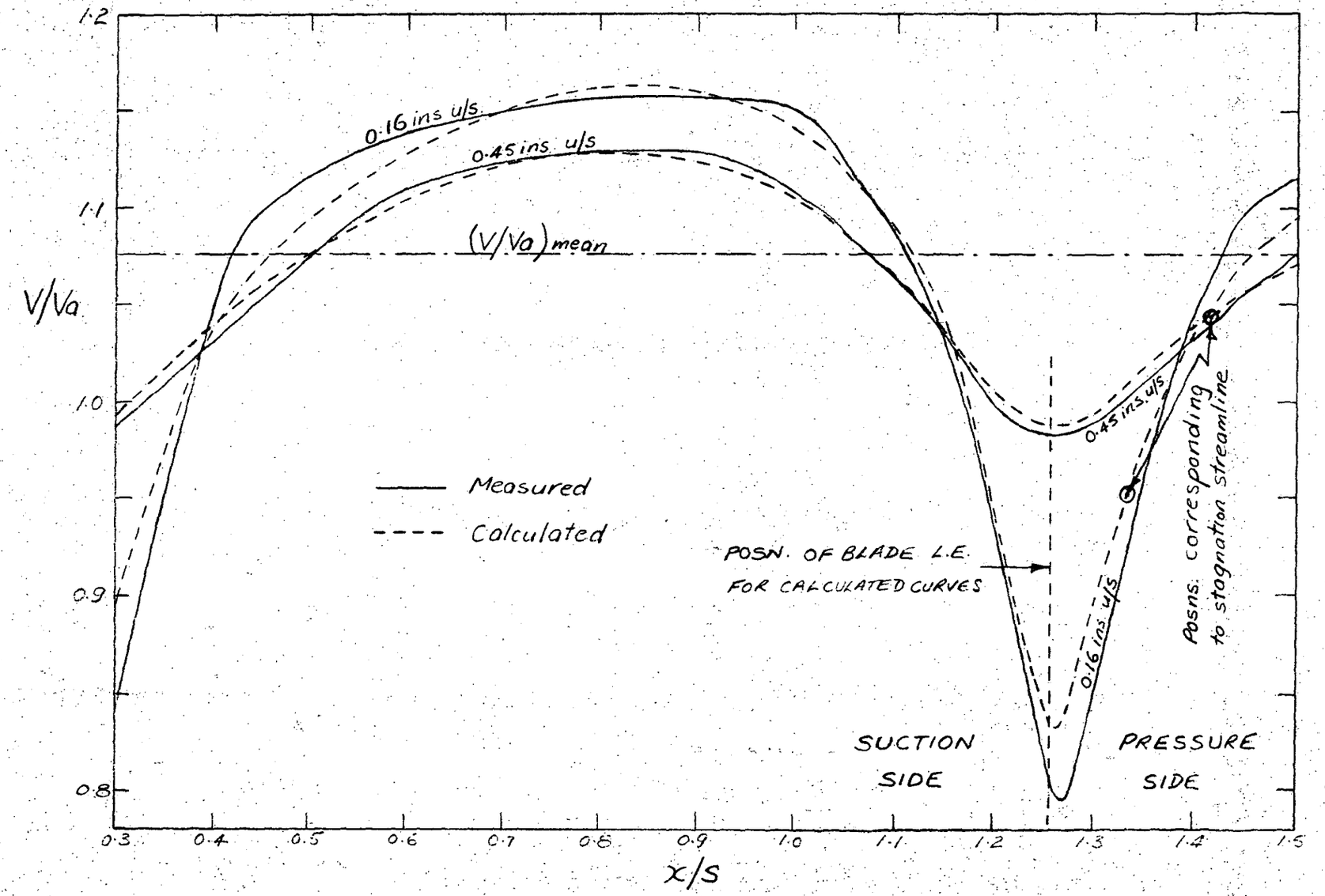

FIG. 3.6 COMPARISON OF MEASURED AND MAPPING MODEL VELOCITY PROFILES

which will certainly affect both the circulation and effective blade shape. Considering these inherent deficiencies, the potential flow model gives a surprisingly good fit to the curves of Fig. 3.2 and provides some justification for the assumption made above, namely that I.G.V. interaction effects are negligible in these "potential flow" considerations. This assumption would certainly be satisfactory for design purposes. The mapping model was also considered suitable for making further predictions about the real flow in the vicinity of the rotor. For example, as there was no way of determining the exact position of the rotor leading edge on the measured velocity profiles, it was felt that there was sufficient justification for assuming for the real flow the same situation as depicted on the calculated profiles.

3.4.3 Loci of Absolute and Relative Velocity Minima

As mentioned above, it was initially expected that the positions of the absolute velocity minima would correspond to the relative stagnation streamline. This reasoning, of course, wrongly assumed that the absolute and relative velocity minima would coincide.

Curves of relative velocity against peripheral position plotted from the mapping model results are shown in Fig. 3.7. The common position of the absolute velocity minima and the positions corresponding to the relative stagnation streamline are indicated on the curves. First of all, it is seen that the absolute and relative velocity minima do not coincide. This is explained by the nature of vector addition in a case where the flow angles are varying. (It should also be noted that even if the relative rotor inlet angle α_1 were constant, the positions of the absolute and relative velocity minima need not be the same.) The situation is illustrated in Fig. 3.8 by velocity diagrams corresponding to the two minima for the axial position 0.45 ins. upstream.

As implied in the above explanation, it had been assumed that the locus of the relative velocity minima would follow the relative stagnation streamline. Fig. 3.7 shows that this, too, is a wrong assumption, with the relative velocity minima approaching the position of the stagnation streamline only near the rotor leading edge. At a position 1.18 ins. (39%C) upstream, the relative minimum is as much as one fifth of a blade spacing from the stagnation streamline. It was thought intuitively that the fluid particle with the minimum velocity at a certain axial position upstream of the rotor would still exhibit the minimum velocity at any position further downstream as it moved closer to the rotor. However, considering the

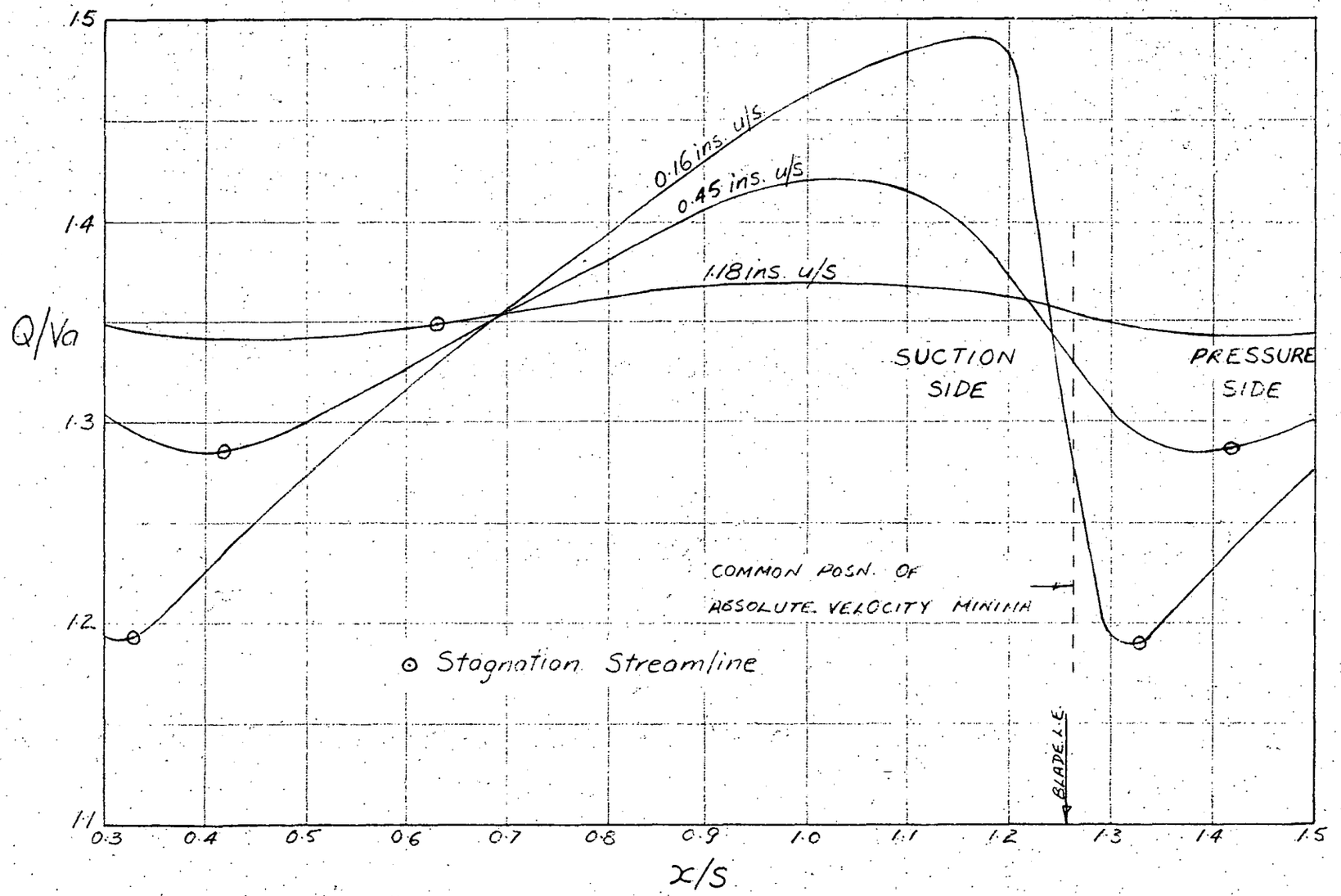

FIG. 3.7 RELATIVE VELOCITY PROFILES (MAPPING MODEL)

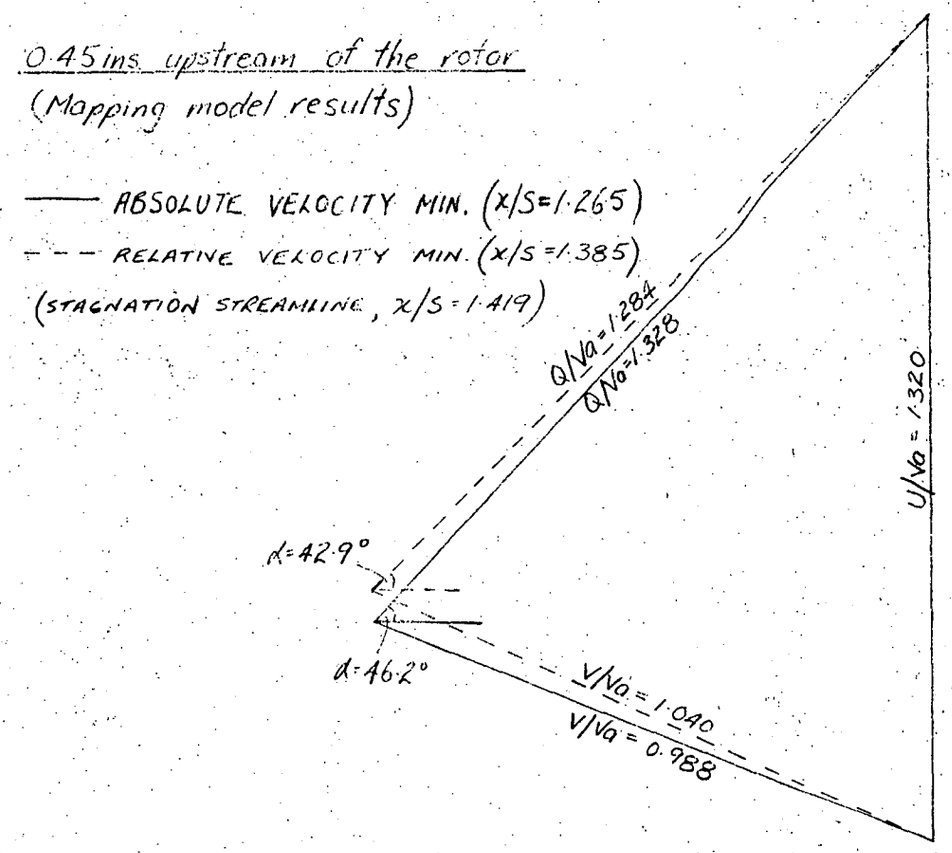

FIG. 3.8 VELOCITY DIAGRAMS CORRESPONDING TO VELOCITY MINIMA

complex nature of the flow around a body as difficult to model as a rotor blade section, there is no reason why this should be the case. The actual situation indicated by the potential flow model - which can be expected to approximate real flow conditions - is shown diagrammatically in Fig. 3.9.

No special reason can be given why the absolute velocity minima should lie on a straight axial line for the particular flow conditions specified by the velocity diagram of Fig. 3.3. The occurrence was investigated further by locating the approximate line of the absolute velocity minima from measurements at other throttle settings. The results, showing that the line was oriented in the axial direction only for the 8 ins. throttle setting, are tabulated below. (In each case, the line was constructed from measurements at two axial positions only - 0.1 ins. (3.3%C) and 1.2 ins. (40%C) upstream of the rotor respectively. The measurements were intended to give only the approximate orientation of what might be a curved locus.)

TABLE 3.2

Approximate Orientation of Line of Absolute Velocity Minima

THROTTLE OPENING (ins.)	5.2	8	22
RELATIVE ROTOR INLET ANGLE (deg.)	47.8	42.4	31.0
ANGLE OF LINE OF Vmin (deg.)	6.2	0	- 13.5

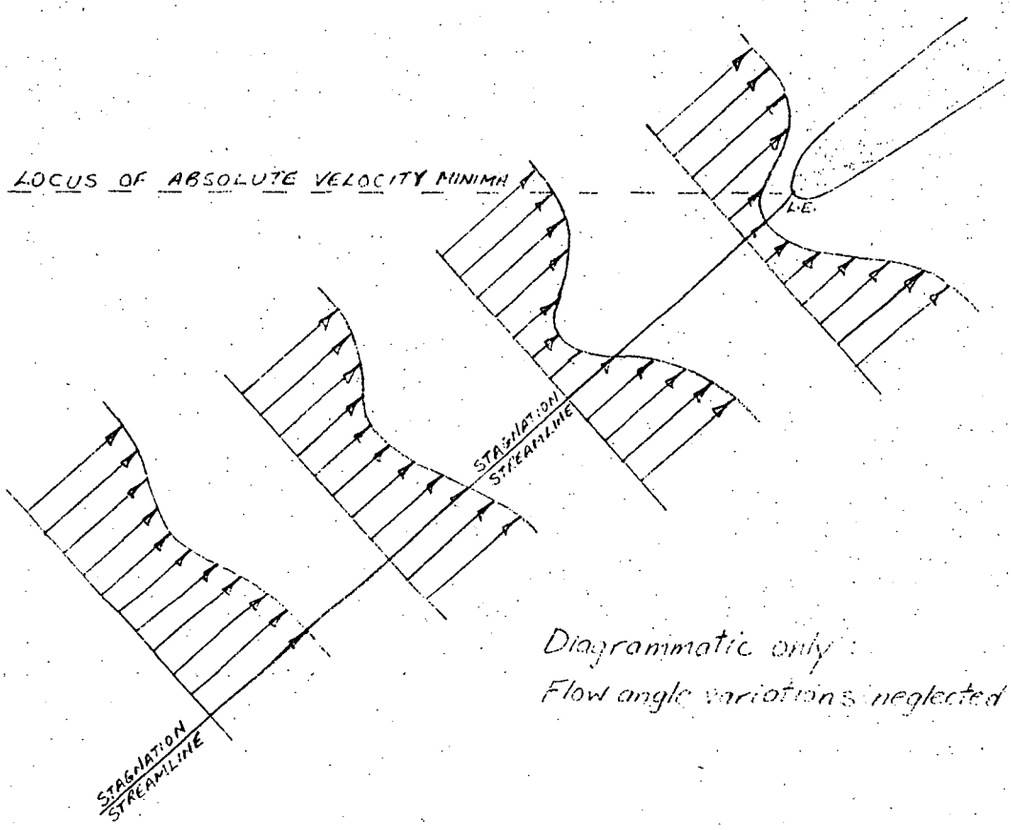

FIG. 3.9 RELATIVE FLOW UPSTREAM OF THE ROTOR

3.5 Traverse through the I.G.V. Wake

The velocity-time curves of Fig. 3.2 were measured with the I.G.V. row rotated to position the hot wire outside of the wake regions. In order to examine the effect of the guide vane wake on the signal detected by the wire and on the general flow pattern in the vicinity of a rotor blade, a further series of measurements were taken, this time rotating the guide vane row to position the hot wire at several different positions inside the wake. These photographs - taken at an axial station 0.37 ins. (12.3%C) upstream of the rotor leading edge - are shown in Fig. 3.10. The instant of triggering is the same for each set of traces.

a. 0.43s TO SUCTION SIDE OF WAKE CENTRE.

Mean Velocity = 64.9 fps.

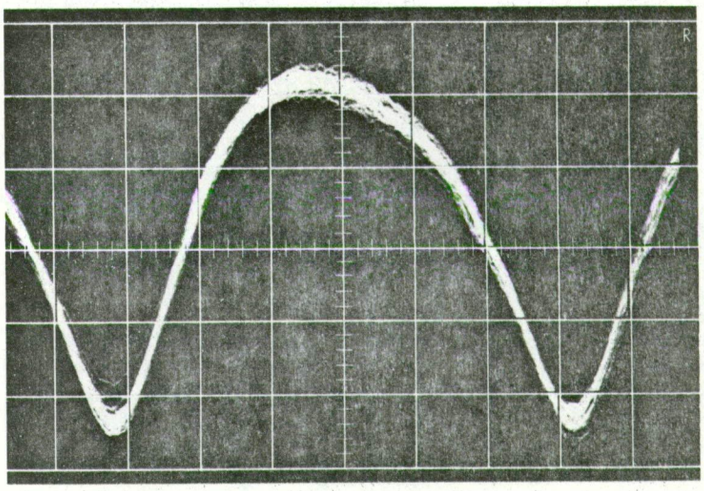

b. 0.17s TO SUCTION SIDE OF WAKE CENTRE.

Mean Velocity = 64.9 fps.

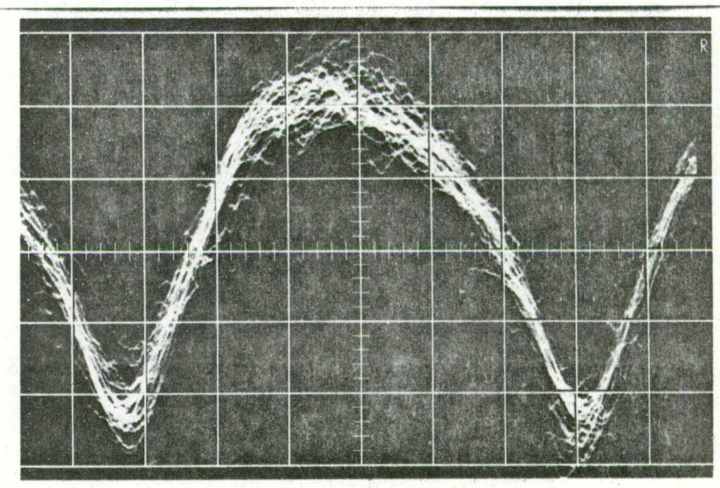

c. PROBE SITUATED AT I.G.V. WAKE CENTRE.

Mean Velocity = 60.2 fps.

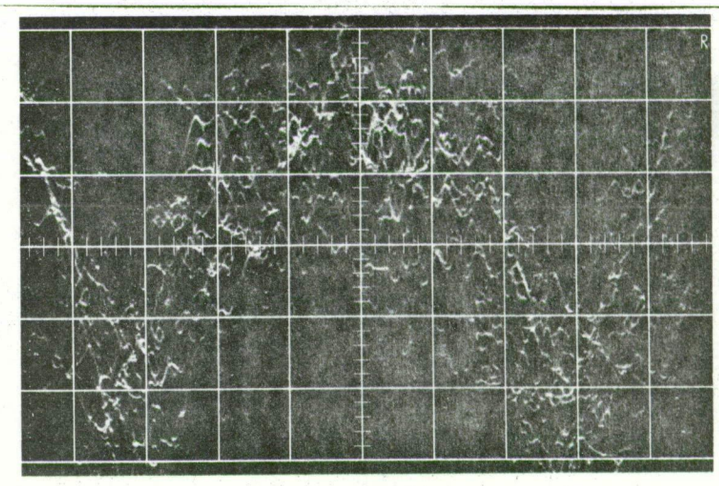

d. 0.12s TO PRESSURE SIDE OF WAKE CENTRE.

Mean Velocity = 64.9 fps.

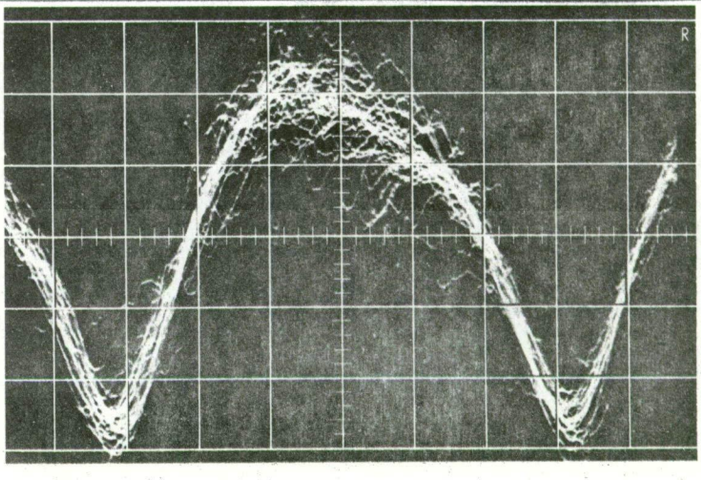

FIG. 3.10
TRAVERSE THROUGH I.G.V. WAKE 0.37 INS. (12.3%C) UPSTREAM OF ROTOR L.E.

Vert. Scale: 2.28 fps/div.

Horl. Scale: 0.5 msec/div.

s = blade spacing (I.G.V.)

The development of the I.G.V. wake in the Vortex Wind Tunnel has been measured to a position 1.50 ins. downstream of the guide vane trailing edge (2.05 ins. upstream of the rotor leading edge) by Boxhall and Nilsson (Ref. 14). These measurements were later extended by the author to a position 0.35 ins. upstream of the rotor. Before discussing the photographs of Fig. 3.10, a brief summary of the results of these investigations is given.

3.5.1 Development of the I.G.V. Wake Upstream of the Rotor

The distributions of the mean velocity, $\bar{V}$, and the RMS value of the velocity fluctuations, V_{RMS}, through the wake were measured at several axial positions between the guide vane and rotor rows using the DISA 55A01 constant temperature anemometer. Typical curves (for a position 0.227 ins. - 7.6%C - downstream of the guide vane trailing edge) are shown in Fig. 3.11. The wake centre-line, defined by the points of maximum mean velocity defect, is plotted in Fig. 3.12 and the decay of the wake defect is shown in a graph of $\bar{V}_{min}/\bar{V}_{max}$ against axial position in Fig. 3.13.

As observed in Fig. 3.11, the wake profiles are far from symmetrical and the velocity distribution outside the wake is distinctly non-uniform. There is always a lack of symmetry in the wake of a lifting aerofoil since the boundary layer on the suction surface is subject to higher pressure gradients and is thus thicker than that on the pressure surface. The variation in the free stream velocity is no doubt due largely to the "potential flow" circulation effect downstream of the guide vanes.

The features described above made it impossible to satisfactorily define the edges of the wake from the mean velocity profile. The distribution of V_{RMS}, however, was approximately symmetrical (at least near the edges of the wake) and fairly constant - at almost zero - outside the wake. Consequently, it was convenient to define the edges of the wake as two points on the profile corresponding to some percentage of the peak V_{RMS} value. Thirty percent of $(V_{RMS})_{max}-(V_{RMS})_{min}$ was finally chosen as a standard. (See Fig. 3.11). Lines representing the edges of the wake based on this definition are shown in Fig. 3.12.

The lack of uniformity in the flow velocity outside the viscous region presented significant difficulties in formulating a suitable definition for the displacement thickness δ^* of the wake. The problem was not considered rigorously at this time, and some approximate values of δ^* were calculated by treating the two halves of the wake in the same way as for a boundary layer. The "expected" values of $\bar{V}$ for the free stream were obtained by extrapolating the nearly linear velocity distribution outside the viscous region to the

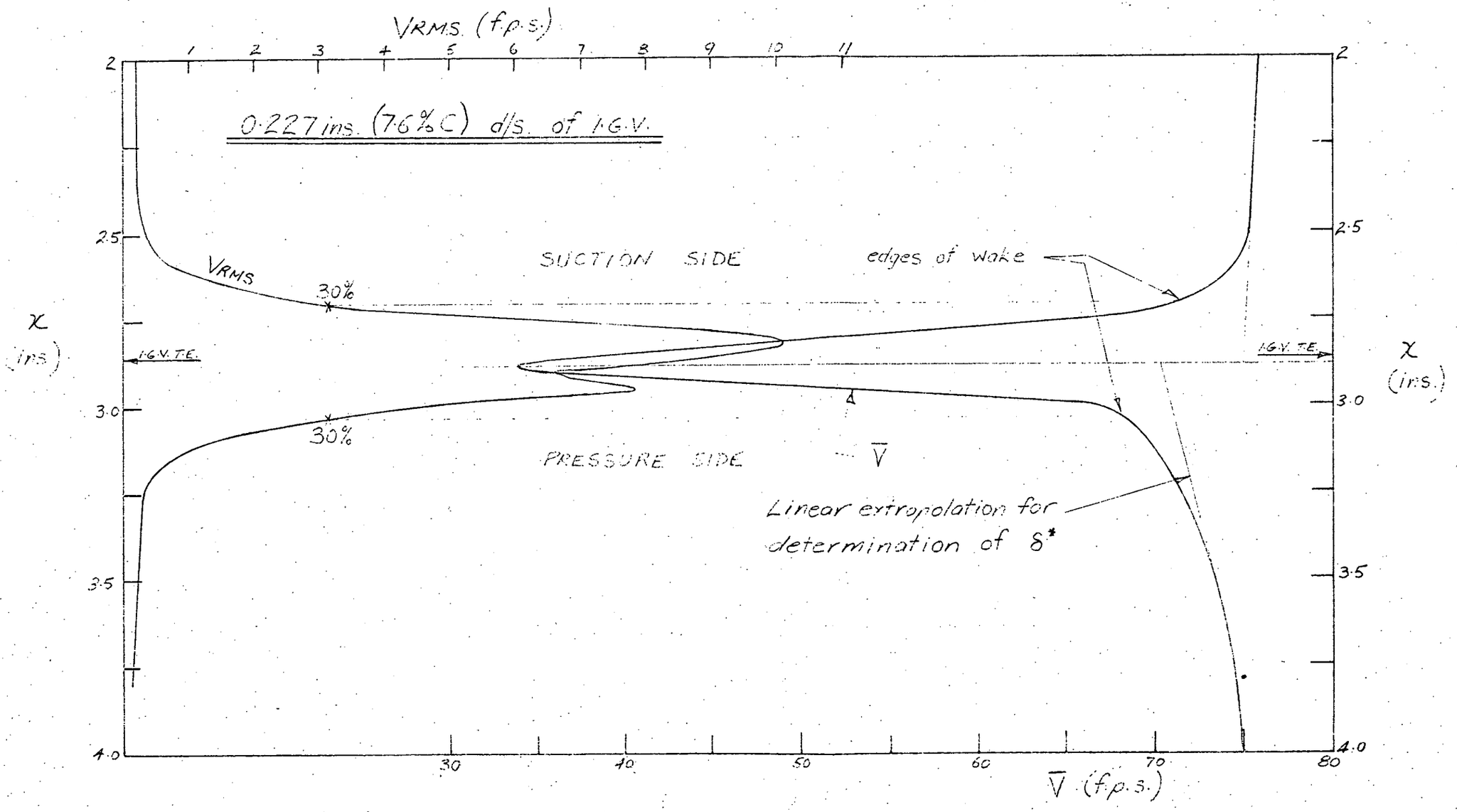

FIG. 3.11 I.G.V. WAKE VELOCITY DISTRIBUTION

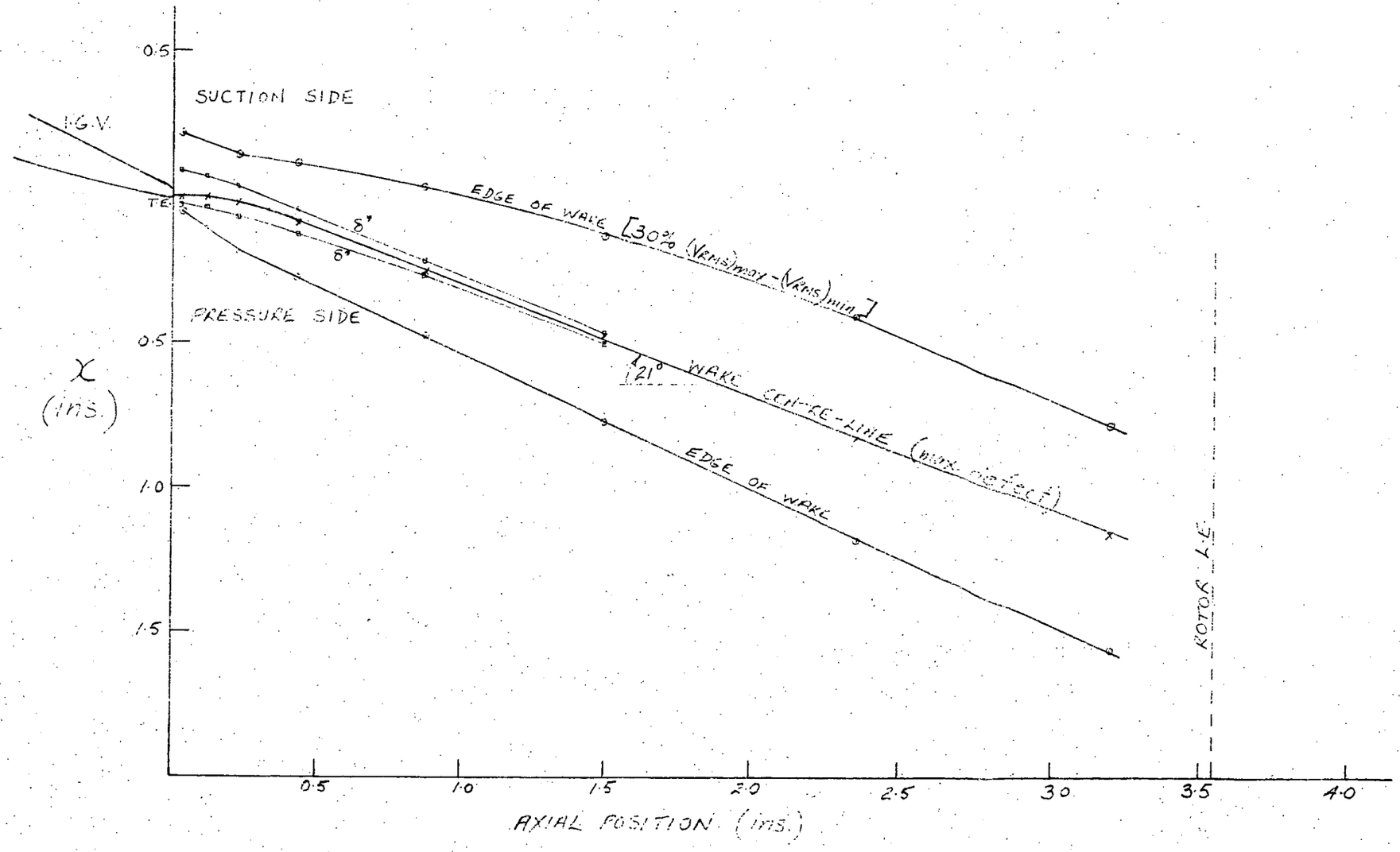

FIG. 3.12 I.G.V. WAKE DEVELOPMENT

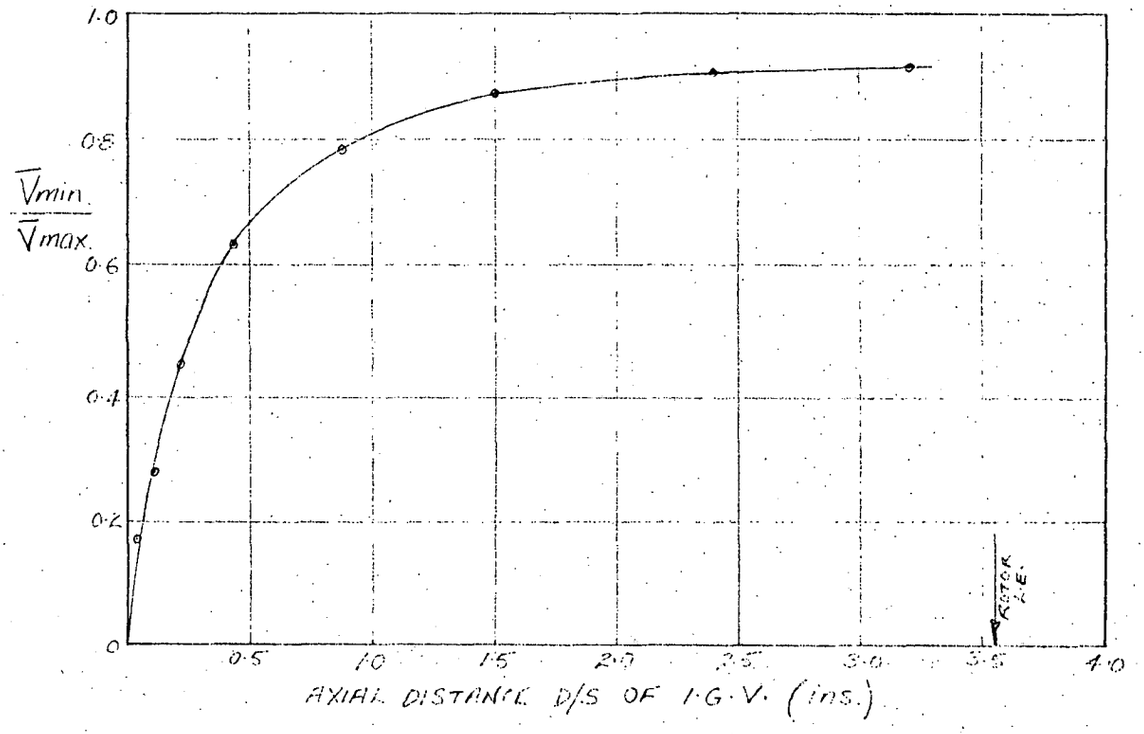

FIG. 3.13 DECAY OF I.G.V. WAKE VELOCITY DEFECT

middle of wake for each half as shown in Fig. 3.11. The calculated displacement thicknesses are plotted on the wake centre-line in Fig. 3.12. The general problem of defining a displacement thickness for a compressor blade wake is considered in more detail in the discussion of the rotor wake in Chapter 5 (Section 5.6).

3.5.2 Interpretation of Photographs

In the photographs of Fig. 3.10, the I.G.V. wake is evident as turbulent fluctuations superimposed on the general velocity-time curve due to the rotor movement. Photograph 3.10c shows the signal recorded by a probe situated at the centre of the wake, which was located as the position of minimum mean velocity. At this station, 0.37 ins. upstream of the rotor leading edge, $\bar{V}min/\bar{V}max = 0.92$ (Fig. 3.13) and the wake is approximately a third of one spacing wide (Fig. 3.12). The change in $\bar{V}$ through the wake is not apparent in the photographs as the A.C. zero on the oscilloscope was adjusted in each case to set the mean velocity at +0.5 on the vertical scale. The measured value of the V_{RMS} component due to the wake at the wake centre was 3.0 f.p.s. compared with a "potential flow" velocity defect of 10.4 f.p.s. (corresponding to a measured V_{RMS} component of 3.1 f.p.s.) and mean velocity 60.2 f.p.s. Despite the high turbulence level, the general shape depicted in the almost wake-free conditions of photograph 3.10a can be easily discerned.

Photographs 3.10b and 3.10d show traces from near each edge of the guide vane wake. It is interesting that the turbulent fluctuations are apparently not uniform in magnitude over the complete trace, but are more noticeable in the region of maximum mean velocity. This is particularly so in photograph 3.10d. This suggests that there is an oscillatory variation in the position of the guide vane wake as the rotor moves past. Such an effect is likely to be the case as the wake particles near the rotor would encounter varying amounts of flow circulation depending on the position of the adjacent rotor blade. Under these conditions, a hot wire near the edge of the wake might effectively be inside the wake for part of the time and outside it the rest, and therefore detect varying levels of turbulence. A similar effect has been observed by the author in measurements downstream of the rotor (see Section 4.4). This phenomenon has also been measured in the Vortex Wind Tunnel by Johnston (Ref. 23).

3.5.3 Effect of the I.G.V. Wake on the Rotor Blade Flow Pattern

Probably the most significant feature of the photographs of Fig. 3.10 is that, apart from the varying levels of wake turbulence, there is no detectable change at all in the mean velocity-time curve due to the rotor movement with the change in the position of the hot wire relative to the wake. The section of the curve between the two minima on each photograph corresponds to a complete traverse of a rotor blade through the I.G.V. wake. (In fact, as there are 38 I.G.Vs. and 37 rotor blades, it represents slightly more than one whole traverse.) However, the same instant on each of the four curves corresponds to different positions of the rotor blade in the I.G.V. wake. Hence any variation in rotor blade circulation with position in the wake would be expected to show up as a change in the general shape and dimensions of the mean velocity-time profile - and this is not the case. It is concluded that there is no apparent measurable change in circulation as the rotor blade passes through the I.G.V. wake.

The passage of a wake over a compressor blade might be expected to cause changes in circulation as a result of any of the following effects:

a. Changes due to general interaction of wake and blade vorticities.

b. The passage of a wake over the surface of a blade could well be expected to produce changes in the positions of the separation points. This would almost certainly be accompanied by changes in the position of the rear stagnation point and hence in the circulation. This argument suggests that the Kutta-Joukowski condition, which fixes the rear stagnation point at the blade trailing edge, is unlikely to apply at all times in unsteady flow. The adequacy of unsteady flow models which assume this condition must surely be questioned. Parker (Refs. 8, 15)

has also expressed uncertainty regarding the Kutta-Joukowski condition in situations involving blade row interaction.

c. Changes in the angle of incidence as the rotor blade encounters the wake velocity defect would be expected to alter the blade circulation. It is difficult to estimate the order of magnitude of possible circulation changes due to this cause in a situation where, at any instant, each point in the flow experiences a different velocity defect and hence different angle of incidence. The effect of a small change in incidence on the circulation around a cascade blade was examined by computing velocity profiles using the mapping model programme for an overall angle of incidence corresponding to the maximum I.G.V. wake defect at the rotor leading edge. The defect was 8%, giving an increase of the order of 3.2 deg. in the angle of incidence. (This was calculated assuming a constant absolute flow angle in the wake.) Fig. 3.14 shows comparisons between the original curves of Fig. 3.6 and the curves with changed incidence for positions 0.16 ins. and 0.45 ins. upstream of the rotor. The differences in the two sets of curves are very noticeable, with an increase in the velocity defect for the position 0.16 ins. upstream of over 70%. These potential flow curves for increased incidence cannot, of course, be related in any way to the real flow conditions. They do, however, show that small changes of incidence due to a wake defect could be expected to alter the blade circulation to some extent.

In the light of the above arguments, it is strange that there is no variation in the "potential flow" velocity profile in the I.G.V. wake traverse of Fig. 3.10. The I.G.V./rotor spacing may be too large for measurable changes in circulation due to the guide vane wake to occur; the measurements should certainly be repeated for a much smaller I.G.V./rotor clearance. Assuming this is not the case, there seem to be two possible explanations.

Firstly, the presence of wakes from the guide vane row may be affecting the rotor circulation, but the latter settles on some mean value as does the position of the rear stagnation point. Under these conditions, the Kutta-Joukowski condition could be satisfied. Secondly, the passage of the I.G.V. wake over a rotor blade may produce changes in the position of the rear stagnation point but they occur too quickly for corresponding changes in the circulation to take place and the circulation again remains on some mean value. Parker (Ref. 8) shows in an argument based on flow visualization films of the starting vortex of an aerofoil, that there is likely to be a considerable time lag between any changes in conditions near the blade and significant resultant changes in circulation. Under the conditions of the second explanation, the Kutta-Joukowski condition would, of course, not be satisfied.

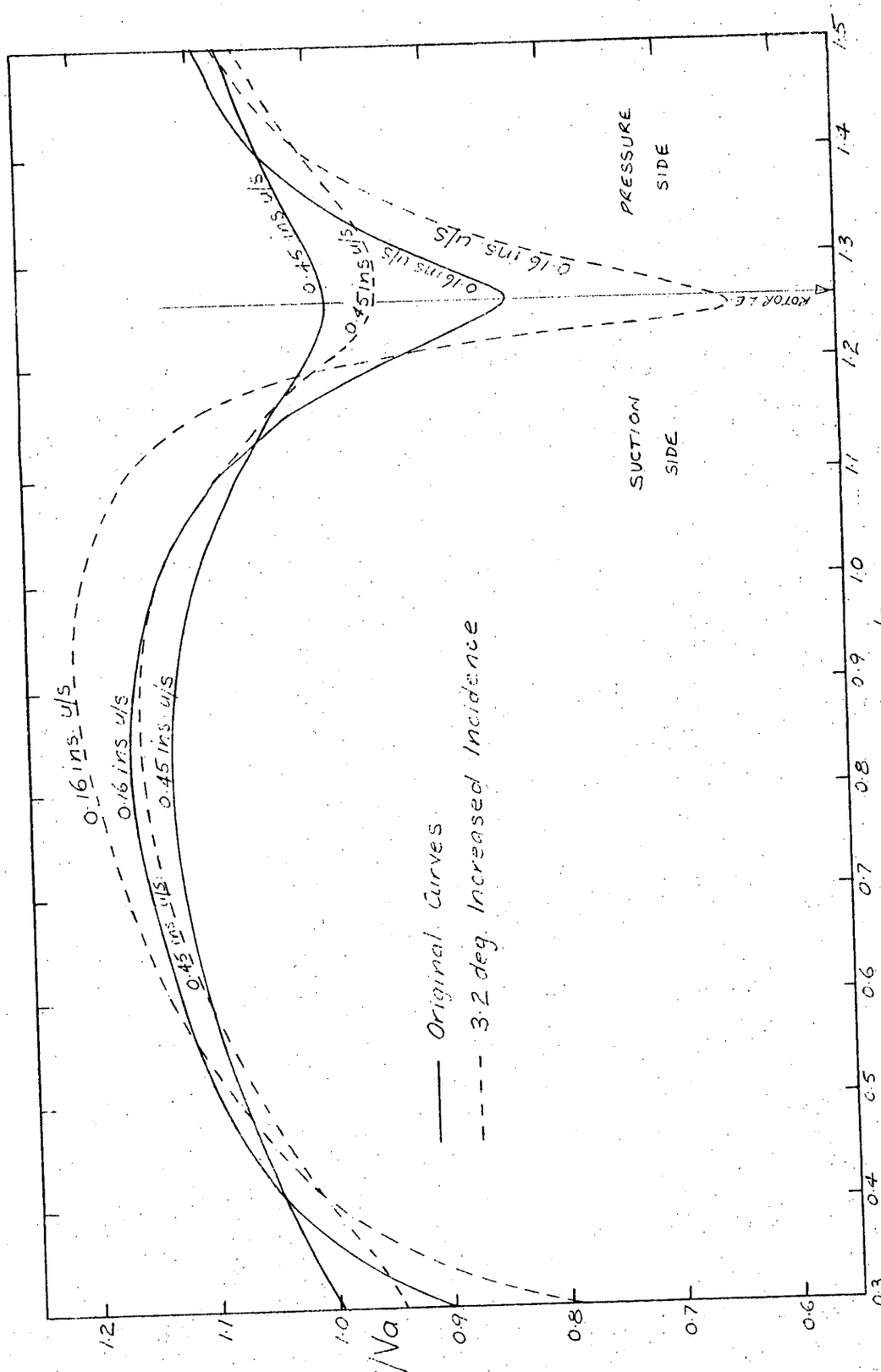

FIG. 3.14 EFFECT OF INCREASED ANGLE OF INCIDENCE ON POTENTIAL FLOW VELOCITY DISTRIBUTIONS UPSTREAM OF THE ROTOR

Parker (Ref. 8), in calculations using a finite difference model of the potential flow interaction between guide vane and rotor rows, considered two extreme conditions for the I.G.Vs.:

a. That the Kutta-Joukowski condition applied at the trailing edge at all times.

b. That the circulation around the guide vanes remained constant at all times.

The calculations based on the assumption of constant circulation tended to show better agreement with experimental results. This is in accord with the photographs of Fig. 3.10 and would seem to suggest the second explanation given above.

3.6 Development of a Thin Aerofoil Model

The thick aerofoil mapping model introduced in Section 3.4 gave a good fit to the measurements of the "potential flow" distribution of velocity upstream of the rotor and was considered very satisfactory for design purposes. The author decided to investigate the possibility of achieving similar agreement with a simpler model based on thin aerofoil theory. This theory replaces each blade profile with a loaded vortex sheet, i.e., vortices arranged along the chord. A good account of the method is given by Csanady (Ref. 10).

3.6.1 Single Vortex Approximation

The simplest model of a compressor row is a single infinite row of bound vortices situated at the mid-points of the blade chords as shown in Fig. 3.15. Preston (Ref. 17) and Horlock (Ref. 2) have used this simple model of a compressor row in discussions of unsteady flow pressure changes in axial flow machines.

Referring to Preston (Ref. 17) and Fig. 3.15 the velocity potential for the row of bound vortices on the real axis is

$$W = \frac{iK}{2\pi} \log \sin\left(\frac{\pi z}{s}\right) \qquad \ldots\ldots(3.1)$$

where s is the spacing and K the circulation in the clock-wise direction.

The velocity components are

$$u_K = \frac{K}{2s} \cdot \frac{\sinh\left(2\pi y/s\right)}{\cosh\left(2\pi y/s\right) - \cos\left(2\pi x/s\right)} \qquad \ldots\ldots(3.2)$$

and

$$v_K = \frac{-K}{2s} \cdot \frac{\sin\left(2\pi x/s\right)}{\cosh\left(2\pi y/s\right) - \cos\left(2\pi x/s\right)} \qquad \ldots\ldots(3.3)$$

When the row is in motion with velocity U, a fixed point in the flow has co-ordinates

$$x = Ut, \text{ and } y$$

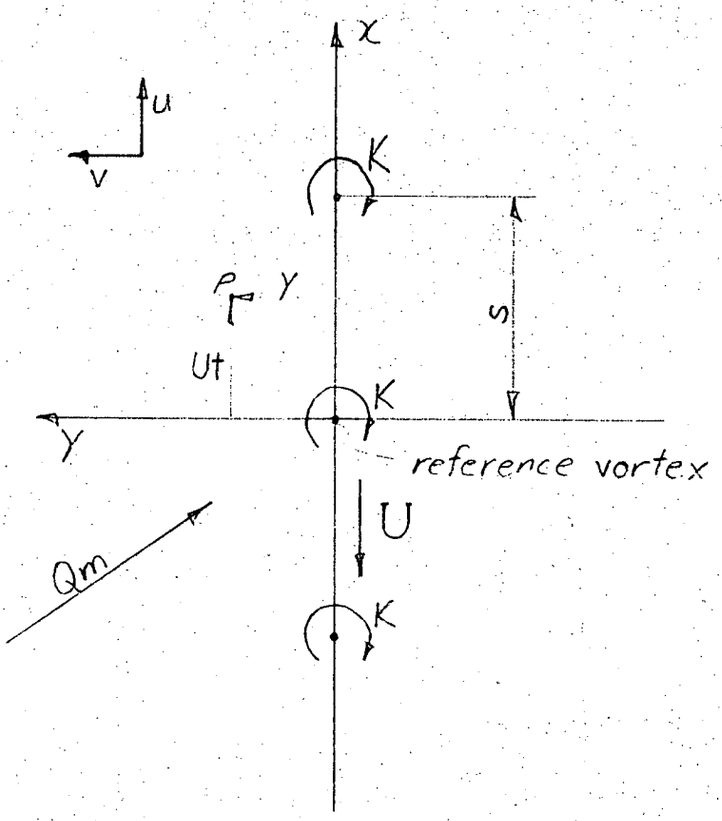

FIG. 3.15 SINGLE VORTEX MODEL OF COMPRESSOR ROW

relative to instantaneous axes moving with the row. Substitution in Eqs. (3.2) and (3.3) then gives the variation in the relative (and absolute) flow velocity components with time at the point.

The total relative velocity at a point (x,y) is obtained by adding u_K and v_K to the vector mean velocity Qm. The total absolute velocity in the case of a moving row is then

$$V = \sqrt{(u_K + Qu_m - U)^2 + (v_K - Va_m)^2} \qquad \ldots\ldots(3.4)$$

Eqs. (3.2), (3.3) and (3.4) were used to compute the absolute velocity distributions at positions upstream of the rotor for comparing with the measurements and the mapping model results. The following values used in the calculations were obtained from the velocity diagram of Fig. 3.3

$$\frac{K}{s} = \Delta Q_u = 27.5 \text{ f.p.s.}$$

$$U - Qu_m = 37.5 \text{ f.p.s.}$$

$$Va_m = 59.5 \text{ f.p.s.}$$

Calculations for the position 0.45 ins. upstream of the rotor leading edge (1.76 ins. upstream of the vortex at mid chord) gave a velocity defect, $(V_{max}-V_{min})/\bar{V}$, of 2.5% compared with the

measured value of 13.8%.

3.6.2 Vortices Distributed along Camber Line

As exemplified in the above calculation, the one vortex model is not very realistic for the purposes of the current investigations. The next step is to replace the blade by a number of vortices arranged along the chord or, better still, along the camber-line.

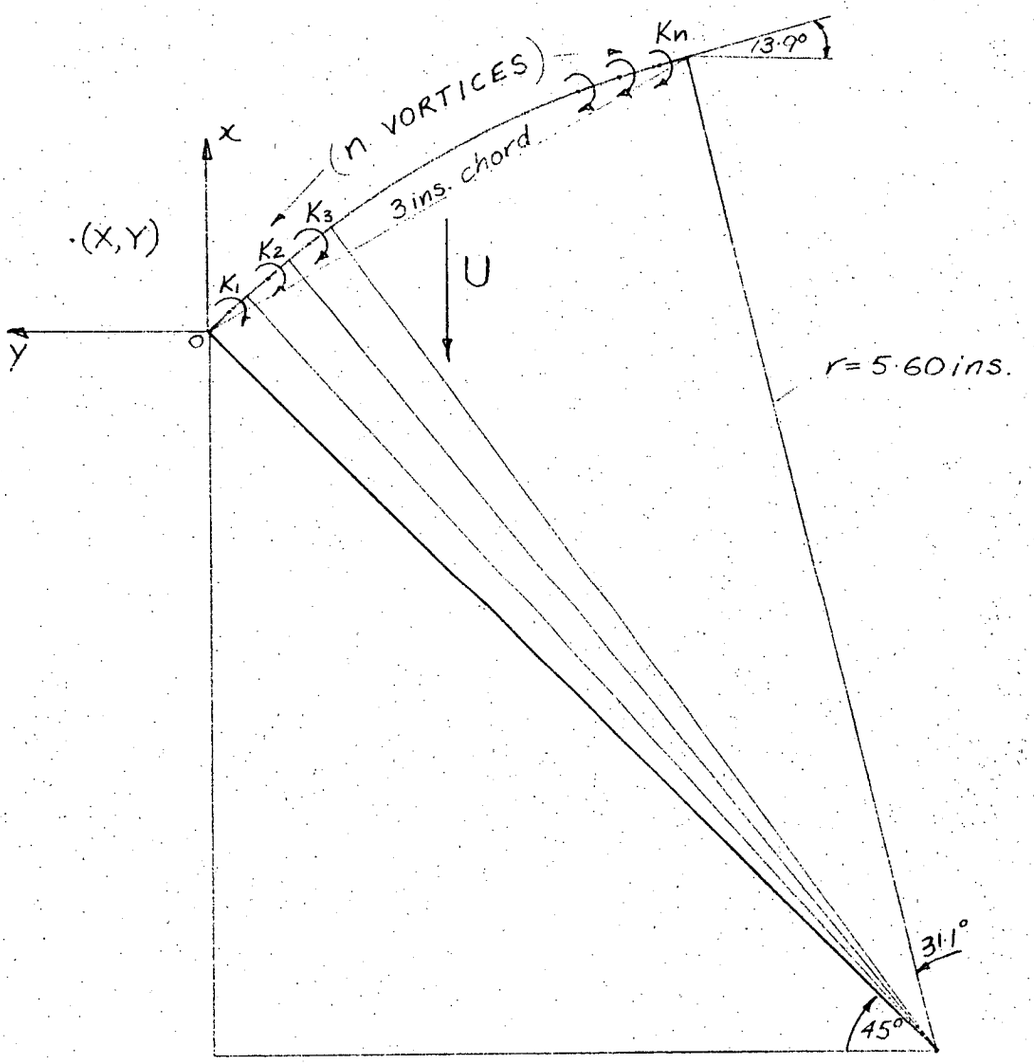

FIG. 3.16 ROTOR BLADE REPLACED BY VORTICES DISTRIBUTED ALONG CAMBER-LINE

A model based on vortices distributed along the circular arc camber line was developed by the author and incorporated into an Elliot 503 digital computer programme. The geometry for one rotor blade is shown in Fig. 3.16. The programme was written to include

the facility for varying the number of vortices, n, used to model the blade. The vortices were situated at the mid-points of n equal arc segments along the camber line. The absolute velocity at a point (X,Y) relative to axes at the leading edge was calculated by summing components due to each of the n single rows of vortices using the Preston analysis incorporated in Eqs. (3.2), (3.3) and (3.4):

$$V = \sqrt{(\Sigma u_K + Qu_m - U)^2 + (\Sigma v_K - Va_m)^2} \qquad \ldots\ldots(3.5)$$

The co-ordinates of the point (X,Y) relative to the i^{th} reference vortex are given by

$$x = X - \left[r \sin(45^\circ + (\tfrac{2i-1}{2n}) \cdot 31.1^\circ) - r \cos 45^\circ\right] \qquad \ldots\ldots(3.6)$$

and $$y = Y + r \cos 45^\circ - r \cos(45^\circ + (\tfrac{2i-1}{2n}) \cdot 31.1^\circ) \qquad \ldots\ldots(3.7)$$

where r is the radius of the circular arc camber line and equals 5.60 ins.

The values of the circulation K for each vortex were obtained from previously measured relative velocity distributions for the suction and pressure surfaces of the rotor blades in the Vortex Wind Tunnel (see Fig. 3.17):

$$K = (Qs - Qp)\Delta\xi \qquad \ldots\ldots(3.8)$$

where Qs and Qp are average suction and pressure surface velocities for the chord segment $\Delta\xi$

The programme was used to compute the variation of absolute velocity with peripheral position (and time) at different axial positions upstream of the rotor with, first of all, 6 vortices per blade. Curves for axial positions 0.16 ins. (y/s = 0.0523) and 0.45 ins. (y/s = 0.1470) upstream are shown in Fig. 3.19. Points corresponding to a later computation with 30 vortices per blade are also shown. It is interesting that the differences between the results for the two different values of n are almost negligible.

The vortex model velocity defects $(\frac{Vmax-Vmin}{Va})$ are only 0.141 (0.16 ins. upstream) and 0.071 (0.45 ins. upstream) compared with the measured values of 0.356 and 0.150.

It was decided to check these large differences by re-running the vortex model programme using values of circulation K obtained from the suction and pressure surface velocity distributions calculated from the mapping model (see Fig. 3.18). For convenience, the computation was carried out using 10 vortices per blade. The resulting velocity profiles are compared with the previous results in Fig. 3.19. The new curves show significant increases in the velocity

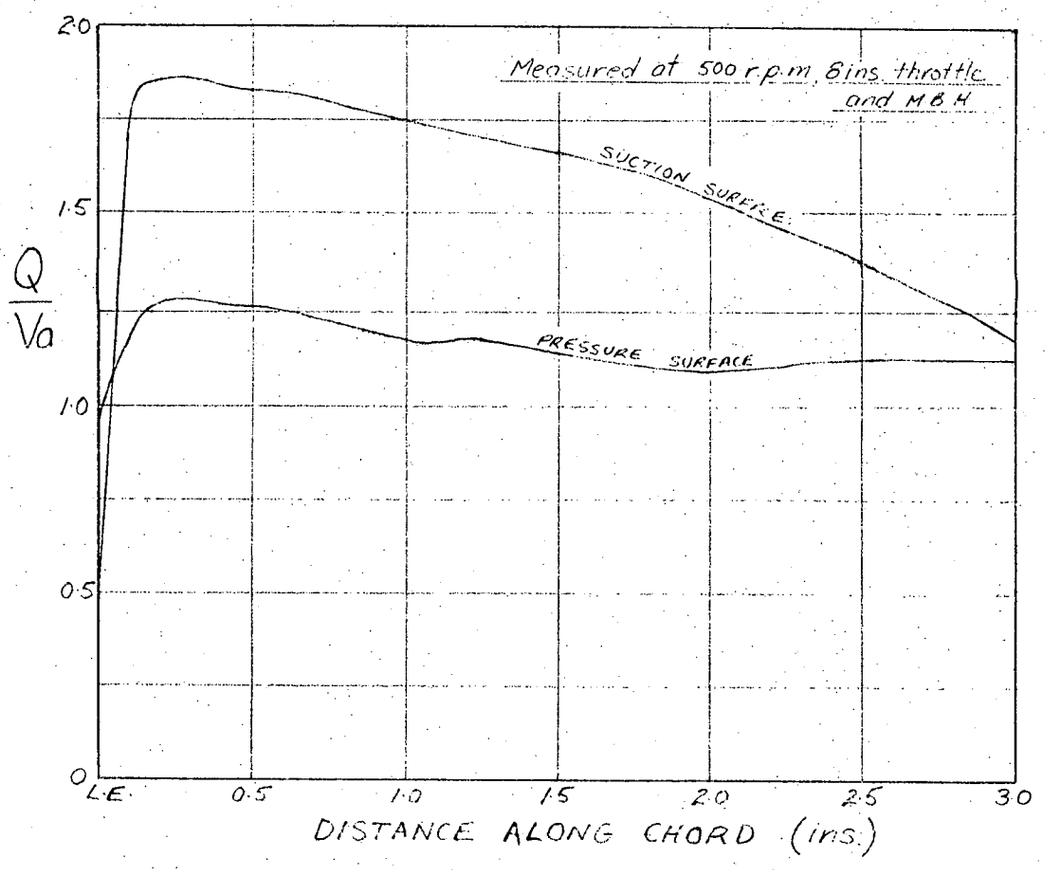

FIG. 3.17 MEASURED ROTOR BLADE SURFACE RELATIVE VELOCITY DISTRIBUTIONS

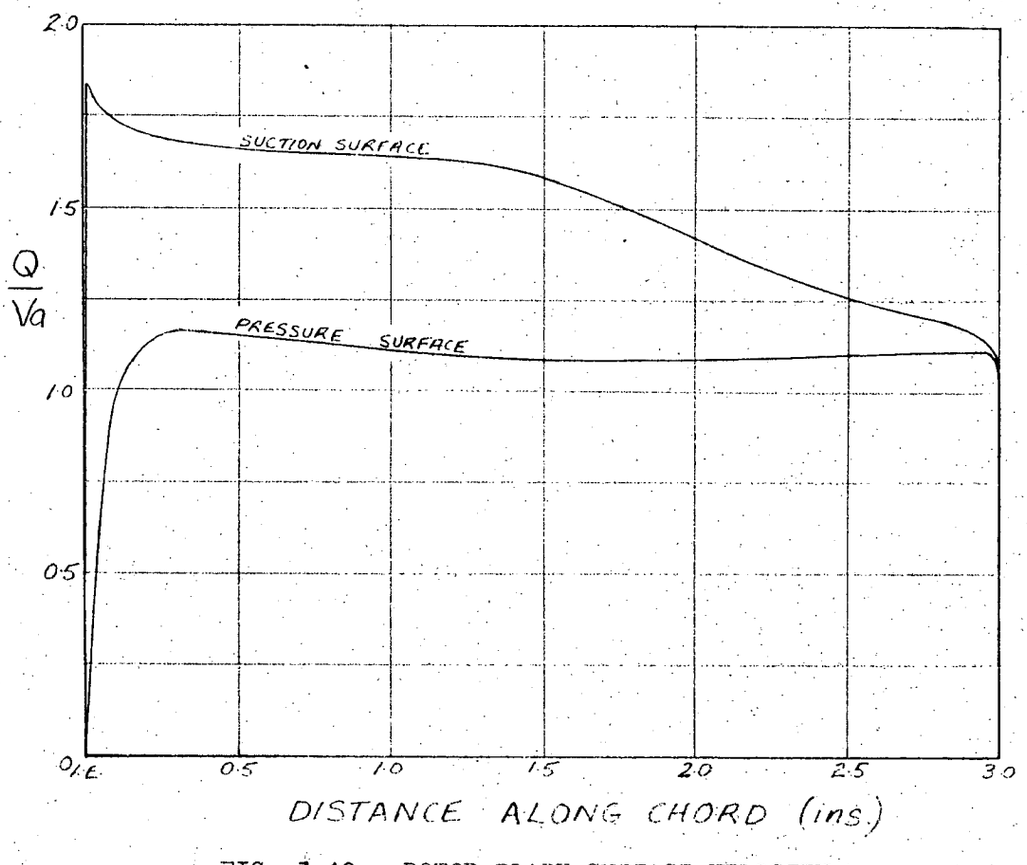

FIG. 3.18 ROTOR BLADE SURFACE VELOCITY DISTRIBUTIONS FROM THE MAPPING MODEL

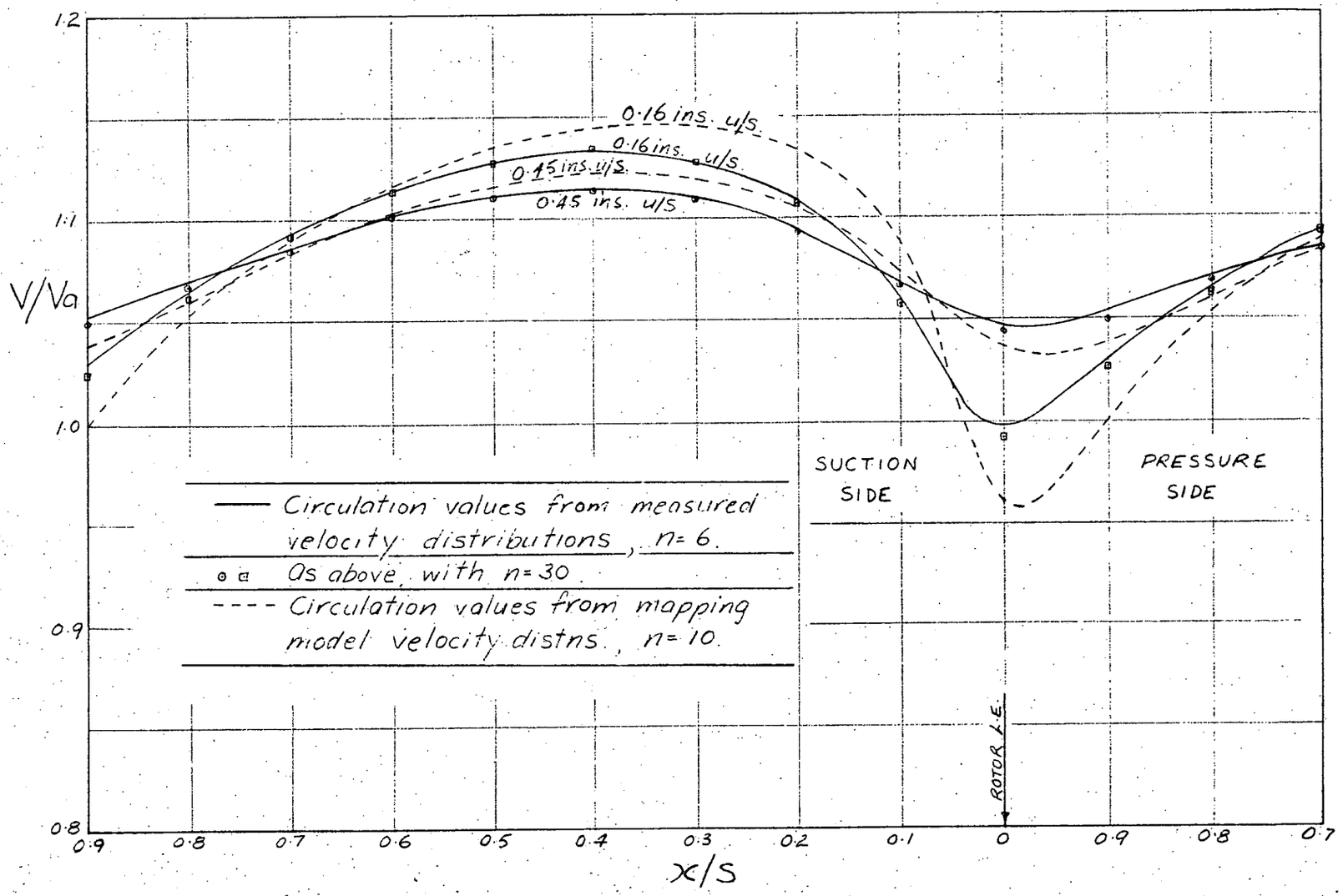

FIG. 3.19 VORTEX MODEL VELOCITY DISTRIBUTIONS

defect, but the values for both axial positions are still approximately 40% less than for the measured curves of Fig. 3.6.

3.6.3 Allowance for Blade Thickness

The above application of the thin aerofoil theory does not give nearly as good an approximation as expected, and is clearly an inadequate model of the real flow. It was therefore necessary to make some allowance for the profile thickness. This was achieved by arranging appropriate sources and sinks (negative sources) along the camber-line, using the method outlined in Csanady (Ref. 16).

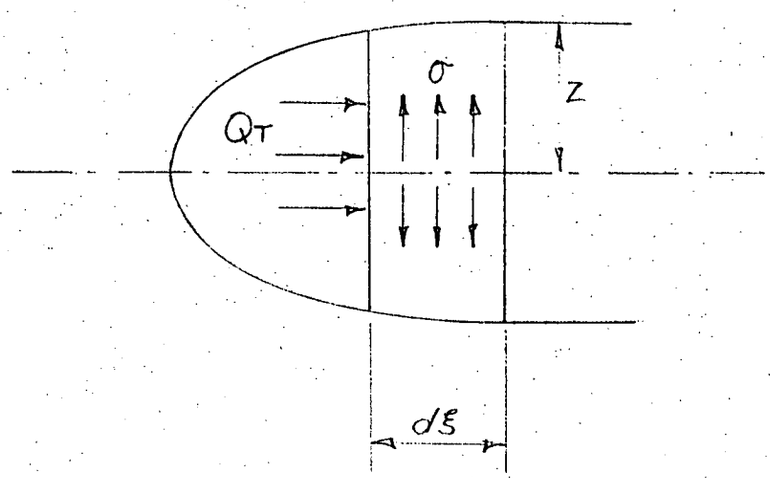

FIG. 3.20

Referring to Fig. 3.20 the relationship between the source distribution and the profile thickness 2z is obtained by considering the mass balance of a profile element:

Fluid entering element $Q_T 2z$

Fluid leaving element $Q_T(2z + 2\frac{dz}{d\xi} d\xi)$

Generated within element $\sigma(\xi)d\xi$

Where Q_T is the transport velocity and $\sigma(\xi)$ the source strength per unit length of chord.

A mass balance gives the relationship

$$\sigma(\xi) = 2Q_T \frac{dz}{d\xi} \qquad \text{.....(3.9)}$$

Clearly one important restriction on the thickness distribution is that the trailing edge must close, i.e.,

$$\int_{\xi=0}^{C} dz = 0 = \int_{0}^{C} \sigma(\xi) d\xi \qquad \text{.....(3.10)}$$

The computer programme was revised to include n sources representing the profile thickness, situated at the same points on the camber line as the vortices. The sources were considered as n single rows as for the Preston vortex analysis. The velocity potential for an infinite row of sources of strength S is

$$W = \frac{-S}{2\pi} \log \sin \left(\frac{\pi z}{s}\right) \qquad \text{.....(3.11)}$$

The velocity components are

$$u_S = \frac{S}{2s} \cdot \frac{\sin(2\pi x/s)}{\cosh(2\pi y/s) - \cos(2\pi x/s)} \qquad \text{.....(3.12)}$$

and $$v_S = \frac{S}{2h} \cdot \frac{\sinh(2\pi y/s)}{\cosh(2\pi y/s) - \cos(2\pi x/s)} \qquad \text{.....(3.13)}$$

The absolute velocity at any point (X,Y) then became

$$V = \sqrt{(\Sigma u_K + \Sigma u_S + Qu_m - U)^2 + (\Sigma v_K + \Sigma v_S - Va_m)^2} \qquad \text{.....(3.14)}$$

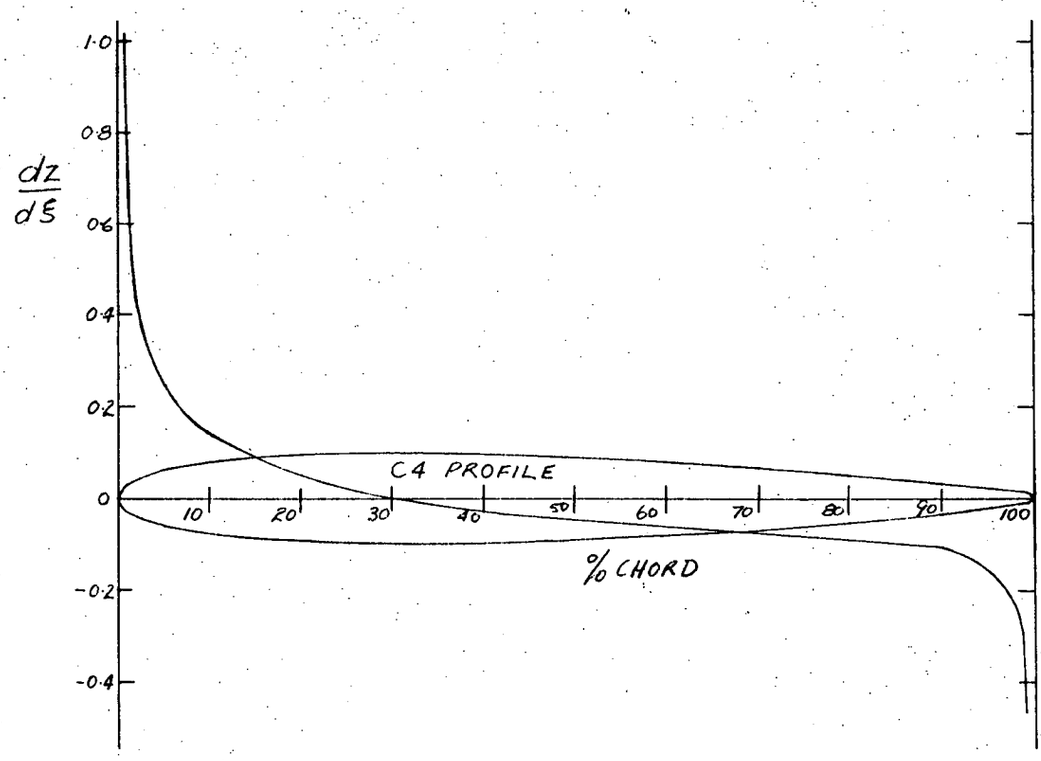

FIG. 3.21 BLADE THICKNESS GRADIENT

The values of the source strength S for each source were calculated using Eq. (3.9). It was considered reasonable to assume, as a first approximation, that the transport velocity Q_T was constant along the chord and equal to the vector mean velocity Q_m.

The thickness gradients $dz/d\xi$ were obtained by graphical differentiation from the C4 section base profile and are plotted in Fig. 3.21. Average values of $dz/d\xi$ for each of the n profile segments were determined from the curve. The average $dz/d\xi$ values for the circular parts of the section forming the leading and trailing edges were determined analytically. As it was difficult to accurately estimate the gradients near the trailing edge by the graphical method, the source strength for the n^{th} segment was chosen to satisfy the closed trailing edge condition of Eq. (3.10).

3.6.4 Comparison with Measurements

The revised thin aerofoil model was used to calculate the absolute velocity profiles for the axial positions 0.16 ins. and 0.45 ins. upstream of the rotor. The resulting curves - for n = 30 and with K values from the measured blade surface velocity distributions - are compared with the measured profiles in Fig. 3.22. The two sets of curves were superimposed by aligning the mean velocities (which differed by only 0.5%) and the peripheral positions of the velocity minima (the same for both axial positions in each case).

The agreement in shape and dimensions between the measured and calculated curves is even better than for the mapping model. (See Fig. 3.6). A comparison of velocity defects is shown in the table below.

TABLE 3.3

Measured and Calculated Velocity Defects $(\frac{Vmax-Vmin}{Va})$

POSITION UPSTREAM OF ROTOR (ins.)	MEASURED	VORTEX-SOURCE MODEL	MAPPING MODEL
0.16	0.356	0.336	0.334
0.45	0.150	0.140	0.143

As for the measured and mapping model velocity distributions, the velocity minima occur at the same peripheral position for both axial stations. However this position is 0.03s to the suction surface side of the rotor leading edge for the vortex-source model compared with a position very slightly to the pressure surface side for the mapping model. The vortex-source model curve gives slightly better general agreement with the measured profile, but it is difficult to guess which model represents the real situation regarding the position of the minima. It is interesting to note the shift in the position of the minima from the pressure surface side of the leading edge to the suction side with the addition of the thickness sources to the thin aerofoil model. (See Figs. 3.19 and 3.22).

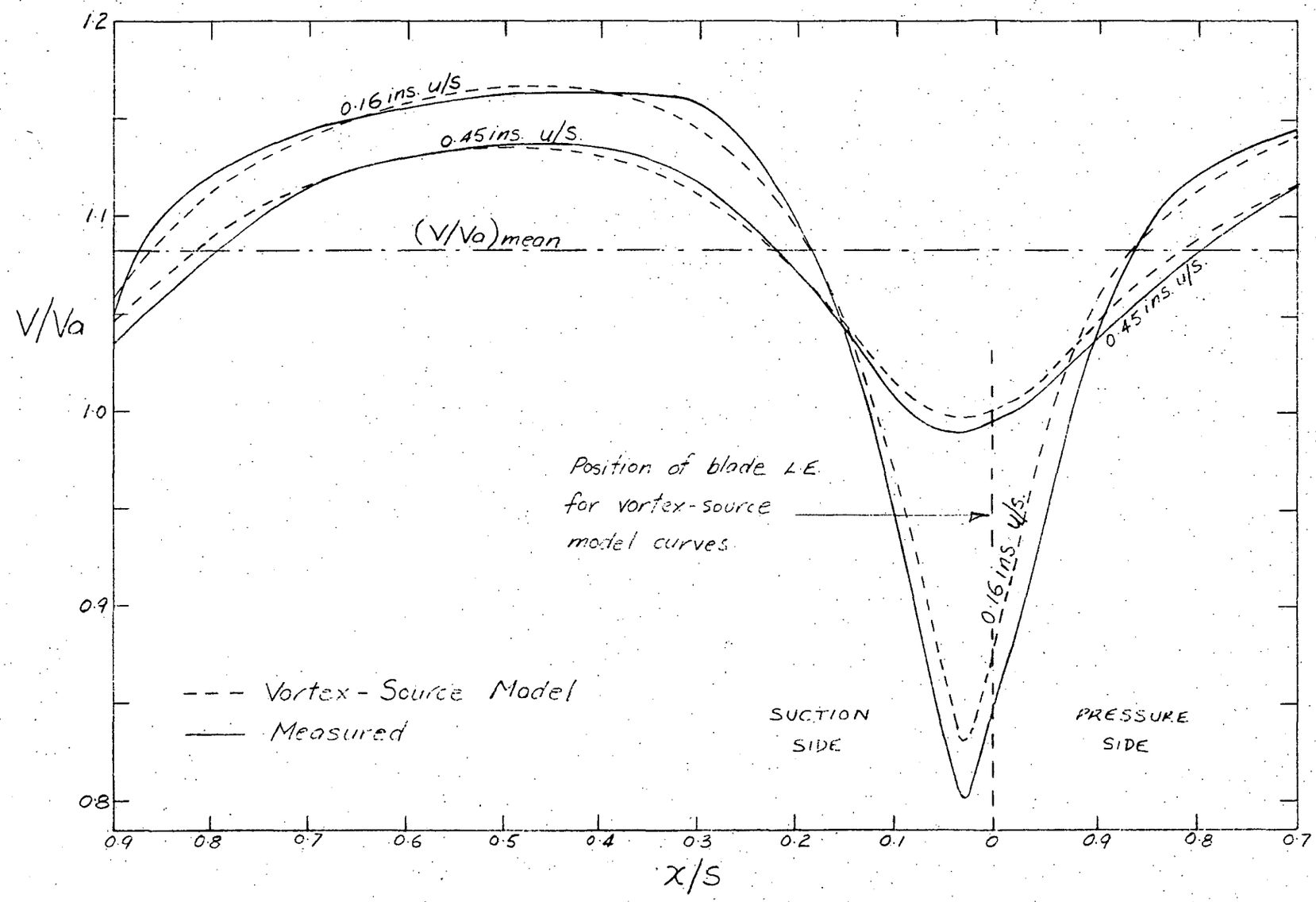

FIG. 3.22 COMPARISON OF VORTEX-SOURCE MODEL AND MEASURED PROFILES

3.6.5 Thickness Effect

The development of the vortex-source model has shown that the "potential flow" defect in velocity upstream of the rotor can be considered as consisting of two separable components - one due to a circulation effect and one to a blade thickness effect. The potential flow model, which is expected to closely approximate the real flow conditions, indicates that roughly 45% of the absolute velocity defect is due to the circulation effect and 55% to the thickness effect.

3.6.6 Advantages of Vortex-Source Model

The vortex-source model, as well as giving a slightly better fit to the measured results, is more versatile than the mapping model in that it can be easily extended to take into account the blade boundary layers and wakes and also three-dimensional effects. The mapping model is limited to the potential flow. The vortex-source model is basically simpler, and satisfactory results for design could be obtained using as few as six vortices (and sources) per blade.

The model, as developed above, conveniently used previously measured blade surface velocity distributions for determining the circulation values for each vortex. This data would not usually be available for design; a practical programme would therefore have to include the calculation of the velocity distributions for the chosen blading.

A model, such as the vortex-source model, in which each blade row can be accurately represented by a small number of discontinuities, would be particularly useful, as it could ultimately enable an entire (multi-stage) machine to be analysed on a computer.

The Wilkinson Model

An alternative method of allowing for the blade thickness using this type of vortex model would have been to replace each blade with two rows of vortices, one along each surface. This is the basis of the Wilkinson potential flow model (Ref. 18) and, as for the vortex-source model, is readily extended to include three dimensional and boundary layer and wake effects. This model is used to calculate potential flow velocity profiles for positions downstream of the stator in Chapter 5.

CHAPTER 4

UNSTEADY FLOW DOWNSTREAM OF THE ROTOR

4.1 Introduction

The hot wire anemometry techniques outlined above were also used to measure the time variation in absolute flow velocity at positions between the rotor and stator. In this region of the compressor the following unsteady flow effects are present:

(i) The "potential flow" variation in velocity due to the rotor movement (as for the measurements upstream of the rotor).

(ii) Unsteadiness due to the presence of rotor blade wakes.

(iii) Unsteadiness due to the I.G.V. wake. The guide vane wake is "chopped" into segments by the rotor blades, as shown in Fig. 1.1, creating an I.G.V. wake avenue.[1] As a result of this, the velocity component due to the I.G.V. wake at a fixed point downstream of the rotor is not constant, as for positions greater than half a chord's length upstream of the rotor,[2] but depends on the position of the rotor. The trend of the velocity defect curve of Fig. 3.13 suggests that the guide vane wake defect downstream of the rotor is likely to still be of the order of 5% to 7%.

(iv) There is also the possibility that effects (i) and (ii) may vary with the position of the rotor relative to the guide vane wake, even though this was not the case for the corresponding measurements upstream of the rotor.

At positions closer to the stator, the mean velocity will also be affected by the "potential flow" variation in velocity upstream of the stator blades. This has been measured by Lockhart (Ref. 19) and is found to be approximately the same as that upstream of the rotor. (This is to be expected as the relative flow geometries for the two rows are almost identical.) The velocity defect is negligible after a distance of about half a chord's length upstream of the blade row. With a rotor/stator spacing of little over a chord length, the effect of the stator on the flow pattern in the vicinity of the rotor blades will be negligible.

---

1. For the purposes of discussion the term "I.G.V. wake avenue" will be used to denote the envelope of the guide vane wake segments taking in all positions of the rotor.

2. Within half a chord's length upstream of the rotor T.E., the guide vane wake is unsteady because of the effect of the "potential flow" variation due to the rotor movement. As discussed in Section 3.5, this is possibly manifest as an oscillatory variation in the wake position.

4.2 Velocity-Time Profiles

The variation in absolute velocity with time at positions 0.1 ins. (3.3%C), 0.2 ins. (6.7%C), 0.58 ins. (19%C) and 1.58 ins. (53%C) downstream of the rotor trailing edge (T.E.), as recorded by a hot wire situated clear of the I.G.V. wake avenue, are shown in the photographs of Fig. 4.1. The measurements were again taken for mean flow conditions corresponding to the velocity diagram of Fig. 3.3.

N.B. a. Approximately 60 consecutive traces are shown on each photograph.

b. Axial positions are quoted relative to the rotor T.E.

c. Each photograph shows the variation in velocity over a time of approximately 1.5τ (τ = time for rotor to travel a distance equal to one blade spacing).

d. The instant of triggering was not the same in each case - the delay time between the photocell circuit pulse and the instant of triggering on the oscilloscope was adjusted to give a display of two complete rotor wake profiles on each photograph.

e. The left hand side of the wake profile corresponds to the pressure surface side of the rotor blade.

f. As for the photographs of Fig. 3.2, the exact position of the rotor blade relative to the hot wire for each point on the trace was not known.

g. In each case the I.G.V. row was moved to locate the hot wire at approximately the same position relative to (and outside) the edge of the guide vane wake avenue.

4.3 Analysis of Photographs

Each set of traces shows the combined effect of (i), the "potential flow" variation in velocity due to blade circulation and thickness effects, and (ii), the velocity defect of particles forming the viscous rotor blade wakes. A further complication is that the velocity at each instant of time on a trace corresponds to the rotor blade being in a different position relative to the I.G.V. wake. The general spread of the traces on each photograph is due to the random fluctuations in the mean flow conditions at the test point. (These are caused by general flow unsteadiness in the room and also by unavoidable variations in the power supply.) Within the rotor wake region, however, there are much greater differences between individual traces due, of course, to the higher turbulence level within the wake.

In order to estimate approximately the respective contributions of effects (i) and (ii) to the profiles of Fig. 4.1, the photographs were compared with potential flow absolute velocity distributions calculated

a. 0.1 INS. (3.3%C) D/S

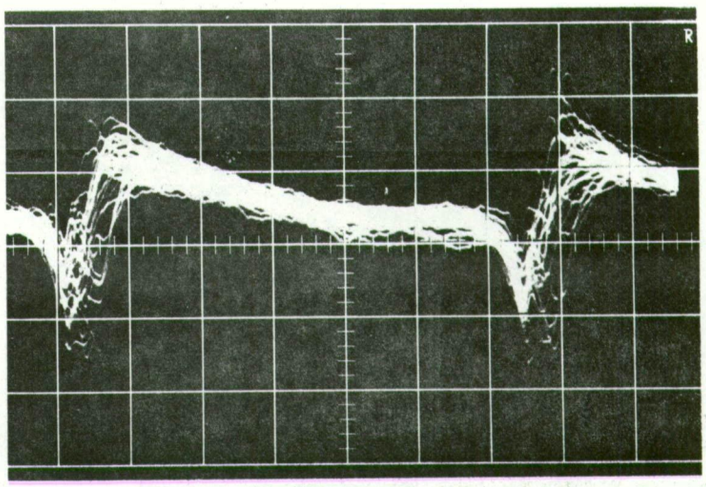

b. 0.2 INS. (6.7%C) D/S

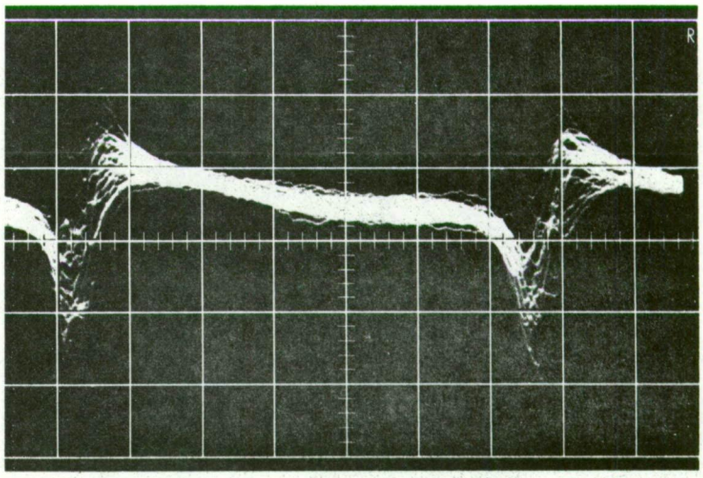

c. 0.58 INS. (19%C) D/S

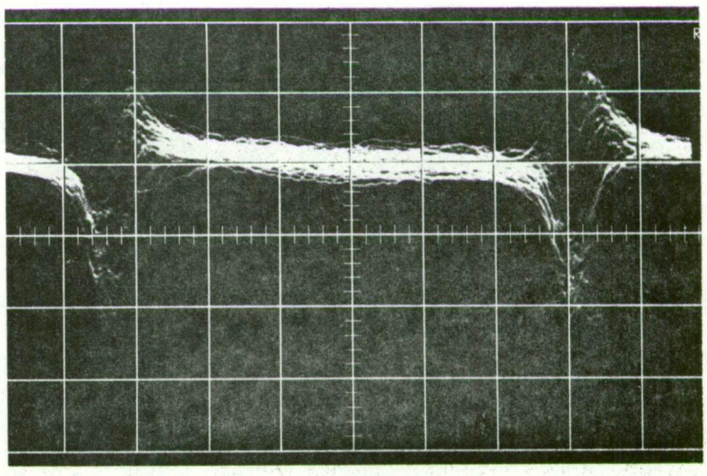

d. 1.58 INS. (53%C) D/S

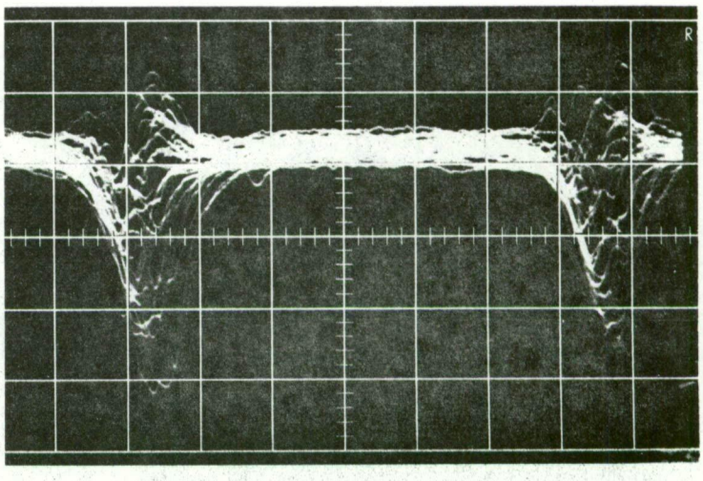

FIG. 4.1
VELOCITY-TIME PROFILES
DOWNSTREAM OF THE ROTOR

Vert. Scale: 5.45 fps/div.

Horl. Scale: 0.5 msec/div.

Mean Velocity = 81.5 fps.

for positions downstream of the rotor from the vortex-source model developed in Section 3.6. In making the comparisons, the following points must be noted:

(1) As in the comparison of the measured and calculated curves for positions upstream of the rotor, any effects due to the I.G.V. wake are being neglected, so that the velocity-time profiles can be considered as instantaneous plots of absolute velocity against peripheral position.

(2) The vorticity in the rotor wake affects, at least to some extent, the flow at all points in the vicinity of the rotor blade (see Ref. 6). The effect is probably most significant near the wake itself. This means that the "actual" potential flow velocity distribution downstream of the rotor for wake conditions is likely to be different to that which would exist were there no wake present. The flow models of course, neglect the effects of blade boundary layers and wakes. The problem of determining the potential flow velocity distribution for the real flow (wake) conditions is discussed further in Section 5.6.

(3) As the position of the rotor T.E. on the photographs is not known, it is difficult to know how to align the measured and calculated curves. The potential flow minima need not correspond to the positions of maximum rotor wake defect. A more detailed consideration of potential flow model velocity distributions in Section 4.5 shows that, in fact, the positions of the two minima approach each other only near the rotor T.E.

A comparison between a mean velocity profile reproduced from a photograph and a curve calculated from the vortex-source model for a position 0.20 ins. downstream of the rotor is shown in Fig. 4.2. The relative peripheral displacement of the two minima was obtained from the loci of the measured and calculated minima plotted in Fig. 4.11 and is likely to be a reasonable approximation of the real situation. (Fig. 4.11 is discussed fully in Section 4.5). The curves were aligned in the vertical direction to give best agreement in the region midway between the positions of maximum rotor wake defect - where the measured profile might be expected to correspond to the "potential flow" velocity distribution. With the curves aligned in this way, the measured absolute velocity value at a common point on the curves was 3% higher than the calculated value. As mentioned previously, this can be accounted for by a small difference in the actual and assumed axial velocities for the measured profiles.

There is excellent agreement between the two curves for the section, 40% of the blade spacing in extent, outside the blade wake regions. It can therefore probably be expected that the vector difference

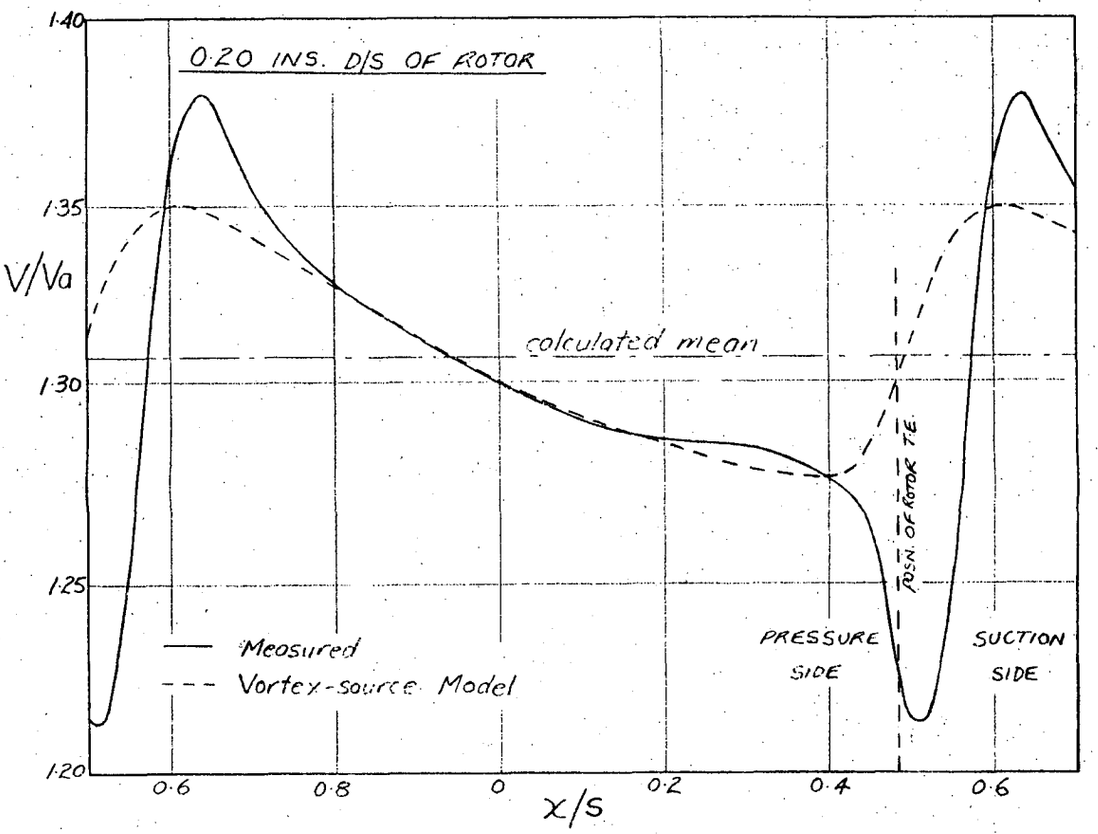

FIG. 4.2 COMPARISON BETWEEN MEASURED AND VORTEX-SOURCE MODEL VELOCITY PROFILES

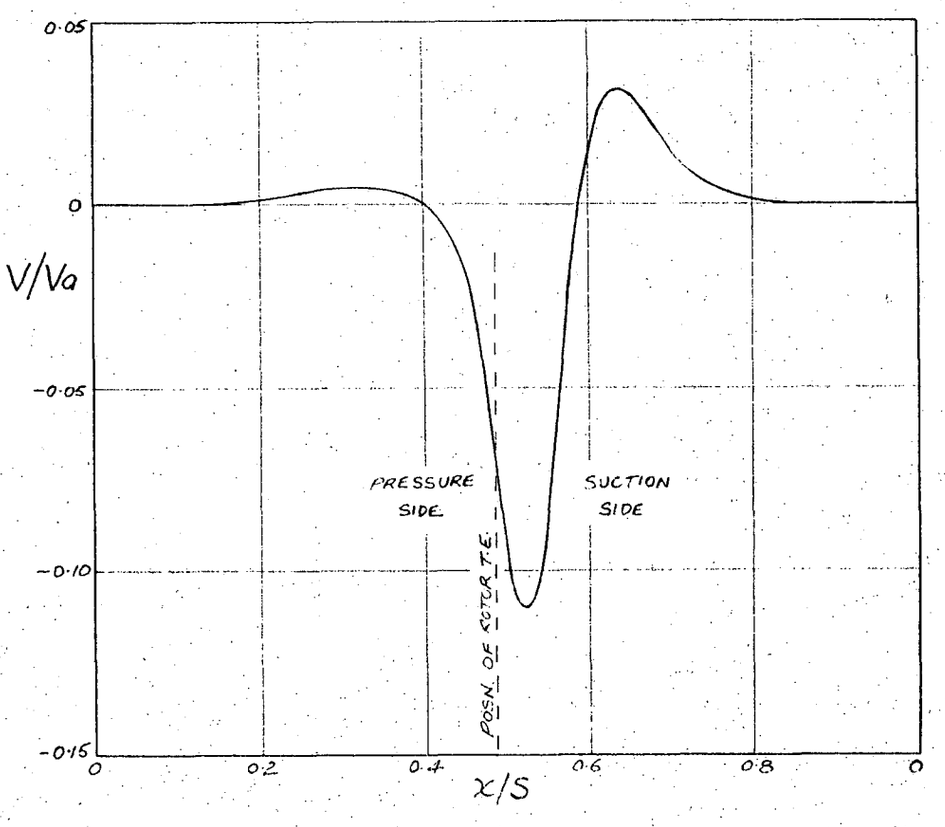

FIG. 4.3 ALGEBRAIC DIFFERENCE OF THE CURVES OF FIG. 4.2

between the measured and potential flow curves represents, to a good approximation, the contribution of the rotor wake to the variation of absolute velocity with time (and distance) downstream of the rotor. As the absolute flow angles corresponding to points on the measured velocity distribution were not known, it was not possible to construct a "true" rotor wake velocity profile. Fig. 4.3, however, shows a wake profile constructed by taking algebraic velocity differences between the two curves of Fig. 4.2. It is considered that the differences in angle between corresponding points on the two curves are at least small enough to justify the use of Fig. 4.3 in interpreting the velocity profiles on the photographs.

Figs. 4.2 and 4.3 suggest that the lack of symmetry in the wake profile and, in particular, the high velocity peak on the suction surface side might be due mainly to the potential flow circulation and thickness effects and not to the actual viscous wake profile itself. Fig. 4.3 indicates that the velocity defect curve due to the wake itself could be approximately symmetrical, apart from a small velocity peak on the suction side. Any peaks which occur in the absolute velocity profile may not be present in the relative velocity profile and could simply be the result of an angle effect in the vector addition. The relationship between the absolute and relative rotor wake velocity profiles is considered in more detail in Chapter 5.

From the photographs it is observed that the velocity outside the wake regions becomes progressively more uniform and the velocity peak on the suction side, progressively smaller, with increasing distance downstream of the rotor. In the light of the above discussion, both these effects are readily explained by the fall off in the "potential flow" velocity defect. For the position 1.58 ins. (53%C) downstream, where the measured circulation and thickness effects appear to be negligible, the vortex-source model gives a velocity defect, V/Va, of 0.005 - or about 0.3 f.p.s.

4.3.1 Wake Defect

The absolute velocity defect (Vmax-Vmin) is approximately the same for all four axial positions and is only of the order of 10 f.p.s. - or 12% of $\bar{V}$. This at first seems unusual in the light of the I.G.V. wake velocity defect curve of Fig. 3.13 which shows, for example, a defect of 56% for a position 0.20 ins. downstream of the blade row, with a rapid fall off in defect for positions further downstream. (Figs. 4.2 and 4.3 indicate that the actual velocity defect due to the wake itself for the positions close to the rotor T.E. is probably even less than the Vmax-Vmin value of about 10 f.p.s.)

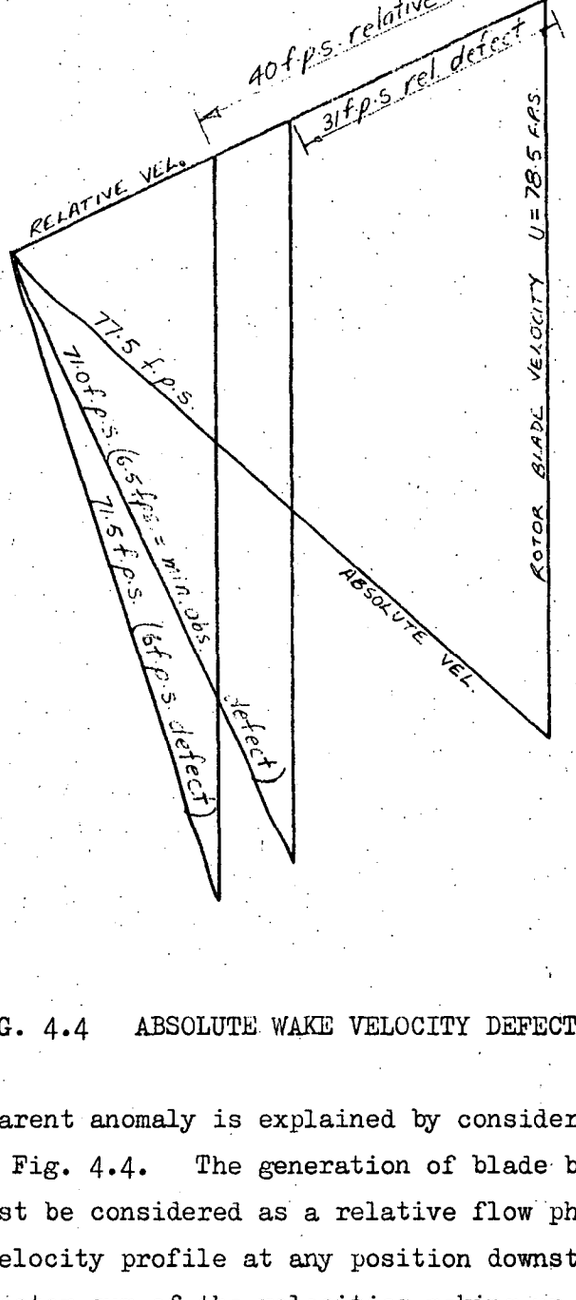

FIG. 4.4 ABSOLUTE WAKE VELOCITY DEFECT

The apparent anomaly is explained by considering the velocity diagram of Fig. 4.4. The generation of blade boundary layers and wakes must be considered as a relative flow phenomenon - the absolute wake velocity profile at any position downstream of a moving row is the vector sum of the velocities making up the relative wake profile and the row velocity U. The figure shows the graphical determination of absolute velocity defects corresponding to particular relative flow defects neglecting, for the purposes of the argument, any changes in the relative flow angle in the wake. It is demonstrated that large changes in the relative flow velocity correspond to comparatively small changes in the absolute velocity. For example, a relative defect of 40 f.p.s. gives a change in the absolute velocity of only 6 f.p.s. (This is of the same order as the measured defects.) An explanation of the constancy of the measured velocity defects is also provided. According to Fig. 4.4, the absolute velocity defect does not continue to increase with increasing relative velocity defect. Instead the geometries of the velocity triangles are such that it

increases to a maximum of 6.5 f.p.s. for a relative velocity defect of 31.0 f.p.s., but thereafter decreases with further increase in the relative defect.

As there are likely to be significant relative flow angle changes in the wake, the constructions of Fig. 4.4 are certainly not realistic and can serve only as a rough guide in the general interpretation of the photographs.

4.3.2 Instantaneous Locus of Absolute Velocity Minima

As mentioned above, the instant of triggering for each set of traces in the photographs of Fig. 4.1 was adjusted to give a display of two complete rotor wake profiles. A repeat series of measurements was taken in which the instant of triggering was kept constant, so that the change in the peripheral position of the wake velocity minimum with axial position could be determined. The observed positions of the minima are plotted on a distance scale in Fig. 4.5. The figure represents the locus at any instant in time of the positions of the fluid particles having the maximum absolute wake velocity defects for each axial position, for a theoretical situation in which the I.G.V. wake is not present. Under these conditions the orientation of the locus is the same relative to the rotor for all instants of time. The band of particles representing a particular rotor blade wake moves around with the rotor blade at velocity U as the separate particles themselves move off downstream in the direction of the absolute flow.

The positions of the wake minima relative to the trailing edge could not be determined experimentally, but can be estimated approximately by considering the relationship between the loci of the absolute and relative flow minima. Far downstream, the rotor wake defect and the variation in flow angle across the wake are small. Under these conditions, the absolute and relative flow velocity minima will co-incide. Hence the locus of the absolute velocity minima in Fig. 4.5 can be expected to approach the relative locus with increasing distance from the T.E.

The centreline of the wake in the relative flow should correspond closely to the relative stagnation streamline. This should approximate to a straight line from the T.E. in the mean relative flow direction. It is seen that the locus of minimum absolute velocity is actually equivalent to such a line after a distance of about 0.3 ins. (10%C) downstream of the T.E. Therefore the approximate position of the rotor blade T.E. in Fig. 4.5 is found by extrapolating the straight line section of the locus to zero as shown.

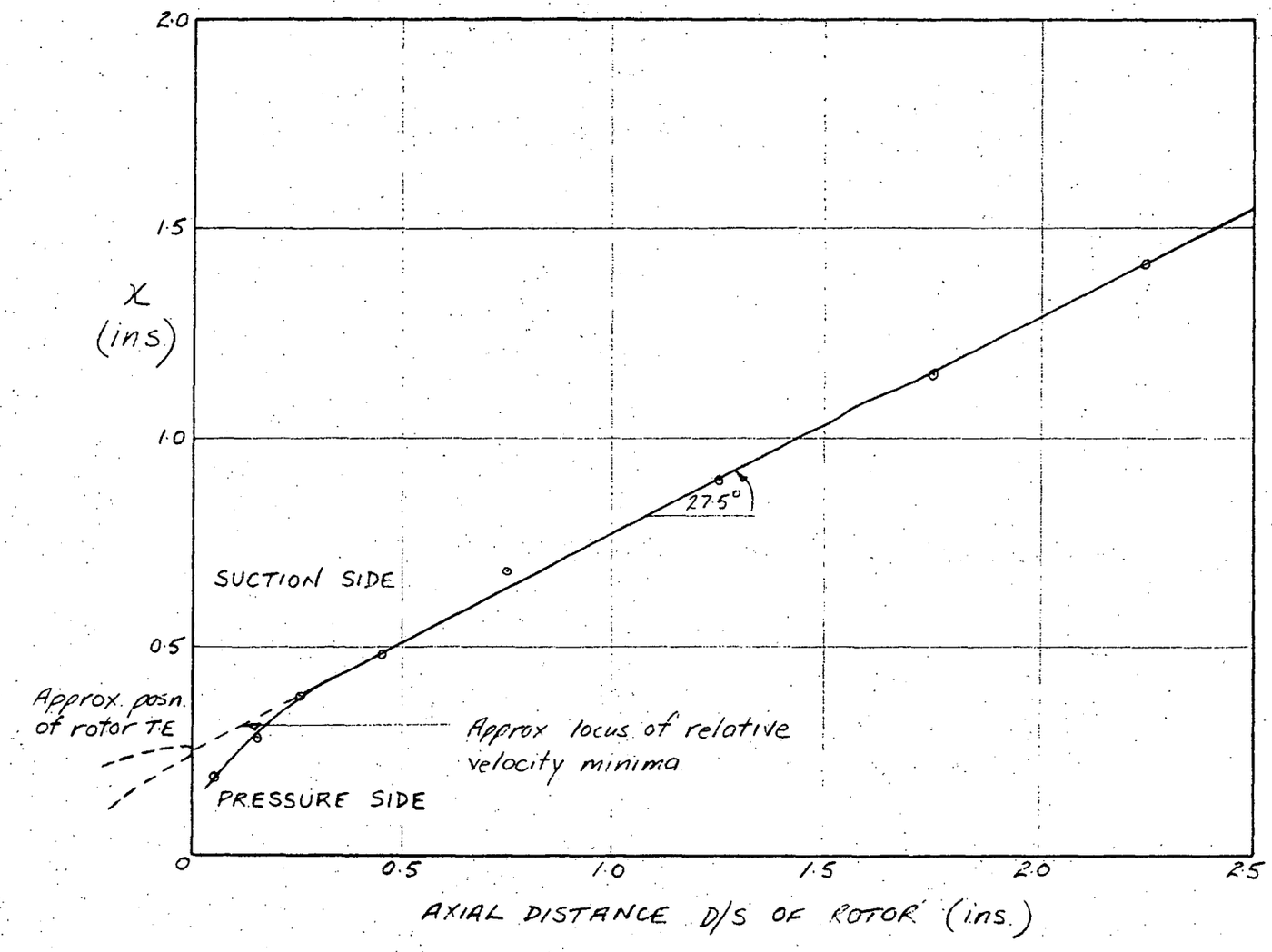

FIG. 4.5 LOCUS OF ABSOLUTE VELOCITY MINIMA

The observed departure of the line of minimum absolute velocity from the relative flow centreline in the region near the T.E. is a consequence of the large relative flow velocity defects and variations in flow angle. In the preceding section it has been shown that, when the relative velocity defect is large, a decrease in the relative flow velocity can actually correspond to an increase in the absolute flow velocity. Clearly, under these conditions and when there are large flow angle variations across the wake, the absolute and relative velocity minima will not co-incide. For example, close to the T.E. at the rear stagnation point, the relative velocity is zero but the absolute velocity is equal to U (78.5 f.p.s.) and this would not be the minimum for this axial position.

4.4 Traverse through I.G.V. Wake

The eight photographs of Fig. 4.6 depict a traverse through the I.G.V. wake avenue at an axial position 0.20 ins. (6.7%C) downstream of the rotor. As for the traverse upstream of the rotor, this was effected by setting the I.G.V. rows at different positions relative to the fixed probe. The instant of triggering is the same for each photograph.

4.4.1 Interpretation of Photographs

Photograph 4.6d shows traces detected by a hot wire situated approximately at the centre of the wake avenue - the general velocity-time profile due to the "potential flow" and rotor wake effects is almost completely masked by the I.G.V. wake turbulence.

Photographs 4.6b and 4.6f correspond roughly to the suction and pressure side edges of the I.G.V. wake avenue respectively. As was noted in the photographs of Fig. 3.10 for the wake traverse upstream of the rotor, the turbulent fluctuations due to the guide vane wake are only present over part of each trace. In Section 3.5, it was suggested that the phenomenon was due to an oscillation in the position of the I.G.V. wake as the rotor moved past; under these conditions a hot wire situated near the edge of the wake could effectively be inside the wake for part of the time and outside it the rest. This is even more likely to be the case downstream of the rotor. As well as the effect of the general variation in flow conditions with changing rotor position, a hot wire situated near the edge of the I.G.V. wake avenue probably detects some discontinuity in the position of the wake due to the "change-over" from one wake segment to the next at the time of passing of the rotor wake. The reasons for expecting this possible "change-over" effect are best seen by considering the diagrammatic representation of the blade wake segments in Fig. 1.1.

a. 0.42s TO SUCTION SIDE OF I.G.V. WAKE AVENUE CENTRE.

Mean Velocity = 79.8 fps.

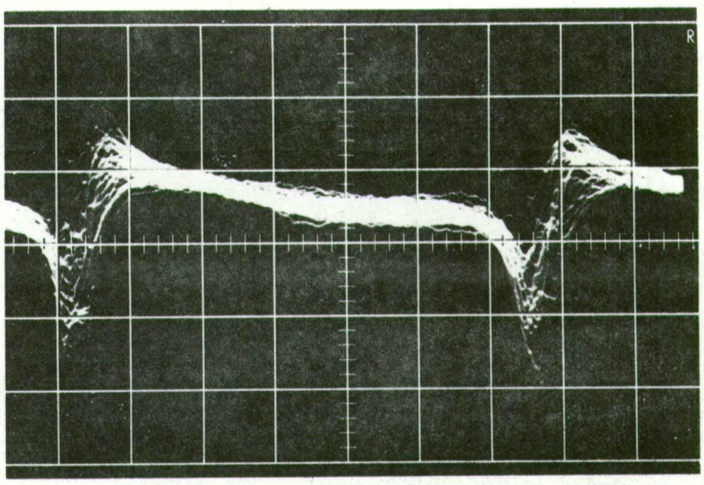

b. 0.22s TO SUCTION SIDE OF I.G.V. WAKE AVENUE CENTRE.

Mean Velocity = 80.3 fps.

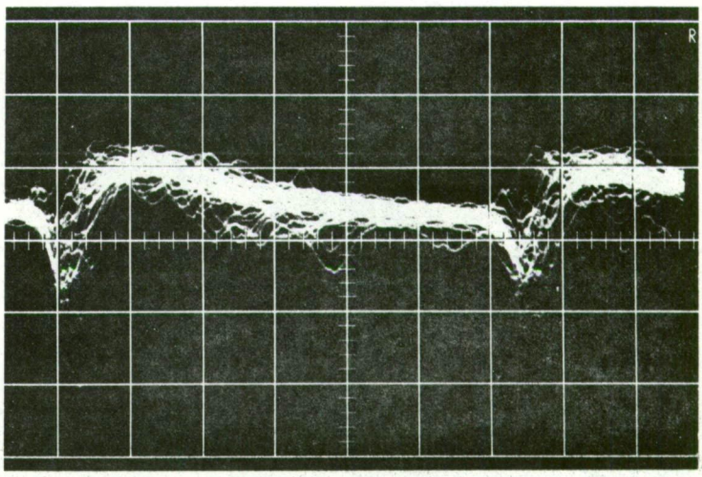

c. 0.08s TO SUCTION SIDE OF I.G.V. WAKE AVENUE CENTRE.

Mean Velocity = 79.8 fps.

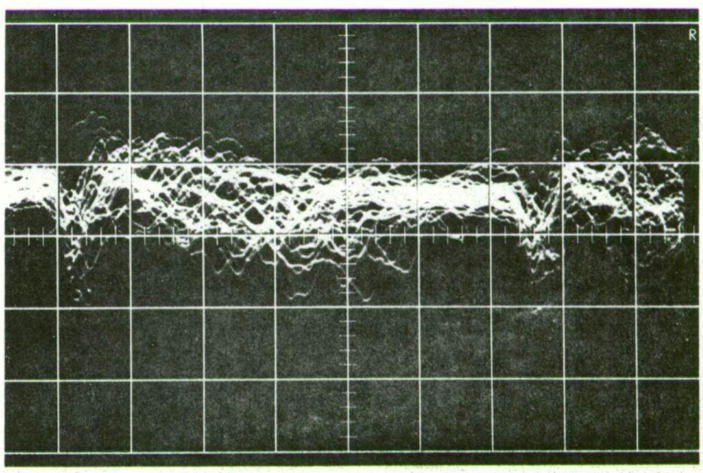

d. PROBE SITUATED AT CENTRE OF I.G.V. WAKE AVENUE.

Mean Velocity = 79.8 fps.

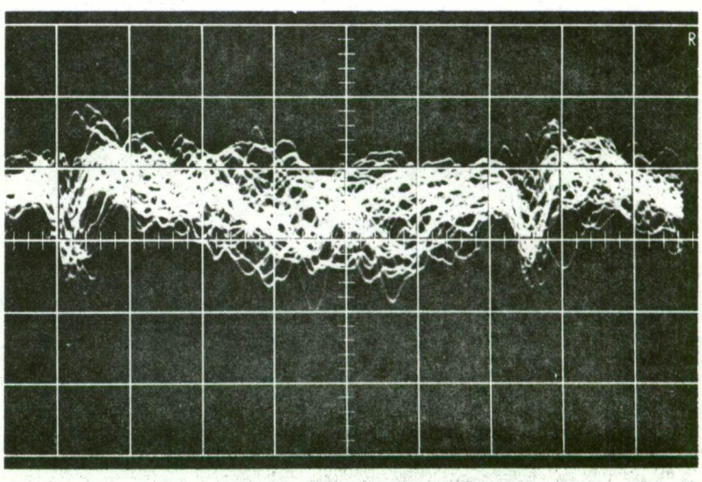

FIG. 4.6 (Cont. next page) TRAVERSE THROUGH I.G.V. WAKE AVENUE 0.2 INS. (6.7%C) DOWNSTREAM OF ROTOR T.E.

Vert. Scale: 5.45 fps/div.

Horl. Scale: 0.5 msec/div.

s = blade spacing (I.G.V.)

e. 0.15s TO PRESSURE SIDE OF I.G.V. WAKE AVENUE CENTRE.

Mean Velocity = 79.8 fps.

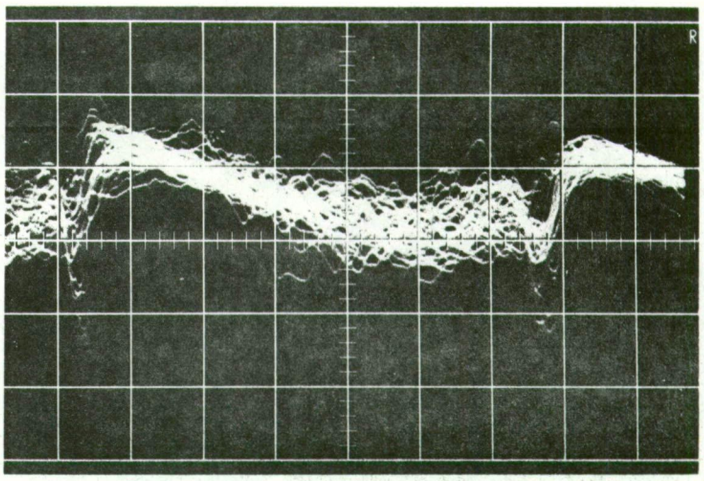

f. 0.35s TO PRESSURE SIDE OF I.G.V. WAKE AVENUE CENTRE.

Mean Velocity = 81.0 fps.

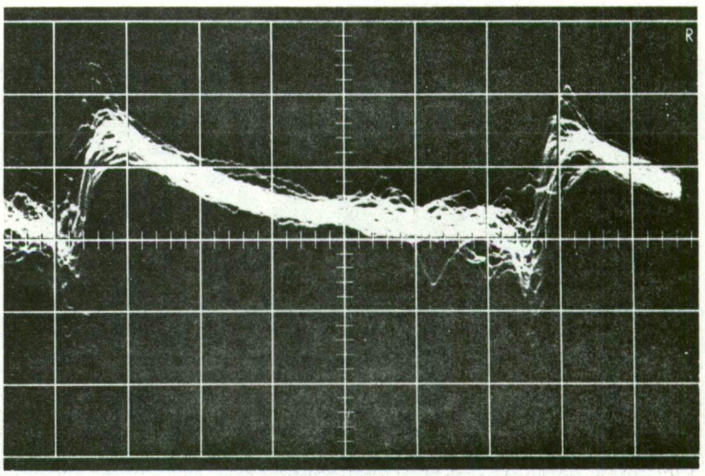

g. 0.49s TO PRESSURE SIDE OF I.G.V. WAKE AVENUE CENTRE.

Mean velocity = 80.6 fps.

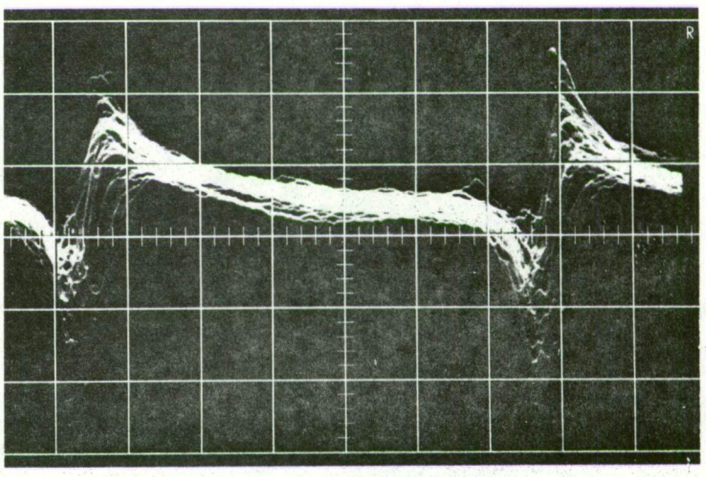

h. 0.66s TO PRESSURE SIDE OF I.G.V. WAKE AVENUE CENTRE.

Mean Velocity = 81.0 fps.

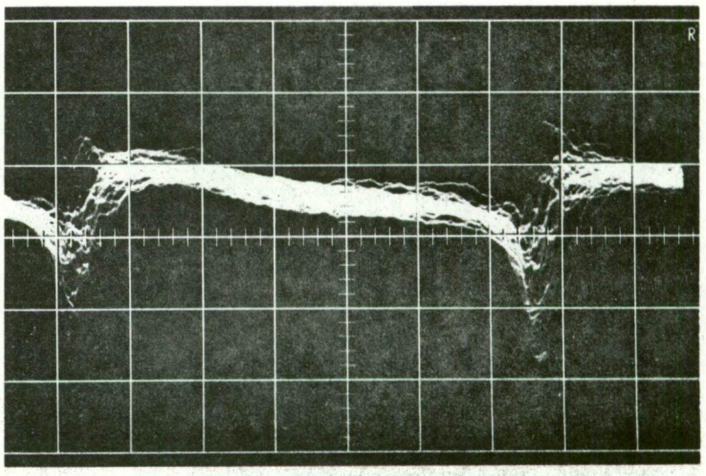

FIG. 4.6 (cont.)

In photograph 4.6b, corresponding to the suction side of the I.G.V. wake avenue, the guide vane wake turbulence is evident only in the region near the suction side of the rotor wake profile and in photograph 4.6f (pressure side of I.G.V. wake avenue) only near the pressure side of the rotor wake profile. This is consistent with a movement of the whole I.G.V. wake segment in the pressure to suction direction at the time when the rotor wake is passing over the wire; during this period a hot wire on the suction side of the I.G.V. wake avenue moves further into the guide vane wake, whereas a hot wire on the pressure side tends to move out of the wake. (This is also consistent with the expected "change-over" effect indicated in Fig. 1.1). It can therefore be said that photograph 4.6b, for example, only corresponds to the edge of the I.G.V. wake segment for a particular position of the rotor relative to the hot wire - in this case the wire is situated at the suction side edge of the wake segment only at the time when it is approximately midway between two rotor wake profiles.

4.4.2 Effect of the I.G.V. Wake on the Flow Downstream of the Rotor

Unlike the I.G.V. wake traverse upstream of the rotor, there are significant changes in the general velocity time curve due to the "potential flow" and rotor wake effects for different positions of the hot wire relative to the I.G.V. row. This was the case for all four axial locations examined. The change is most apparent in the variation of the magnitude of the velocity defect, Vmax-Vmin, in the rotor wake regions of the profile. It is difficult to determine from the photograph whether this is due mainly to a change in the "potential flow" component (i) or mainly to a change in the rotor wake component (ii) - or equally to both. The conclusions drawn from the guide vane wake traverse upstream of the rotor (Section 3.5) would suggest that there is not likely to be any change in the "potential flow" variation in velocity either upstream or downstream of the rotor. However any change in the rotor wake due to the effect of the I.G.V. wake could cause a corresponding change in the potential flow, as discussed in Section 4.3(2).

The most obvious change in the velocity profile with changing I.G.V. wake position is seen in photographs 4.6g and 4.6h, both of which were recorded with the hot wire itself situated clear of the guide vane wake. The average value of Vmax-Vmin changes from 10.9 f.p.s. to 6.5 f.p.s. (approximately). It is interesting that most of this change is actually due to a considerable drop in the magnitude of the suction side velocity peak. However, it cannot be concluded from this that the changes in the velocity defect are due mainly to variations in the "potential flow" components of the curves.

There also appears to be a significant fall off in the velocity defect of the mean profile within the I.G.V. wake avenue. This is also indicated by the measured RMS values of the velocity fluctuations (V_{RMS}) corresponding to each photograph of Fig. 4.6. Fig. 4.7 shows a plot of V_{RMS} against peripheral position relative to the I.G.V. wake avenue.

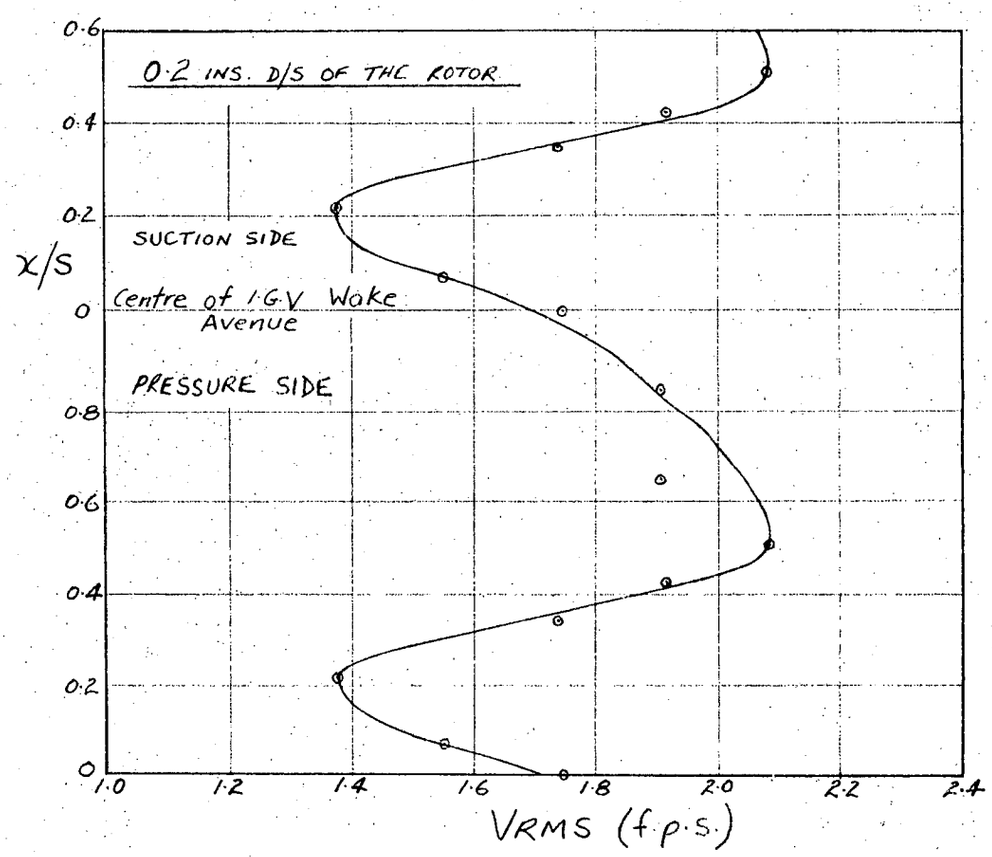

FIG. 4.7 VARIATION OF V_{RMS} ACROSS I.G.V. WAKE AVENUE

Each V_{RMS} value can be considered as the sum of two components - one representing the average time variation in velocity downstream of the rotor due to the "potential flow" and rotor wake effects and one representing the guide vane wake turbulence. If there were no change in the average profile due to the "potential flow" and rotor wake effects with position relative to the I.G.V. wake, then clearly the value of V_{RMS} would be determined by the I.G.V. wake turbulence level and would be expected to reach a maximum at the centre of the wake avenue. The curve of Fig. 4.7 shows that this is certainly not the case. For the position 0.20 ins. downstream of the rotor, the maximum V_{RMS} actually occurs midway between successive I.G.V. wake avenue centres, and the wake avenue centre itself is closer to a minimum V_{RMS} value. Hence it is apparent that, although the component

due to guide vane wake turbulence is greatest at the wake avenue centre, the velocity variation due to the "potential flow" and rotor wake effects has fallen off giving a relatively low overall value of V_{RMS}.

Owing to the large velocity fluctuations in the rotor wake regions of the traces (due to both rotor wake and guide vane wake turbulence) it was not possible to determine conclusively whether there was any shift in the position of maximum rotor wake defect with changing I.G.V. wake position.

Discussion

As explained in Section 3.5, points corresponding to the same instant of time (and position of the rotor relative to the hot wire) on each photograph of the traverse correspond to different positions of the rotor relative to the guide vane wake. Any changes in the average velocity-time profile could therefore be the result of variations in the flow pattern around a rotor blade with changing position relative to the I.G.V. wake. Although there was no apparent variation in the "potential flow" velocity distribution upstream of the rotor with rotor position relative to the guide vane wake, this need not be the case downstream. For example, changes in the position of the rotor blade rear stagnation point due to the I.G.V. wake, may noticeably alter the flow downstream of the rotor but not significantly affect the flow upstream. Some justification for expecting this to be the case is given in the next section (4.5). It is shown that, although the mapping and vortex-source potential flow models give remarkably similar predictions of the flow upstream of the rotor, they do not agree nearly as well at positions downstream of the rotor; this is attributed to the inherent difference between the models in conditions at the blade trailing edge.

Even if the I.G.V. wake does not directly affect the "potential flow" downstream of the rotor, it could well affect the generation of the rotor wake. In this case, the "potential flow" could also be indirectly affected as flow conditions downstream of the rotor are probably influenced considerably by the vorticity in the rotor wake, as mentioned in Section 4.3.

Alternatively, the changes in the velocity profile could be due to a local guide vane wake effect at the measuring point. This immediately raises the question, as yet unanswerable, as to what happens when two wakes interact. (Many of the fluid particles are obviously common to both the rotor and I.G.V. wakes.) The different average velocity defects on the photographs could be accounted for by changes in the average relative (and absolute) flow angle across the I.G.V. wake avenue. This would allow the same relative velocity defect to correspond to varying absolute velocity defects. An approximate calculation based on the velocity diagram of Fig.

3.3 and a relative rotor wake defect of 50% (cf. Fig. 3.13) showed that the observed defect changes could be attributed to relative flow angle variations of less than 10 deg. As the wake flow angle distribution could not be measured (owing to the very small spatial discrimination required and the fluctuations in velocity), this possible explanation of the variation in the velocity profiles could not be investigated further.

4.5 Potential Flow Velocity Distribution

The presence of the rotor blade wakes made it impossible to measure the "potential flow" variation in absolute velocity with time at axial stations downstream of the rotor in the same way as was practicable upstream. As the two flow models introduced in Chapter 3 gave good agreement with the "potential flow" velocity distributions upstream of the rotor, it was likely that they would also closely approximate the "potential flow" component of the velocity variation downstream. In Section 4.3, curves calculated from the vortex-source model were used to estimate the respective contributions of the "potential flow" effects and the rotor wakes to the measured velocity profiles downstream of the rotor.

4.5.1 Comparison of Models

Figs. 4.8 and 4.9 show potential flow absolute velocity distributions at axial positions 0.20 ins. (6.7%C) and 0.55 ins. (18.3%C) downstream of the rotor calculated from:

a. the thick aerofoil mapping model
b. the vortex-source model
c. the thin aerofoil model (vortices only).

The mapping and vortex-source model curves for each axial position are essentially the same in shape but differ to some extent in velocity defect as shown in the following table.

TABLE 4.1

Comparison of Potential Flow Velocity Defects

POSITION D/S OF ROTOR (ins.)	$\frac{V_{max}-V_{min}}{V_a}$ (MAPPING)	$\frac{V_{max}-V_{min}}{V_a}$ (VORTEX-SOURCE)	% DIFFERENCE (w.r.t. average)
0.20	0.064	0.071	10
0.55	0.027	0.031	14

It was interesting that the differences in defect were as large as these, considering the excellent agreement between the two models upstream of the rotor. (See Table 3.3). The poorer agreement downstream of the rotor can probably be ascribed to differences between the two models in flow conditions

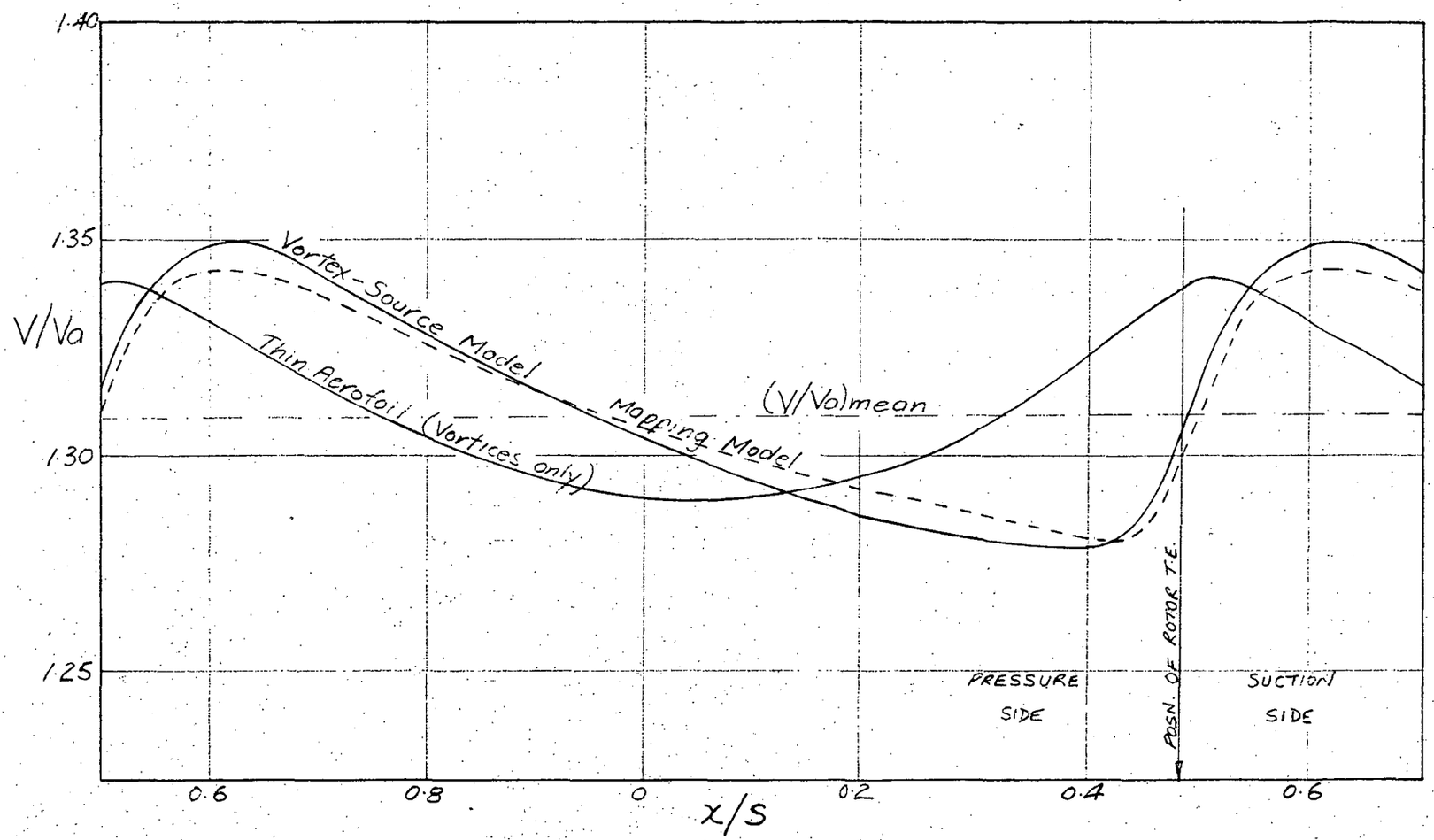

FIG. 4.8 ABSOLUTE VELOCITY DISTRIBUTIONS 0.20 INS. (6.7%C) DOWNSTREAM OF THE ROTOR

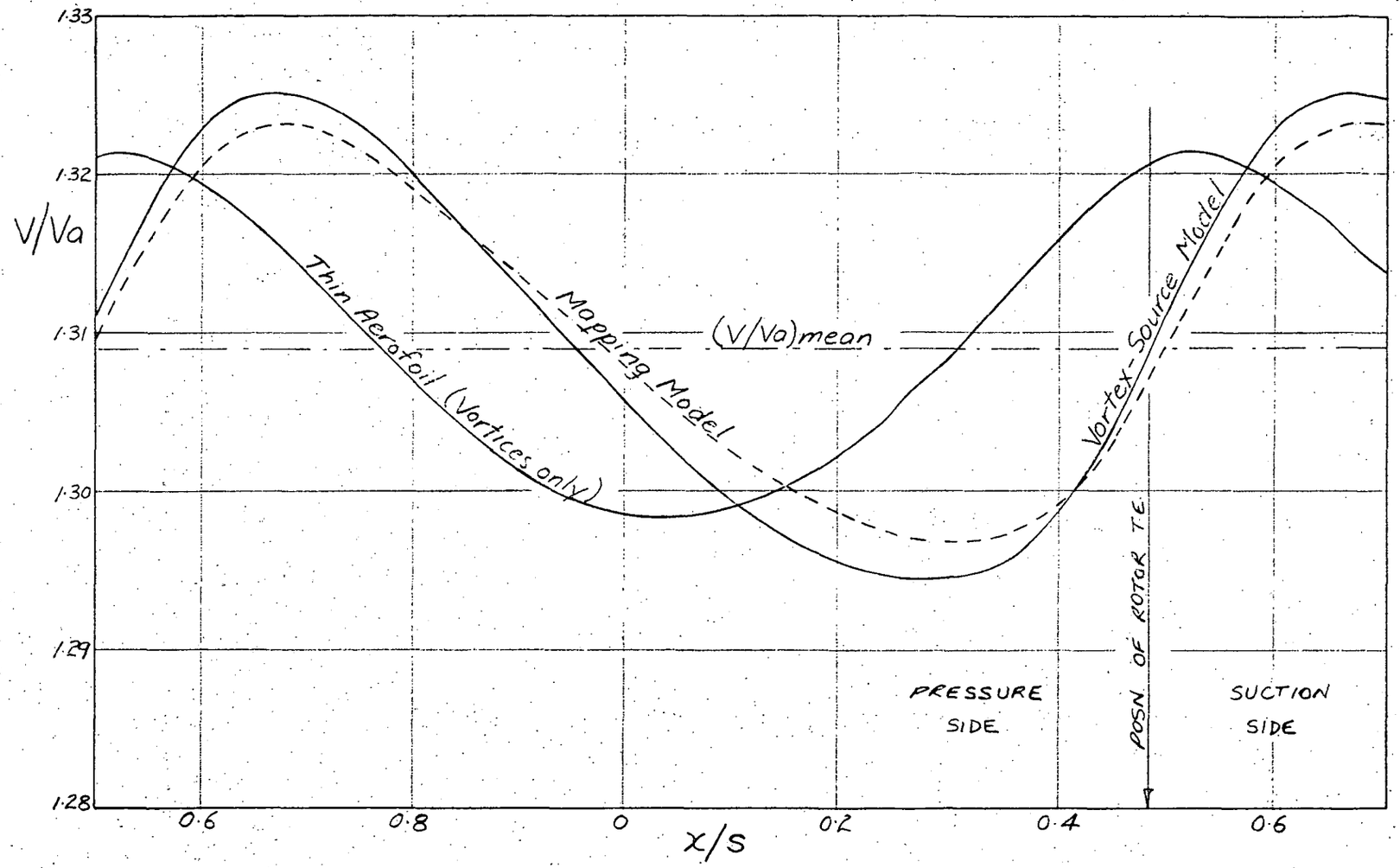

FIG. 4.9 ABSOLUTE VELOCITY DISTRIBUTIONS 0.55 INS. (18.3%C) DOWNSTREAM OF THE ROTOR

in the region of the blade trailing edge. Investigations carried out by Oliver (Ref. 13) based on the Wilkinson flow model (Ref. 18) have indicated that the potential flow downstream of a cascade blade may be extremely sensitive to the conditions at the trailing edge, e.g. blade shape, position of rear stagnation point.

In the case of the mapping model, which necessitated the use of an approximation of the actual C4 section, there would probably be relatively large deviations from the true blade shape near the trailing edge. The simulation of thickness using sources in the vortex-source model also gave only an approximation of the true blade section. (This influenced only the thickness effect, the circulation being controlled by the chosen vortex distribution.) The models are also likely to differ in regard to the position of the rear stagnation point. The mapping model incorporates the Kutta-Joukowski condition which fixes the rear stagnation point at the trailing edge. The vortex-source model, however, is based on the measured blade surface velocity distributions and as a result, the effective rear stagnation point position for this model is likely to be approximately the same as for the real flow conditions. As argued in Section 3.5, this will probably not be in accordance with the Kutta-Joukowski condition.

The above discussion suggests that the vortex-source model is likely to give the better prediction of real flow conditions as it uses the actual measured vorticity and thus includes the true T.E. effect. However, it is possible that neither model adequately approximates the real "potential flow" component of the downstream velocity distribution as both neglect the effects of the I.G.V. and rotor wakes. Nevertheless, the vortex-source model gave an excellent fit to the measured velocity profiles of Fig. 4.1 in the sections outside the rotor wake regions. (See Fig. 4.2.)

For calculations upstream of the rotor, the adding of thickness sources to the thin aerofoil model had the effect of increasing the velocity defect by over 100% and slightly shifting the position of the velocity minimum in the pressure to suction direction (less than 0.1s). The general shape of the velocity profile, however, was basically the same for both models. As shown in Figs. 4.8 and 4.9, the situation downstream of the rotor is considerably different. The allowance for thickness drastically alters the shape, as well as the velocity defect, of the thin aerofoil model curves.

There is a large shift in the position of the velocity minimum. The minimum position for the vortex model is approximately constant with axial distance downstream and almost midway between adjacent rotor T.E.'s

(see Fig. 4.11). At 0.2 ins. downstream of the rotor, the minimum for the vortex-source model is situated only 0.103s. to the pressure side of the T.E. position; this represents a shift in the position of the minimum due to the added thickness effect of about 0.33s. For 0.55 ins. downstream the shift is 0.24s. The increase in velocity defect due to the allowance for thickness is much smaller than for positions upstream - 39% increase at 0.20 ins. downstream and 35% at 0.55 ins.

4.5.2 Velocity Defect

A curve showing the variation of the potential flow absolute velocity defect with axial position downstream of the rotor is shown in Fig. 4.10; the defects were obtained from the vortex-source model curves. The decay of the measured "potential flow" defect upstream of the rotor is shown for comparison. The downstream defects are only about 20% of the defects for the corresponding upstream positions. This is not surprising in view of the large general fall in both profile thickness and potential flow circulation along the blade.

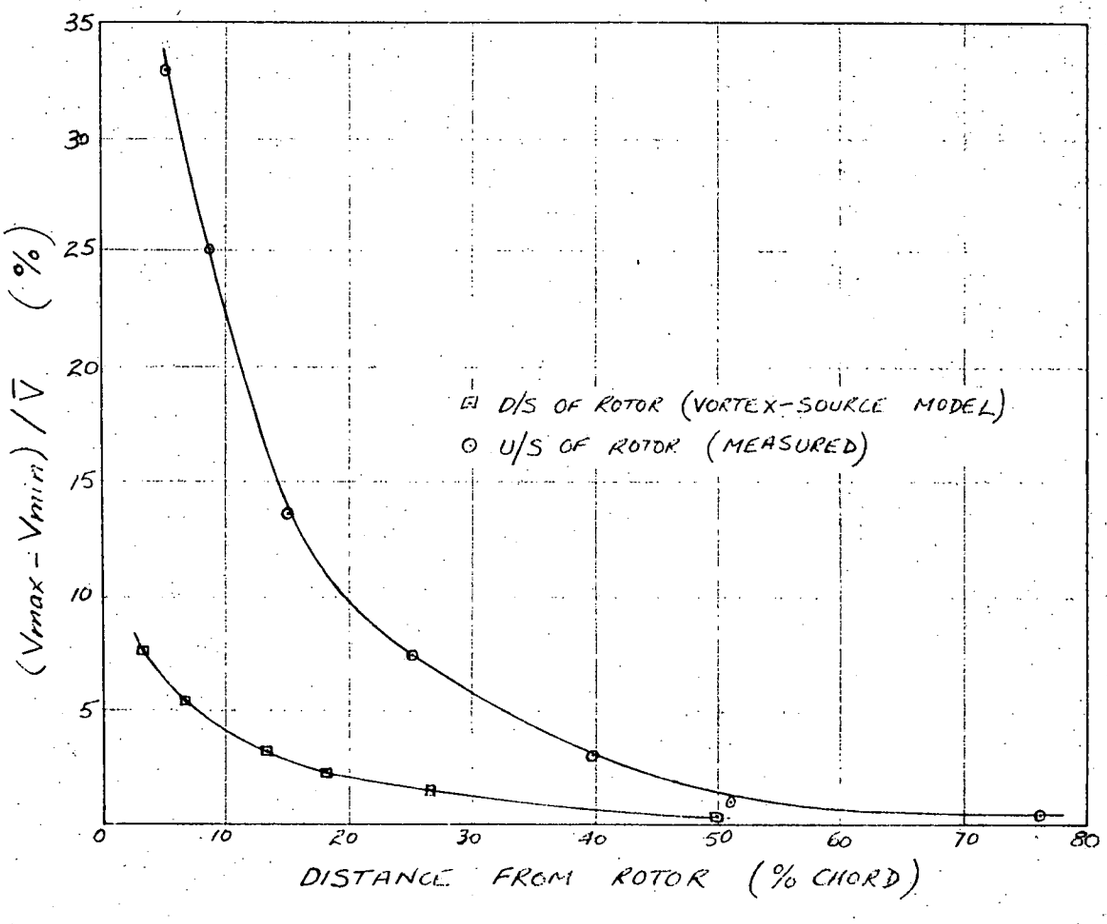

FIG. 4.10 VARIATION OF VELOCITY DEFECT WITH AXIAL POSITION

4.5.3 Loci of Velocity Minima

The positions of maximum potential flow absolute velocity defect downstream of the rotor for each of the three models are plotted in Fig. 4.11; the loci of the relative velocity minima (calculated from the vortex-source model) and of the measured absolute rotor wake minima are also shown. As for the measurements upstream of the rotor, the loci of the vortex-source and mapping model minima are very similar, but slightly separated (by an almost constant amount) in peripheral position. Also as was the case upstream, the potential flow minima (and the relative flow minima) do not lie at all close to the likely position of the relative rotor stagnation streamline.

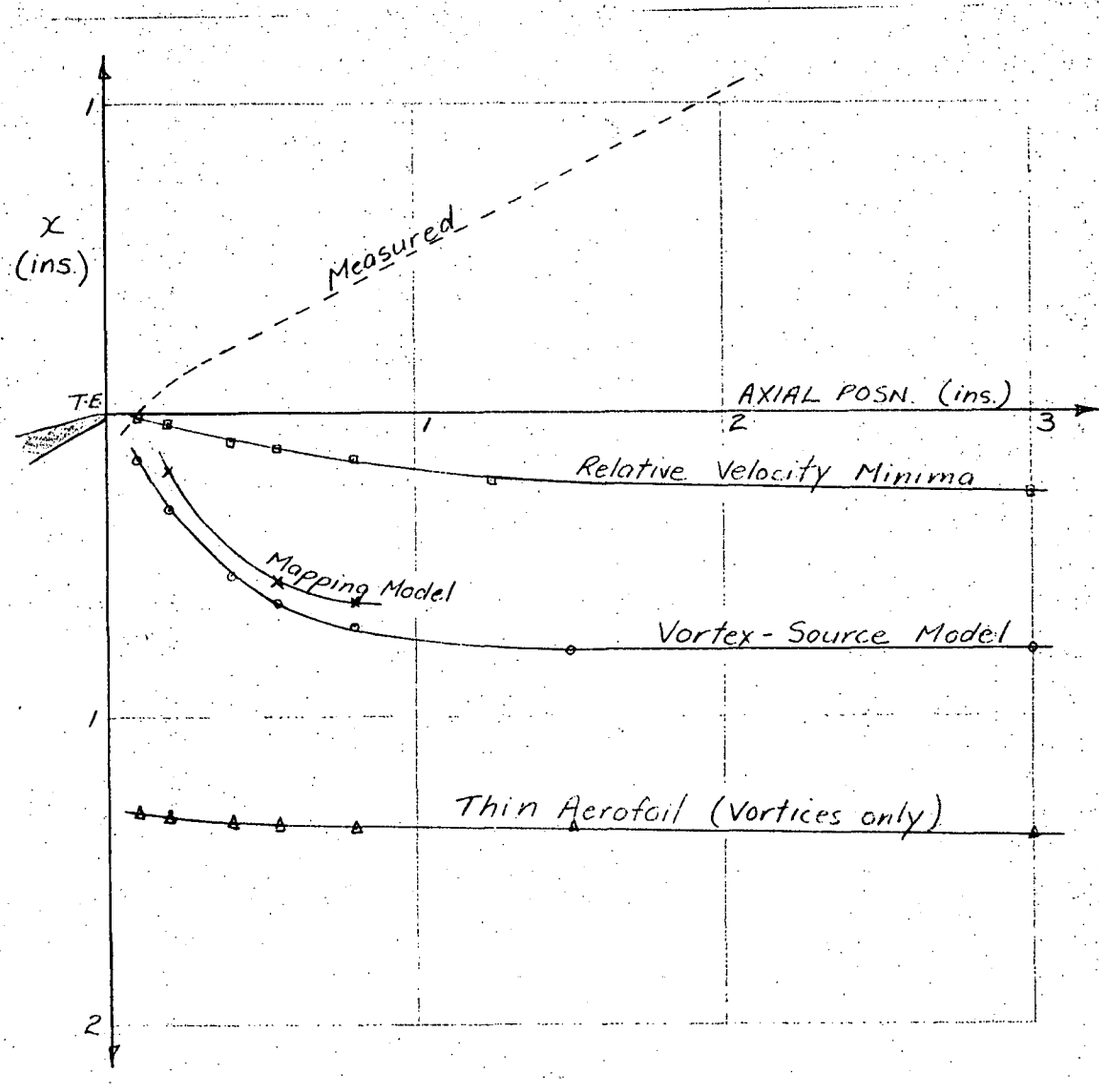

FIG. 4.11 LOCI OF VELOCITY MINIMA

It is interesting to note that the peripheral position of the thin aerofoil model (vortices only) minimum is approximately constant with axial position and is situated almost midway between adjacent trailing edges. (This corresponds closely to the constant peripheral position of

the measured and calculated absolute velocity minima upstream of the rotor.) The addition of the thickness sources to the thin aerofoil model shifts the minima considerably closer to the trailing edge as shown. (At 0.1 ins. downstream, the shift due to added thickness is just over one third of the blade spacing.) This trend suggests that it would be worthwhile investigating the result of adding to the model extra thickness to account for the effect of the blade boundary layer and wake. This is considered in the next chapter. (Section 5.7).

CHAPTER 5

DEVELOPMENT OF A ROTOR WAKE MODEL

5.1. Introduction

One of the aims of the present study is, having measured the various unsteady flow phenomena which occur in an axial flow compressor, to produce mathematical models suitable for use in accounting for these effects in compressor design. Models which give close approximations of the measured "potential flow" variations in velocity upstream and downstream of a moving row have been presented in the previous two chapters. In order to investigate more closely the contribution of blade wakes to flow unsteadiness and the interaction effect of wakes from one row impinging on a following row, there is a need for a suitable mathematical model to describe a compressor blade wake.

This chapter considers the possibility of extending the vortex-source model developed above to take into account the rotor blade wakes. The measurements of the flow downstream of the rotor presented in Chapter 4 were not suitable for use in defining a wake model for the following reasons:

a. It was not possible to determine the true contribution of the viscous rotor wake to the measured velocity distribution.

b. The general development (profile shapes, velocity defect decay, wake spread etc.) of the relative rotor wake could not be determined from the absolute flow measurements as the flow angle variation in the wake was not known (and could not be measured).

At mid blade height in the Vortex Wind Tunnel, the blade angles for the rotor and stator are identical and, for the flow conditions being considered for the current investigations, the average relative flow angles and velocities for the rotor are almost the same as those for the stator (see velocity diagram, Fig. 3.3). It is therefore expected that the stator wake would be very similar to the rotor wake in the relative flow and could be used in formulating a model of the rotor wake.

The first part of this chapter is devoted to a discussion of hot wire measurements of the velocity distribution downstream of the stator. Next, the equivalence between the relative rotor and stator wakes is examined by

1. constructing an absolute rotor wake profile from a measured stator wake velocity distribution (considered as a relative rotor wake

distribution) and an approximate relative flow angle distribution calculated from the potential flow; and

2. using a measured absolute rotor wake velocity profile and a measured stator wake distribution (again considered as a relative rotor wake distribution) to predict the relative flow angle distribution in the rotor wake.

The measured stator wake profiles are employed to construct an approximate effective rotor blade shape. The latter is incorporated in a revised vortex-source model in an attempt to improve the prediction of the flow by accounting for the added thickness effect of the rotor blade boundary layer and wake. The revised model is used to calculate absolute velocity distributions downstream of the rotor in the same way as before, and these are compared with the previous distributions presented in Section 4.5.

5.2 Measurements of Stator Wake Velocity Distribution

Measurements of the mean velocity distribution in the stator wake at several axial stations downstream of the stator were carried out using the constant temperature anemometer for the same flow conditions as the previous measurements, i.e., those corresponding to the velocity diagram of Fig. 3.3. Downstream of the stator row, a hot wire detects unsteadiness due to the following effects:

1. The general turbulence associated with the stator wake.
2. The passing of the rotor wakes as for the measurements upstream of the stator. The rotor wake is effectively "chopped" into segments by the stator row in the same way as described above for the case of the I.G.V. wake passing through the rotor. (See Fig. 1.1.)
3. The inlet guide vane wake avenue. As well as the general turbulence associated with the wake, unsteadiness also arises because the position of a fixed point relative to the wake segment centre-line varies with time. This is due to the rotation of the I.G.V. wake segments as they pass through the rotor and stator rows, with the result that the centre-lines of the segments downstream of the stator are not oriented in the direction of the flow.

The hot wire therefore recorded the time average of a velocity varying under the influence of all the above factors. This average velocity could well be expected to vary with the position of the stator relative to the I.G.V. row. The I.G.V. wake avenue, as well as having a possible direct effect on the flow around a stator blade, is also likely to have an indirect influence due to interaction with the rotor wakes. In Section 4.4, it was seen that the guide vane wake avenue significantly

altered the velocity deficiencies of the rotor wakes; in this way, the position of the I.G.V. row relative to the stator could influence the effect that the rotor wakes have on the flow in the vicinity of the stator.

For these reasons, the stator wake traverses were performed by moving both the I.G.V. and stator rows together relative to the stationary probe, so that the position of the stator blade relative to the I.G.V. wake avenue was always the same. The particular situation considered had both sets of blades at the same peripheral setting at mid blade height (M.B.H.) - i.e., each stator blade centre was located axially downstream of a guide vane centre. The only criterion for choosing this situation was that, as will be shown later in Chapter 6, it corresponded to a minimum level of generated noise in the Vortex Wind Tunnel.

5.3 Discussion of Stator Wake Profiles

5.3.1 Comparison with I.G.V. and Rotor Wake Measurements

The measured stator wake velocity profiles are shown in Figs. 5.1 to 5.6. As was observed for the I.G.V. wake, the velocity profiles are far from symmetrical. This, as explained in Section 3.5.1, is because the boundary layer on the suction surface of any lifting aerofoil is subject to higher pressure gradients and is thus thicker than that on the pressure surface.

Perhaps the most interesting feature of the profiles, however, is the almost uniform velocity distribution outside the wake, particularly for the positions closest to the T.E. - further downstream, a noticeable variation in the free-stream velocity does appear. This apparent uniformity in the velocity outside the wake was unexpected in view of the significant free stream "potential flow" effect observed in the I.G.V. wake profiles (see Fig. 3.11) and in the absolute velocity variation downstream of the rotor as recorded in the photographs of Fig. 4.1.

The blade angles and flow conditions for the I.G.Vs. are quite different to those for the stator blades and reasonably large differences in the wake development and the general distribution of velocity downstream of the two rows could be expected. There is also experimental evidence to suggest that the boundary layer on the guide vane pressure surface is laminar over the whole of chord and undergoes transition to turbulence only near the trailing edge; the boundary layers on the rotor and stator blades are turbulent over at least the last half chordlength. If this be the case, significant differences between the I.G.V. and stator wake developments could certainly be expected.

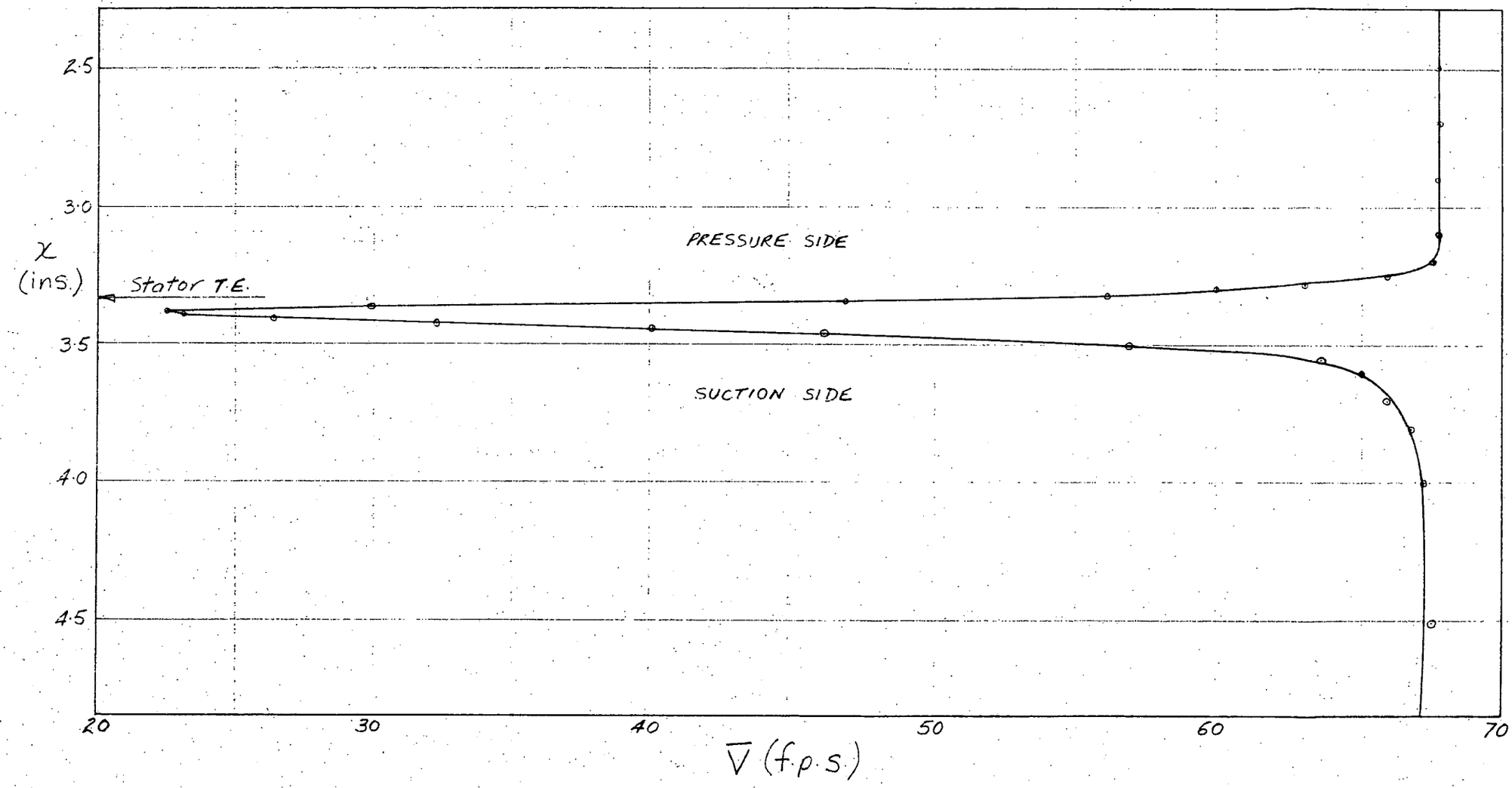

FIG. 5.1 STATOR WAKE VELOCITY DISTRIBUTION 0.10 INS. (3.3%C) DOWNSTREAM OF T.E.

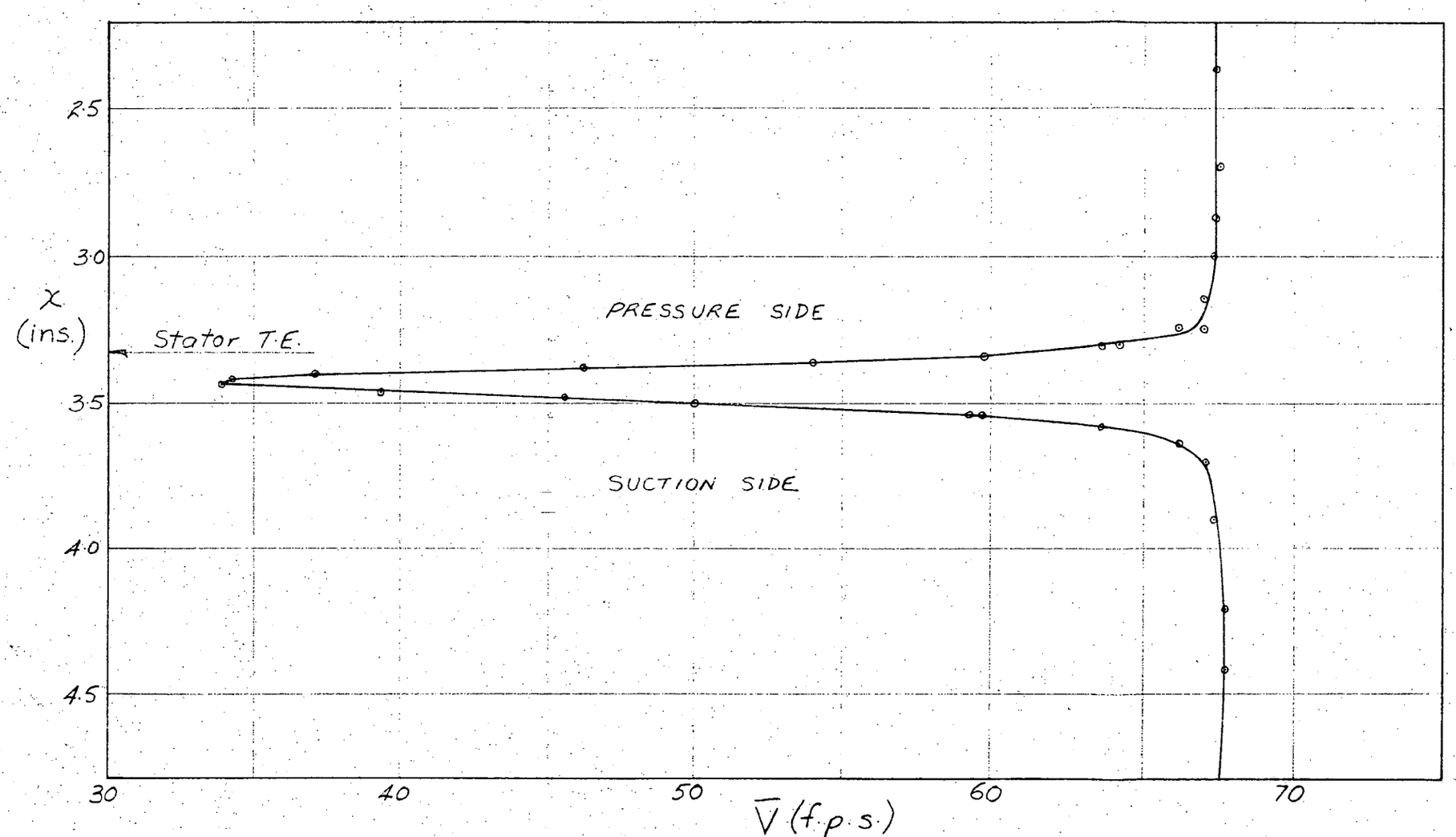

FIG. 5.2 STATOR WAKE VELOCITY DISTRIBUTION 0.20 INS. (6.7%C) DOWNSTREAM OF T.E.

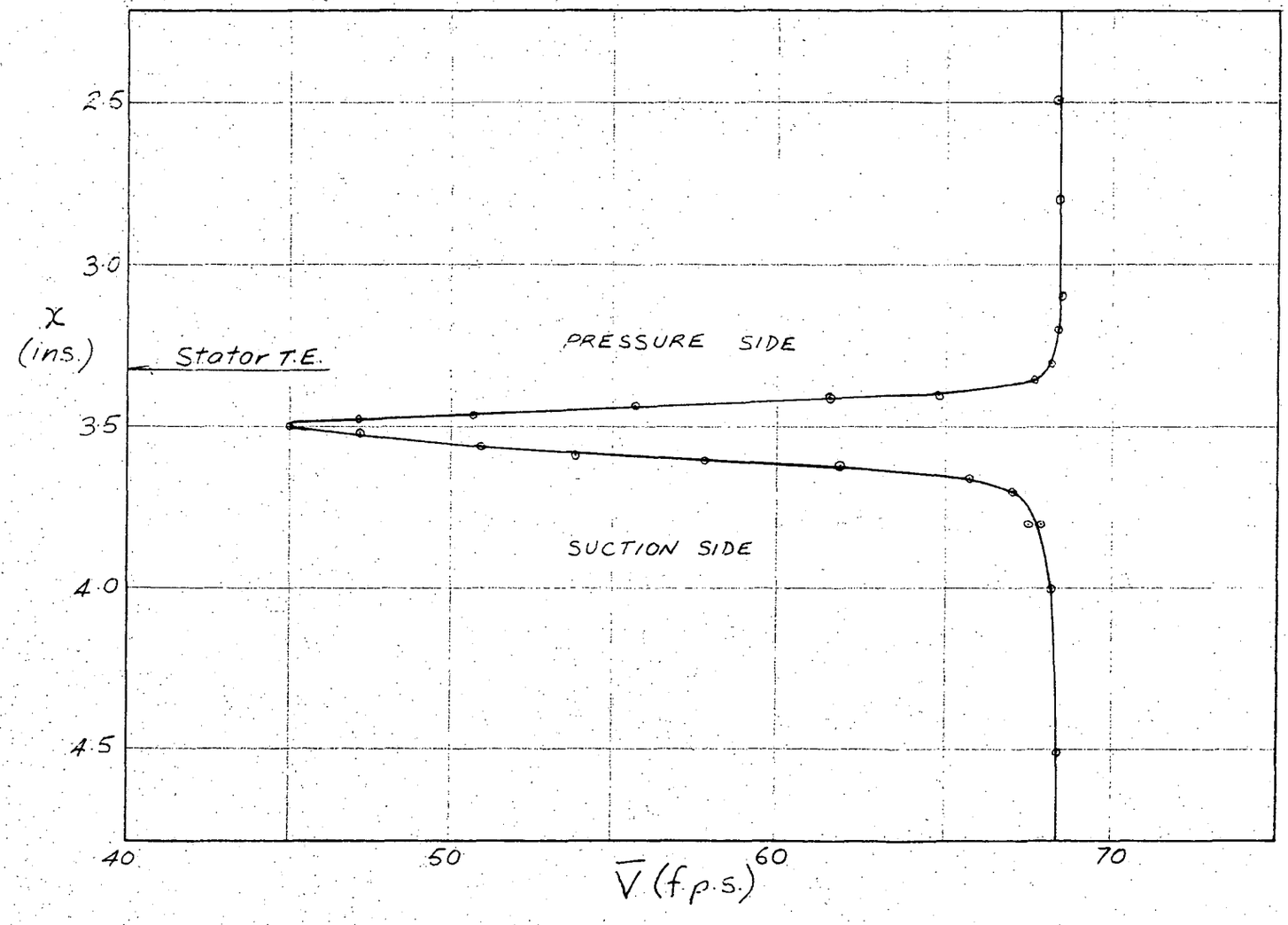

FIG. 5.3 STATOR WAKE VELOCITY DISTRIBUTION 0.40 INS. (13.3%C) DOWNSTREAM OF T.E.

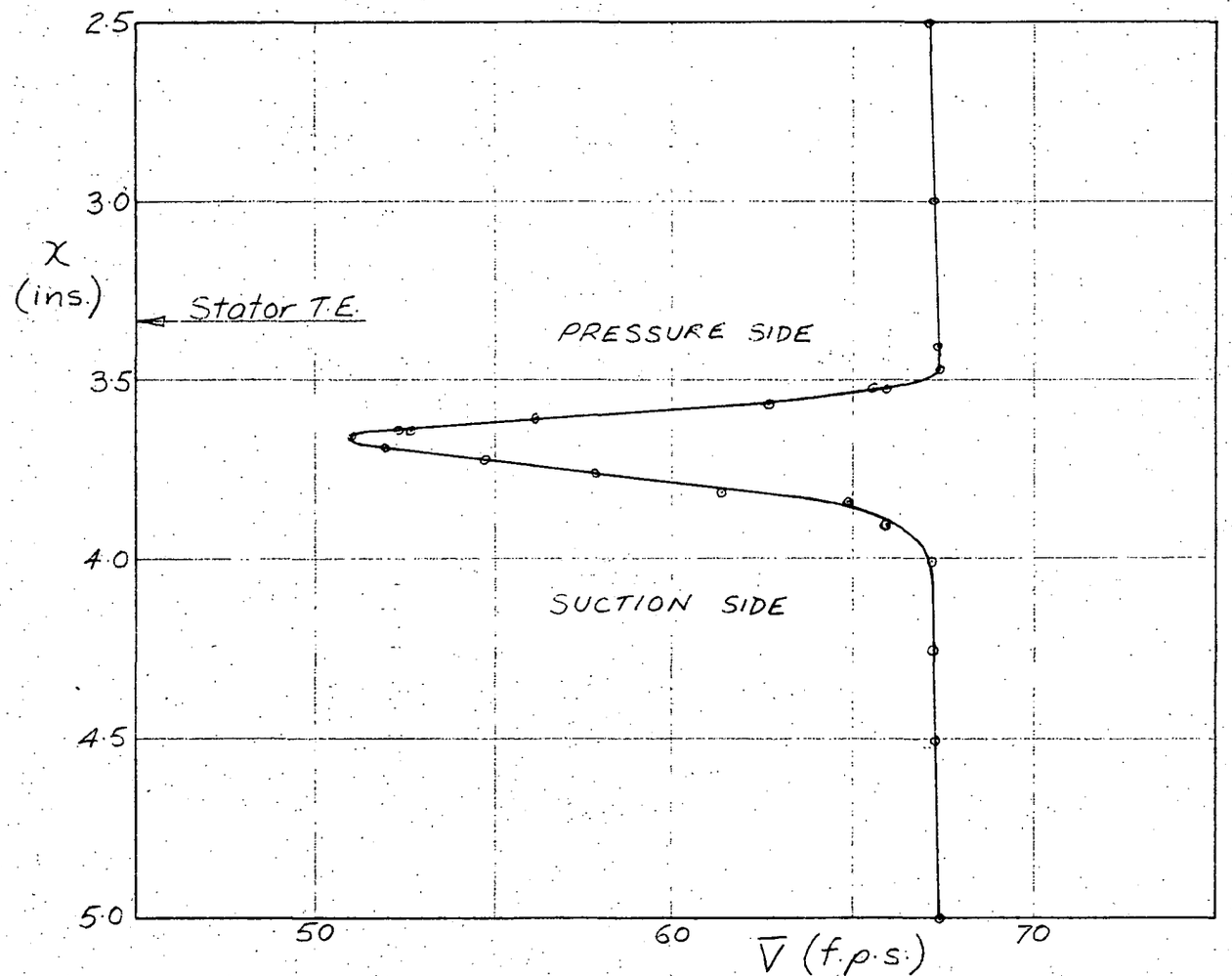

FIG. 5.4 STATOR WAKE VELOCITY DISTRIBUTION
0.80 INS. (26.7%C) DOWNSTREAM OF T.E.

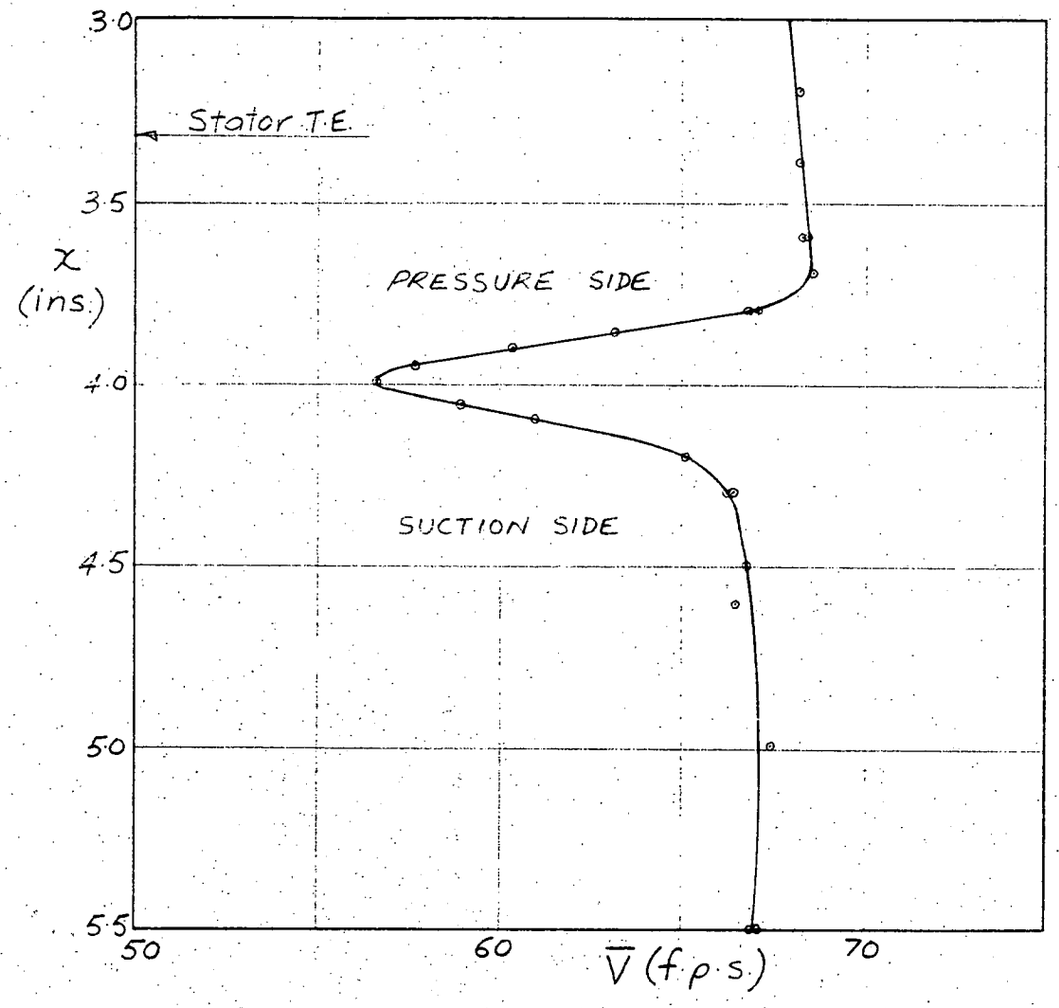

FIG. 5.5 STATOR WAKE VELOCITY DISTRIBUTION
1.5 INS. (50%C) DOWNSTREAM OF T.E.

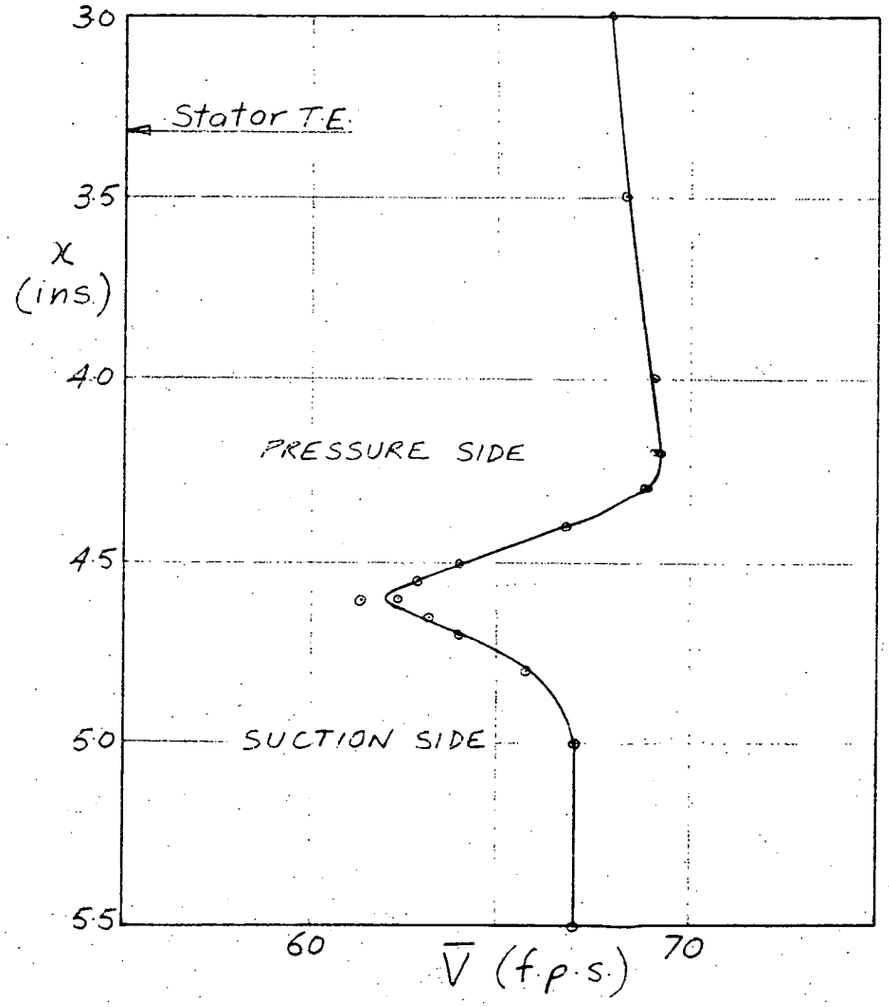

FIG. 5.6 STATOR WAKE VELOCITY DISTRIBUTION
3.0 INS. (100%C) DOWNSTREAM OF T.E.

The stator wake profiles could also not be expected to resemble the absolute velocity distributions downstream of the rotor (Fig. 4.1). The contribution of the "potential flow" variation to the absolute velocity distributions of Fig. 4.1 is accentuated because of the relatively small wake velocity defect in the absolute flow. For example, in Fig. 4.2 (0.20 ins. downstream of the rotor), the potential flow (vortex-source model) velocity defect is about half the overall defect. The relatively large "potential flow" effect observed in the rotor absolute velocity distributions would not appear in the rotor relative velocity profiles and could therefore not be expected to be observed to nearly the same extent in the velocity variation downstream of the stator. (The explanation for the very small absolute wake velocity defects has been given in Section 4.3: an absolute velocity defect of the order of 8 f.p.s. at the position 0.20 ins. downstream is to be compared with a stator wake defect, and likely relative rotor wake defect, of 33 f.p.s. - Fig. 5.2.) The shape of the absolute rotor wake profiles is also a function of the relative positions of the "potential flow" and wake minima (see Fig. 4.2). As indicated in Fig. 4.11, the relationship between the loci of the potential flow and wake minima is considerably different for the relative flow. The same is no doubt true of the flow downstream of the stator.

5.3.2 Free Stream Velocity Distribution

A possible explanation for the uniform velocity distribution in the free stream for positions close to the stator trailing edge could be that velocity gradients due to the "potential flow" and viscous wake components of the flow add in such a way as to give virtually zero variation outside the wake.

In Figs. 5.5 and 5.6, for positions 1.5 ins. and 3.0 ins. downstream of the T.E., there are significant velocity gradients in the free stream. This far downstream, the "potential flow" velocity defects are expected to be negligible - e.g. the velocity defect calculated from a potential flow model for the stator (Wilkinson, Ref. 18) for 3.00 ins. downstream is 0.011 f.p.s. For the same position there is a measured velocity variation in the region outside the wake of approximately 2 f.p.s. This suggests that, well downstream of the stator, there is a "free stream" velocity gradient due to the wake itself. Such an effect could be thought of as an alteration of the "potential flow" velocity distribution due to the presence of the wake, as referred to in Section 4.3. It should be noted that the observed free stream variation is an increase from the suction to pressure side. This is the reverse of the normal "potential flow" situation.

Any "free stream" velocity gradient due to the wake is likely to be present at all axial positions downstream of the stator. As suggested above, the uniform velocity distribution outside the wake for positions close to the T.E. could then be the result of opposing "potential flow" and wake free stream velocity gradients.

This hypothesis was tested by comparing the measured profiles of Figs. 5.1 to 5.6 with velocity distributions calculated from a potential flow model developed by Oliver (Ref. 13) based on the Wilkinson method (Ref. 18). (This method is discussed briefly in Section 3.6). Fig. 5.7 shows, for the position 0.20 ins. downstream of the stator, the potential flow profile superimposed on the measured profile by roughly aligning the two mean velocities. It is noted that the two velocity minima, although certainly not concurrent, are much closer than in the case of the absolute velocity curves shown in Fig. 4.2 for the same axial position with respect to the rotor T.E. Also shown in Fig. 5.7 is the algebraic difference (neglecting flow angle changes) between the measured and potential flow curves. This should at least be similar in shape to the vector difference of the two curves which would represent the contribution of wake effects to the velocity distribution.

The constructed curve is essentially similar in shape to the profiles of Figs. 5.5 and 5.6 (which correspond to virtually zero potential flow variation) and exhibits the same general free stream velocity gradient due to the wake. It would appear that the above hypothesis is correct - i.e., that the presence of the wake produces a free stream velocity gradient which tends to oppose the velocity gradient due to blade circulation and thickness effects, so that just downstream of the stator T.E. the resultant velocity distribution outside the wake is approximately uniform. This is in apparent contrast to the situation downstream of the inlet guide vanes. The measurements of Boxhall and Nilsson (Ref. 14) showed a significant free stream velocity gradient to exist just downstream of the T.E. (see Fig. 3.11), whereas at a position 1.50 ins. downstream the velocity distribution outside the wake was approximately uniform.

The free stream velocity gradient can be thought of as being induced by a net total vorticity in the wake. That is, the magnitudes of the opposing vorticities in each half of the wake are not equal and there is a total non-zero vorticity for the wake as a whole; this is characteristic of a curved wake.

It is interesting to note that, apart from the velocity gradient outside the wake, the constructed stator wake curve of Fig. 5.7 is very similar in shape to the construction of the contribution of the

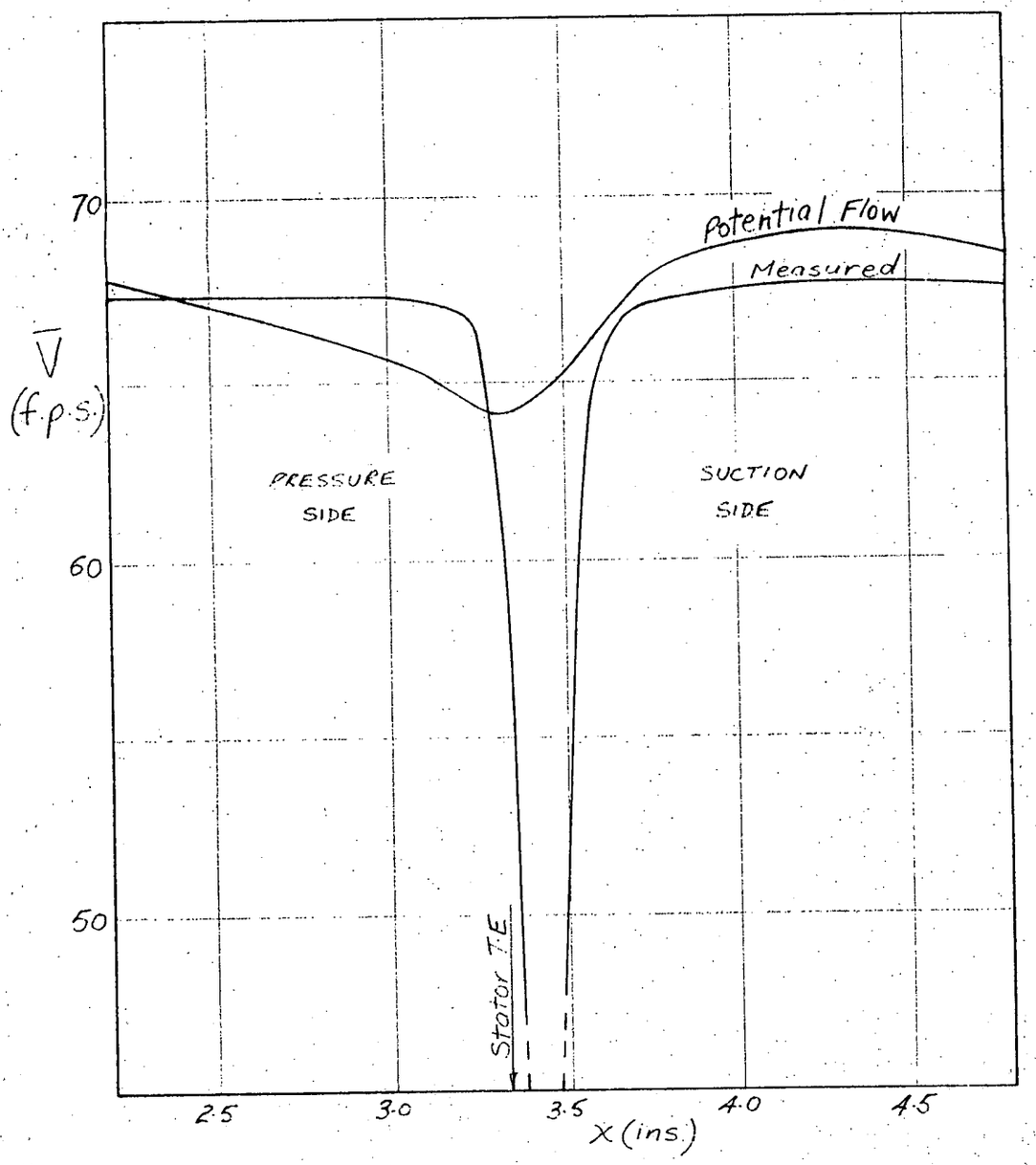

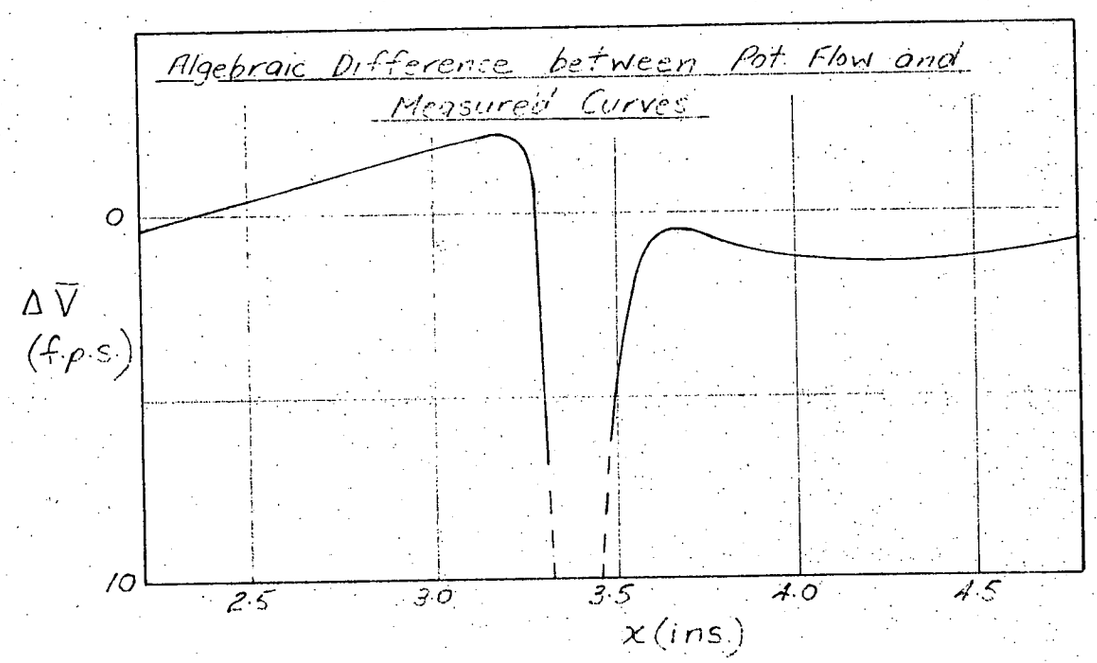

FIG. 5.7 COMPARISON BETWEEN POTENTIAL FLOW AND MEASURED PROFILES 0.20 INS. (6.7%C) DOWNSTREAM OF THE STATOR

rotor wake to the absolute velocity distribution downstream of the rotor (Fig. 4.3). (However these curves are only approximate in that:

1. calculated potential flow velocity profiles are used with the measured distributions

and 2. the possibly large differences between the calculated and real flow angles are neglected.)

5.3.3 Stator Wake Centre-Line and Velocity Defect

The wake centre-line as defined by positions of maximum velocity defect is plotted in Fig. 5.8. Apart from a slightly curved section near the T.E., it is a straight line in the mean flow direction. The line curves into the trailing edge in the same sense as for the I.G.V. wake (see Fig. 3.12), but the effect is not nearly as marked. The larger curvature of the I.G.V. wake centre-line near the trailing edge could possibly be the result of a laminar pressure surface boundary layer as discussed in Section 5.3.1 above. (In this case the boundary layer would undergo transition near the T.E.). It is expected that the centre-line of the relative rotor wake will be essentially the same as for the stator wake.

In Fig. 4.5 in the previous chapter, the approximate position of the rotor T.E. relative to the locus of the absolute velocity minima downstream of the rotor was determined by assuming the relative wake centre-line to be a straight line. In the light of the above, the true position of the T.E. is probably very slightly to the pressure side of the one shown.

The decay of the stator wake velocity defect is shown in the graph of $\bar{V}min/\bar{V}max$ against axial position in Fig. 5.9. The measured I.G.V. wake defect curve is shown for comparison.

5.4 Effect of the I.G.V./Stator Peripheral Relationship on the Velocity Distribution Downstream of the Stator

The stator wake profiles presented above were measured for a particular I.G.V./stator peripheral relationship in which each stator blade centre was located axially downstream of a guide vane centre at M.B.H. Johnston and Lockhart (Ref. 20) have performed traverses downstream of stator in the Vortex Wind Tunnel for different relative peripheral settings of the I.G.V. and stator rows using a Conrad three hole pressure probe. The results of their investigations are considered briefly in this section.

Fig. 5.10 shows the velocity distributions for the same flow conditions considered by the author 0.20 ins. downstream of the stator obtained from Conrad probe measurements for 4 different I.G.V./stator configurations. (It was, of course, not possible to obtain accurate

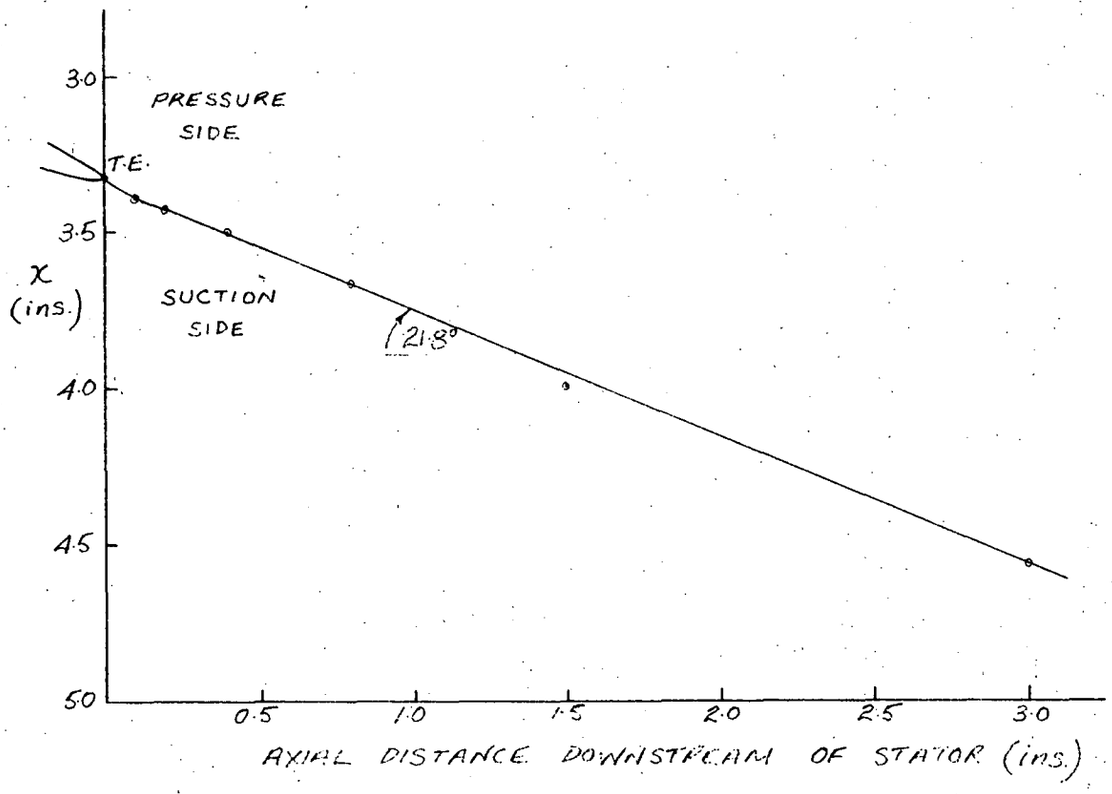

FIG. 5.8 STATOR WAKE CENTRE-LINE

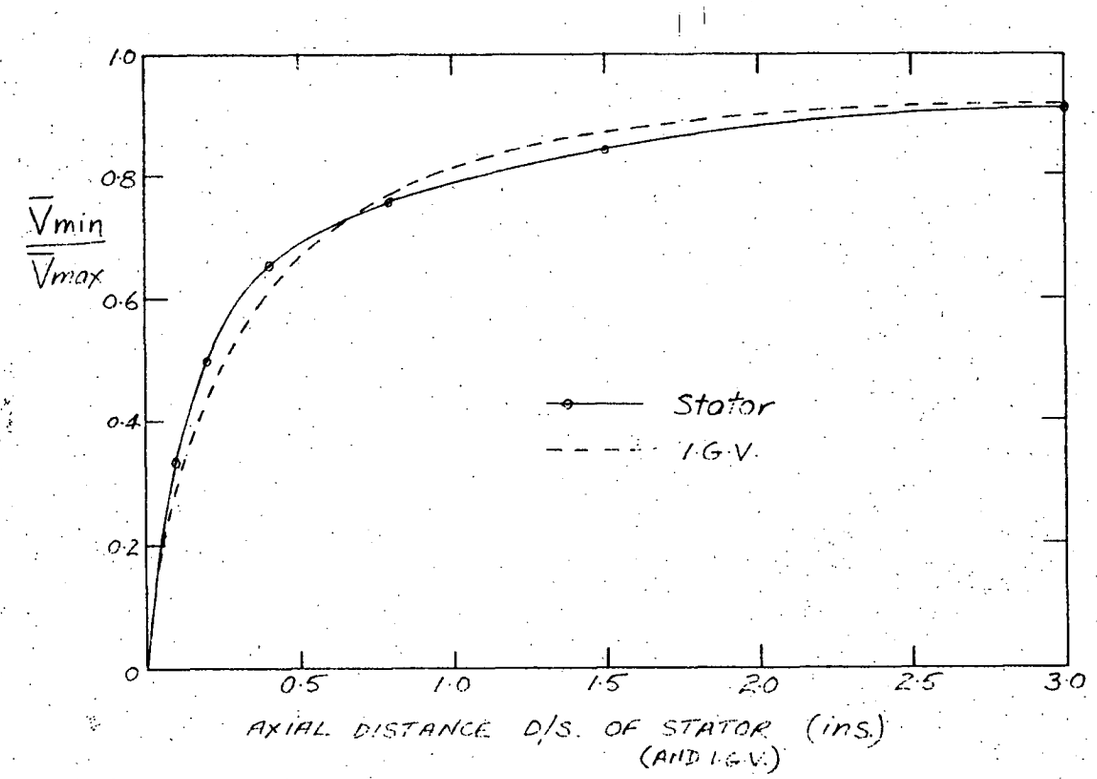

FIG. 5.9 DECAY OF STATOR WAKE VELOCITY DEFECT

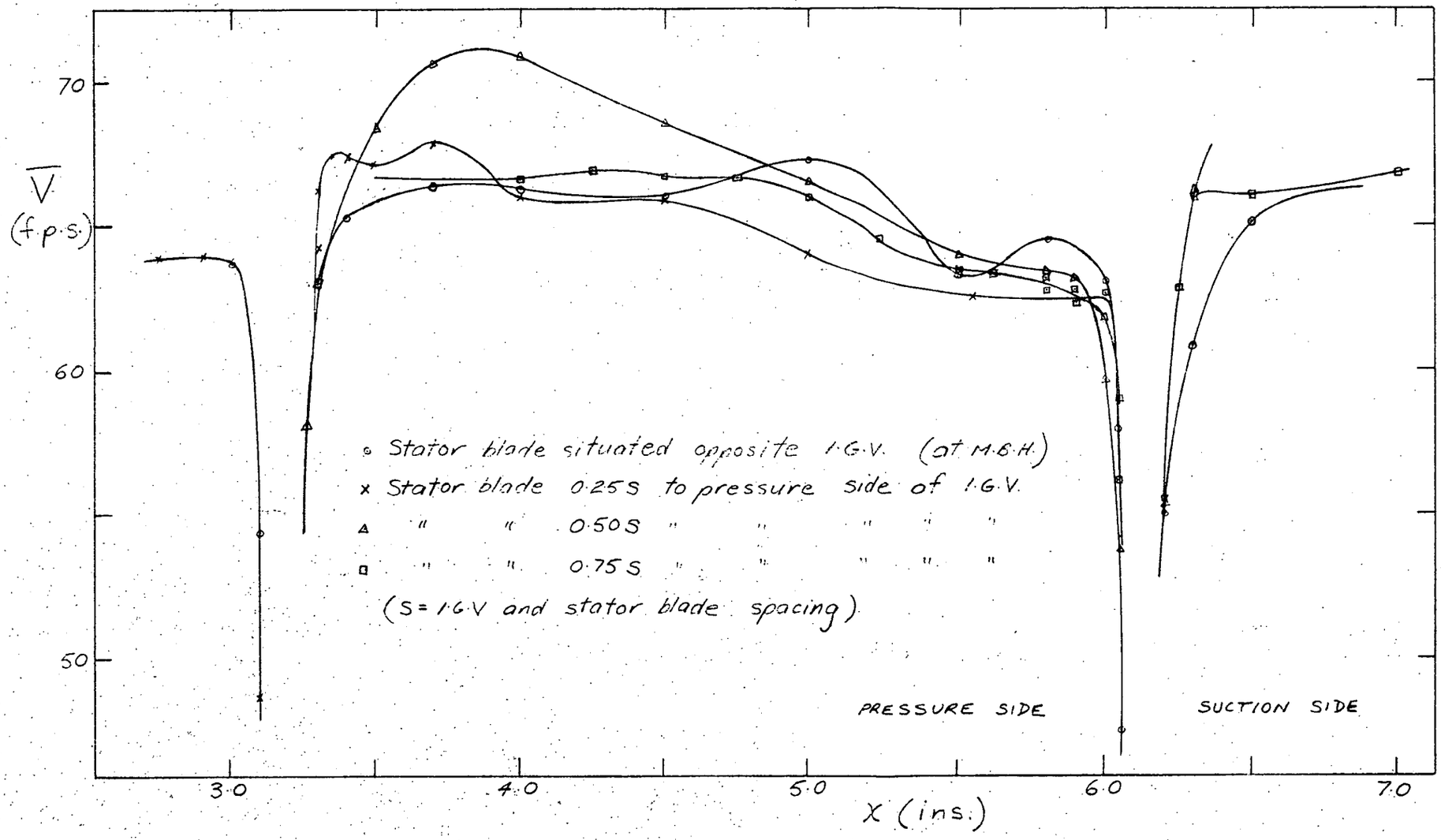

FIG. 5.10 CONRAD PROBE TRAVERSES 0.20 INS. (6.7%C) DOWNSTREAM OF THE STATOR

measurements with the Conrad probe in the wake regions.) The curves indicate that the velocity distribution downstream of the stator varies considerably with changing I.G.V./stator relationship. For the situation in which each stator blade is situated peripherally midway between two guide vanes (at M.B.H.) there is a substantial free stream velocity gradient, unlike the situation shown in the measured profile of Fig. 5.2.

Johnston and Lockhart observed in total head traverses a localized free stream peak of higher energy, the position of which could be made to traverse the free stream by changing the relative peripheral positions of the stator and I.G.Vs. This total head peak may have represented higher energy fluid near the centre of the I.G.V. wake avenue which is produced as the I.G.V. wake passes through the rotor. Smith (Ref. 7) has pointed out that, although the fluid in a blade wake passing through a rotating row is subject to the same static pressure field as the free stream fluid, it has a different through flow velocity and is therefore subject to a different amount of energy exchange with the blading. In the case of a compressor, the I.G.V. wake fluid resides longer in the rotor and can therefore be expected to gain more energy. However, it is difficult to determine from the limited measurements available whether this is actually the situation being observed in the distributions downstream of the stator. Further investigation is warranted.

A brief investigation of the change in the stator wake profile 0.20 ins. downstream for different I.G.V./stator configurations carried out by the author showed an increase in the velocity defect of about 4% when the relative peripheral displacement between the two rows was changed by half a blade spacing.

In the sections that follow, the variation in the stator wake profile with changing I.G.V./stator relationship is neglected and all discussion is based on the velocity profiles of Figs. 5.1 to 5.6.

5.5 Equivalence of the Relative Rotor and Stator Wakes

5.5.1 Comparison of Profiles

As explained above, the stator wake is expected to closely approximate the relative rotor wake. If the flow angle distribution in the wake were known, it would, of course, be possible to check this equivalence by performing the vector addition of the blade speed U to the velocities of the measured stator wake profiles and comparing the resultant velocity profiles with the measured absolute rotor wake profiles. As it was not possible to measure the wake flow angle distribution, the author decided to carry out the constructions using relative flow angle

distributions calculated from the Wilkinson potential flow model. These distributions would not be expected to resemble the real wake angle distributions, but should indicate the effect of the variation in flow angle across the wake on the shape of the absolute velocity profiles.

Fig. 5.12 shows the absolute velocity distribution for the position 0.20 ins. downstream of the rotor, constructed from the stator wake profile of Fig. 5.2 using the calculated relative potential flow angle distribution shown in Fig. 5.11. The constructed velocity distribution includes both the "potential flow" and wake effects and is to be compared with the measured absolute velocity distribution in Fig. 4.2.

The constructed curve shows the effect of the varying flow angle and the general properties of the vector addition in producing large velocity peaks on either side of the absolute profile from a uniform free stream velocity distribution in the relative flow. Although the measured and constructed curves are considerably different in shape in the pressure side of the wake region, they are very similar in shape on the suction side and have approximately the same overall defect (Vmax-Vmin) of about 10 f.p.s. Considering that there are likely to be large differences between the real and potential flow angle distributions, the agreement is surprisingly good. The large velocity peak on the pressure side of the constructed profile could probably be accounted for by the calculated flow angle distribution being a poor approximation of the real flow conditions in this region.

5.5.2 Predicted Wake Flow Angle Distribution

As an alternative check on the equivalence of the stator and relative rotor wakes, the measured profiles - rotor absolute (Fig. 4.2) and stator (Fig. 5.2) - were used to predict the relative flow angle distribution 0.20 ins. downstream of the rotor by simple calculation from velocity diagrams constructed from the three known velocities, V, Q, and U. Clearly, the calculated angle distribution would vary depending on the chosen relative peripheral positions of the two curves.

Fig. 5.13 shows the flow angle distribution calculated assuming the relative and absolute rotor wake minima to be co-incident. The common position of the velocity minima was found to also correspond to the position of minimum relative flow angle. The general variation in flow angle across the blade spacing is basically similar to the potential flow distribution of Fig. 5.11 and, somewhat surprisingly, the difference between the extreme flow angle values is almost exactly the same (8.5 deg.) in both cases. However the occurrence of the secondary maximum and

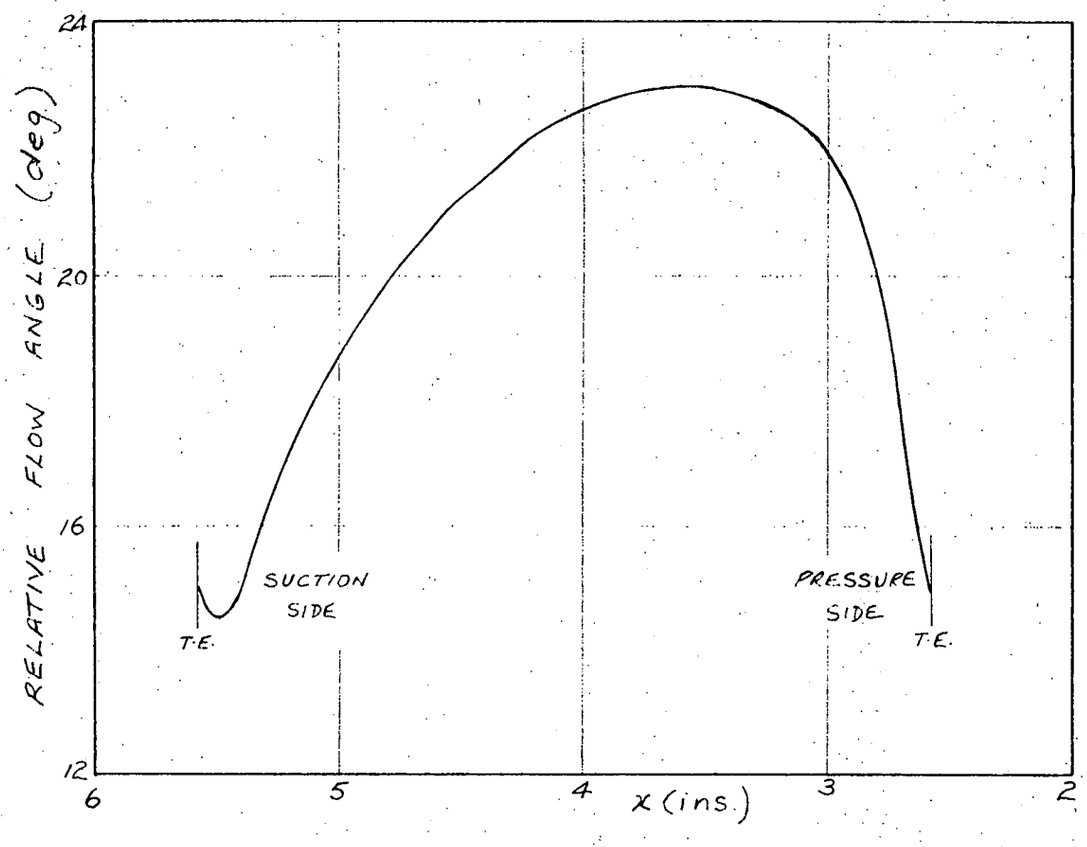

FIG. 5.11 WILKINSON POTENTIAL FLOW ANGLE DISTRIBUTION 0.20 INS. DOWNSTREAM OF THE STATOR

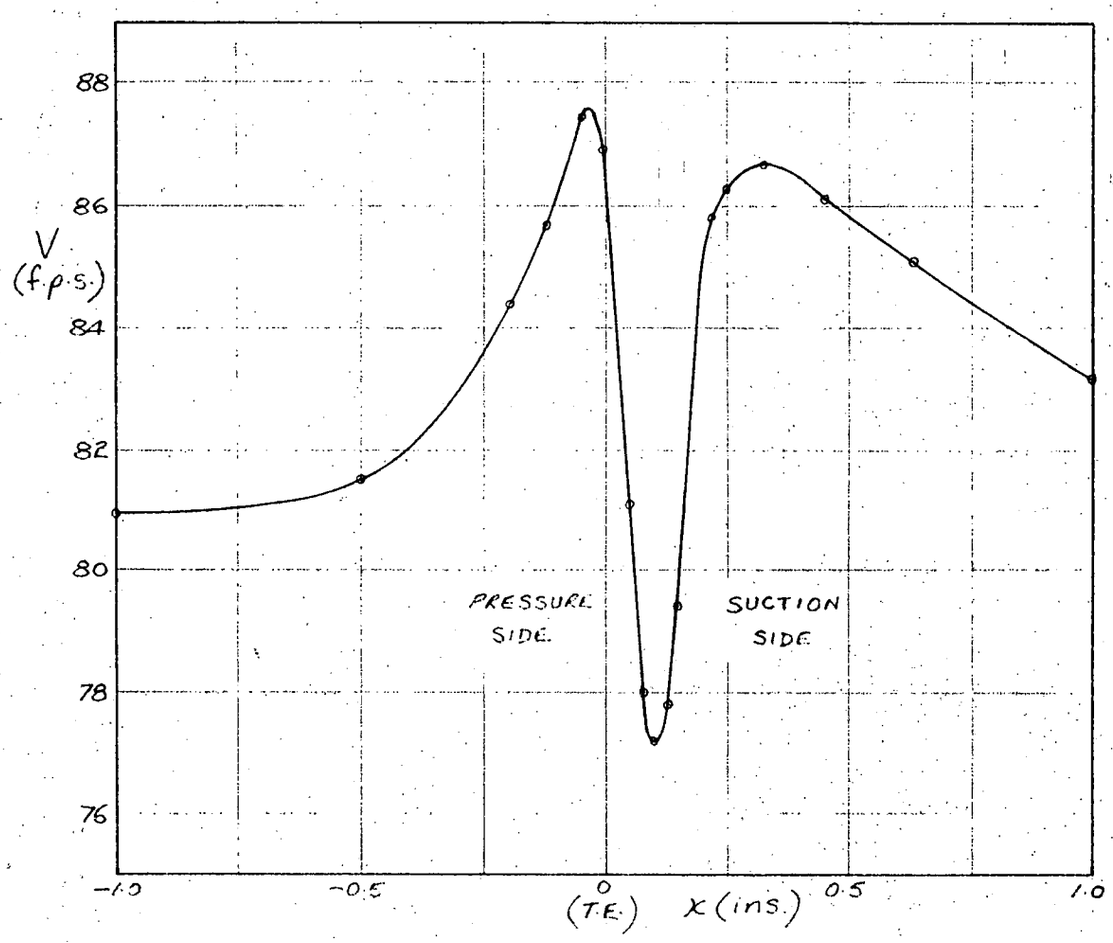

FIG. 5.12 ABSOLUTE ROTOR WAKE VELOCITY PROFILE CONSTRUCTED FROM MEASURED STATOR WAKE PROFILE 0.20 INS. DOWNSTREAM OF THE ROTOR

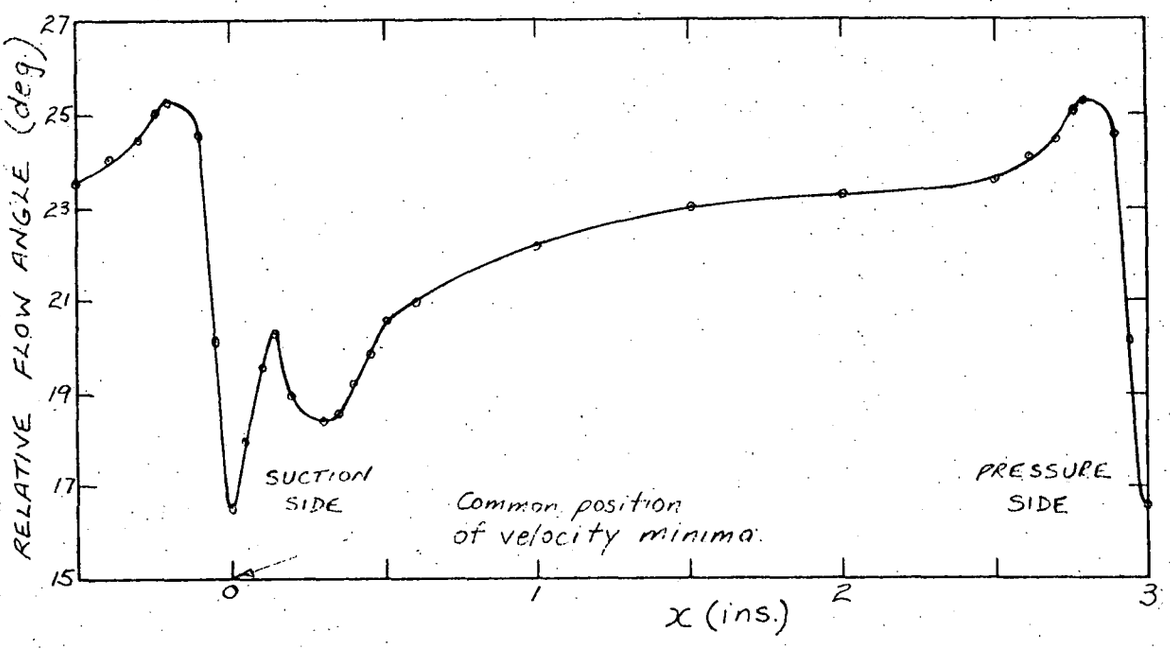

FIG. 5.13 PREDICTED RELATIVE FLOW ANGLE DISTRIBUTION 0.20 INS. DOWNSTREAM OF THE ROTOR ASSUMING RELATIVE AND ABSOLUTE WAKE MINIMA CO-INCIDENT

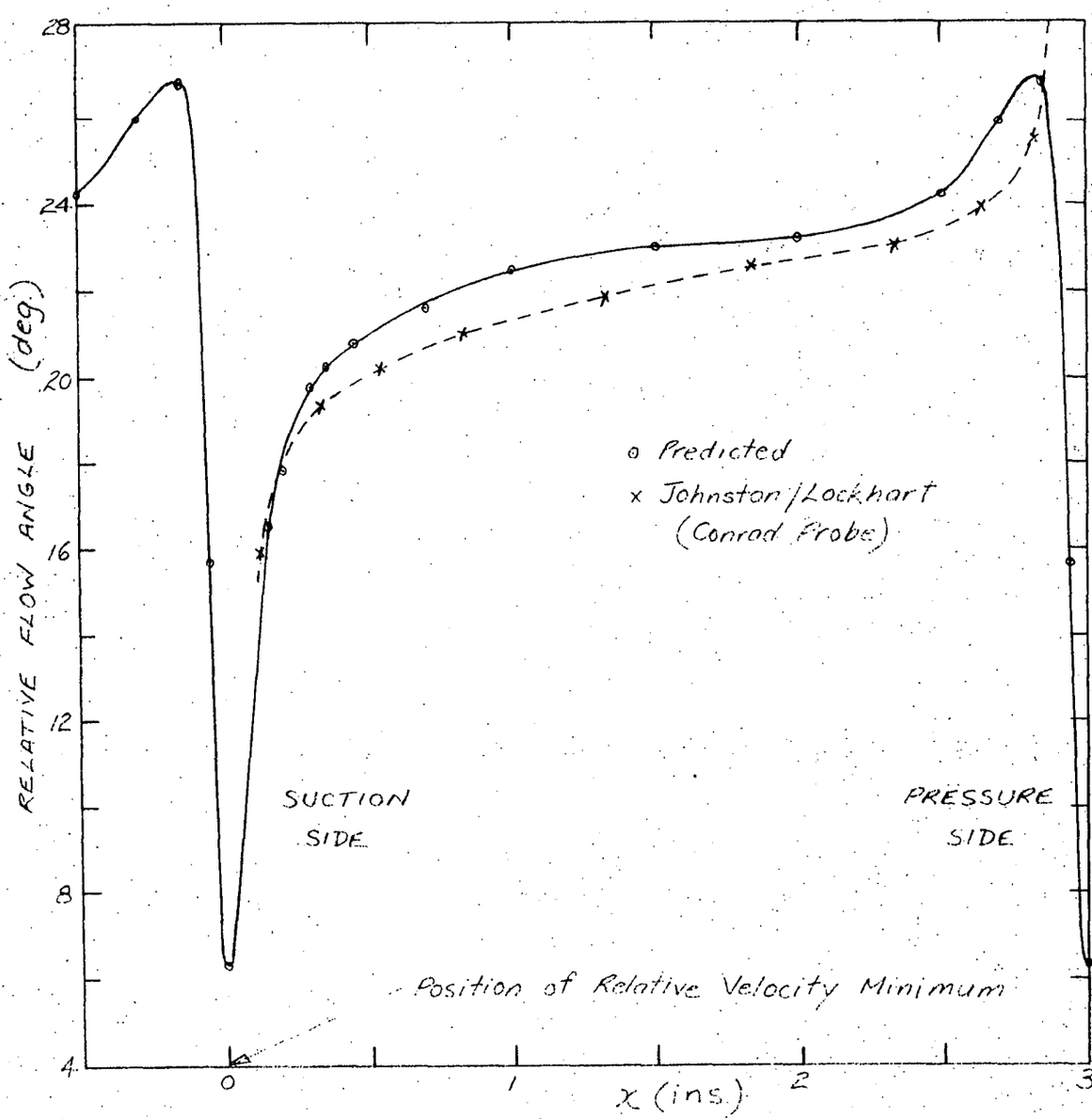

FIG. 5.14 PREDICTED RELATIVE FLOW ANGLE DISTRIBUTION 0.20 INS. DOWNSTREAM OF THE ROTOR ASSUMING 0.15 INS. DISPLACEMENT OF ABSOLUTE VELOCITY MINIMUM TO PRESSURE SIDE OF RELATIVE MINIMUM

minimum on the suction side edge of the wake is difficult to explain in terms of the likely real flow conditions.

The possibility of removing the secondary maximum and minimum from the constructed angle distribution by adjusting the relative peripheral displacement of the absolute and relative velocity minima was investigated. It was found that this could be achieved by displacing the absolute velocity minimum 0.15 ins. to the pressure side of the relative minimum; the resulting angle distribution is shown in Fig. 5.14.

This curve is similar in shape to an approximate angle distribution for the same position downstream of the stator measured by Johnston and Lockhart (Ref. 20) using a Conrad probe (also shown in Fig. 5.14). Fig. 4.5 shows that a slight separation of the velocity minima in the required direction can, in fact, be expected. The difference between 0.15 ins. and the much smaller separation shown in Fig. 4.5 could possibly be attributed at least partly to experimental error involved in the determination of the positions of minimum absolute velocity and also to the (small) differences between the relative rotor wake and the stator wake.

The distribution of Fig. 5.14 shows much greater variations in relative flow angle through the wake than the previous curve (Fig. 5.13) - for which the difference between the extreme flow angles was approximately the same as for the potential flow. There is for the new angle distribution a variation in α_2 from 6.3 deg. to 26.8 deg. - corresponding to $2\frac{1}{2}$ times the variation in the potential flow angle distribution. This larger variation in the flow angle is expected to represent a more realistic description of the real flow conditions in the wake.

5.6 Wake Model Considerations

The results of the previous section provide some indication that the stator wake is, as would be expected from the similar mean relative flow conditions for the two rows, a close approximation to the relative rotor wake. It is felt that there is certainly sufficient justification for using the stator wake measurements (the only suitable data available in any case) in formulating an approximate model of the relative rotor wake for the purposes of extending the vortex source model to give a more accurate description of the real flow.

As has been advocated by Lighthill (Ref. 21), a convenient method for describing a boundary layer is in terms of its vorticity. The blade plus its boundary layer can be replaced by a vortex sheet at the displaced surface, i.e. at a surface which is one boundary layer

displacement thickness from the blade surface. This represents the obvious next improvement on the Wilkinson model discussed above. Clearly, the blade wake could also be taken into account in a similar way by replacing each half of the wake with a vortex sheet at the displacement thickness. Alternatively, in terms of the vortex-source model used above, the effective extra blade thickness due to the boundary layer and wake could be modelled by extending the row of sources into the wake and calculating the source strengths from the geometry of the displaced surface. However, considerable difficulties arise in defining a displacement thickness δ^* for a wake.

5.6.1 Wake Displacement Thickness

In the case of a boundary layer, the displacement thickness is usually thought of as a flow deficiency thickness and represents, in the case of an aerofoil, the extra thickness which would have to be added to the original profile such that the flow outside it with all the fluid travelling at the free stream velocity Q is the same as the real flow (with the boundary layer deficiency). The boundary layer displacement thickness is then defined by the expression

$$\delta^* = \int_0^\infty (1 - q/Q)\,dy \qquad \ldots\ldots(5.1)$$

where q is the velocity in the boundary layer

and Q the (free stream) velocity which would exist were there no viscous effects.

As the "potential flow" velocity gradients outside a boundary layer are small and the boundary layer itself is thin, Q can be assumed to be constant at the free stream velocity just outside the boundary layer.

It is not possible to apply the same simple definition of δ^* to a wake, especially in the region close to the blade trailing edge. Here the wake is unsymmetrical, with the velocity outside the wake usually different for each side. (This is particularly so in the case of the I.G.V. wake - see Fig. 3.11.) The particles which follow a path over the suction side of a blade have more strongly curved paths near the trailing edge than those which travel over the pressure surface.

Another complication is that there is a significant "potential flow" velocity defect in the vicinity of the wake as shown, for example, in Fig. 5.7. At this position (0.20 ins. downstream of the stator T.E.), the calculated potential flow defect is about 15% of the defect in the wake; at 0.1 ins. downstream, it is almost 20%. Furthermore, the "potential flow" velocity distribution both inside and outside the wake is, itself, likely to be affected considerably by the presence of the wake. Under these conditions, it is difficult to see how to apply a definition

of the displacement thickness in terms of a flow deficiency in the same way as for a boundary layer. Also, from a practical viewpoint, there is no way of determining the actual "potential flow" velocity distribution for the region inside the wake, were it desired to use this to define q/Q values. Nor would it be possible to determine the "potential flow" distribution that would exist without the wake present - apart from the calculated one.

As a first approximation for curved flow, the flow outside the viscous region can be regarded as being a vortex flow with Qr = constant. For this approximation the radii of curvature of the streamlines in the vicinity of the wake are large enough for the centre of curvature to be taken as lying in the same circumferential plane as the measurements. The radius of curvature at any point can then be calculated from the local slope of the velocity distribution:

$$\partial(Qr)/\partial r = 0 \qquad \text{.....(5.2)}$$

and $$r = -Q/(\partial Q/\partial r) \qquad \text{.....(5.3)}$$

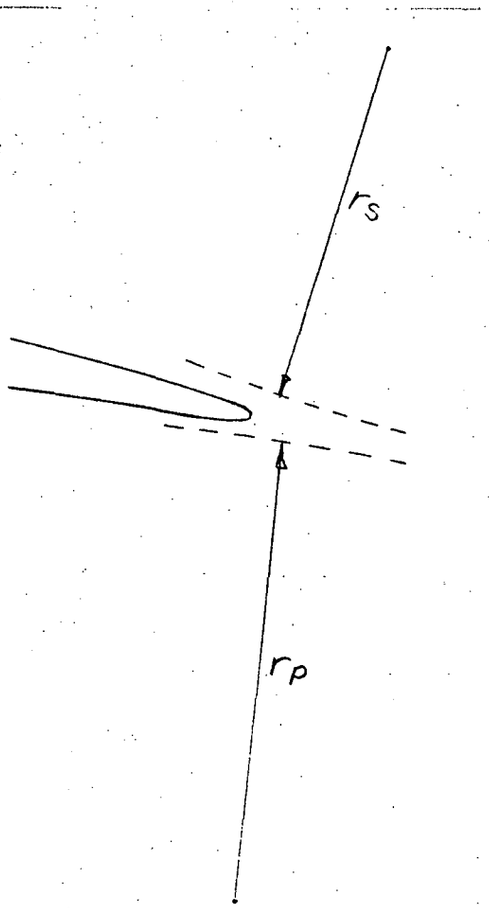

FIG. 5.15

The situation is then as sketched in Fig. 5.15, with a different curvature and velocity distribution for each side of the

wake. With the radius near each edge of the wake large enough, there is a good argument for extrapolating the nearly linear velocity distributions on each side to the middle of the wake (defined as the position of minimum velocity). Approximate displacement thickness values for each side of the wake can then be calculated from the measurements in the same sort of way as for uniform velocity outside the wake, except that the potential flow distribution is taken as varying linearly. This approximate method was used by Boxhall and Nilsson (Ref. 14) to determine values of δ^* for the I.G.V. wake (Section 3.5) and is illustrated in Fig. 3.11.

5.6.2 Vortex Sheet Models of the Wake

The above model has been extended by Oliver (Ref. 22) to include the wake by defining a vortex sheet (positioned at the displaced surface) to represent each side of the wake. This is equivalent to approximating the rather odd shape of the wake profile by a rectangular distribution which satisfies the same continuity requirements as the real flow - see Fig. 5.16. This is a very attractive model and is easily incorporated into the discontinuity methods of flow calculation described above.

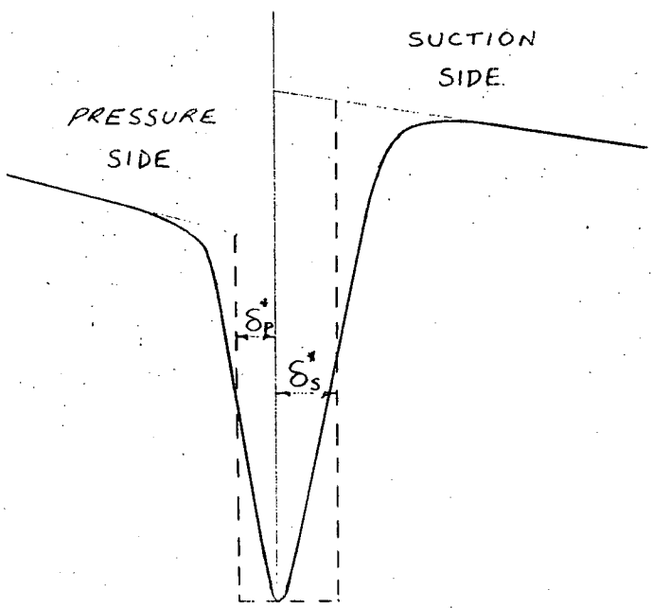

FIG. 5.16 SINGLE VORTEX SHEET MODEL OF WAKE

However, the single vortex sheet model is limited in application as, although it satisfies the flow deficiency requirement of the real wake, there is no allowance for the momentum deficiency. It could therefore not be used in the context of the current investigations,

where it is desired, for example, to examine the fluctuations in pressure on a blade due to the influence of wakes from an upstream row.

Both the flow deficiency and momentum deficiency requirements can be satisfied by introducing a second vortex sheet on each side of the wake. Oliver has found it convenient to arbitrarily place the inner vortex sheet for each side at the wake centre. The position of the outer vortex sheet on each side is then determined and is given by

$$d/\delta^* = H/(H-1) \qquad \ldots\ldots(5.4)$$

where d is the distance of the outer vortex sheet from the wake centre and H is the shape factor δ^*/θ.
The two vortex sheet model is illustrated in Fig. 5.17

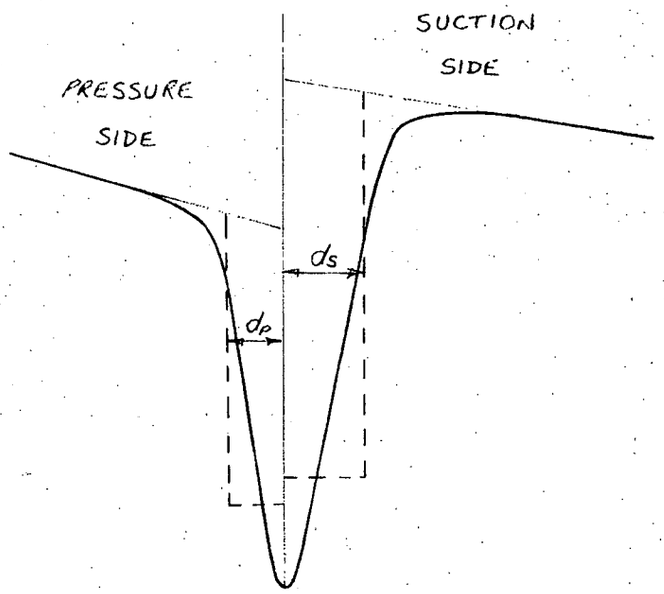

FIG. 5.17 TWO VORTEX SHEET MODEL OF WAKE

5.7 Boundary Layer and Wake Thickness Model

At the same time as Oliver was contemplating the development of a vortex sheet model of the wake, the author decided to investigate the effect of extending the vortex-source model developed in Section 3.6 just to include the extra thickness effect due to the rotor blade boundary layer and wake.

The importance of blade thickness effects has been demonstrated above. Upstream of the rotor, over 50% of the "potential flow" velocity defect can be attributed to thickness effects (Section 3.6.5) - downstream, 30% - 40% (Section 4.5.1). Possibly a more interesting effect was the

large shift in the position of the downstream velocity minimum with the addition of the blade thickness sources to the thin aerofoil potential flow model. The inclusion of the boundary layer and wake thickness effects might therefore be expected to significantly alter the predicted potential flow velocity distribution.

5.7.1 Determination of Displaced Surface

The vortex-source model programme was revised to include a further row of sources representing the relative rotor wake distributed along a straight line extending from the trailing edge. All source strength values were calculated using thickness gradients, $dz/d\xi$, determined from an approximate construction of the effective blade shape, i.e. the displaced surface.

The displaced surface for the relative rotor wake was assumed to be the same as for the stator wake. Approximate values of the displacement thickness δ^* for each side of the wake were first calculated from the measured stator wake profiles using the curved flow approximation of extrapolating the free stream velocity distributions for each side to the centre of the wake as described above. The corresponding values of δ^*, obtained by numerical integration in the same way as for a boundary layer using Eq. (5.1), are plotted against axial position in Fig. 5.18.

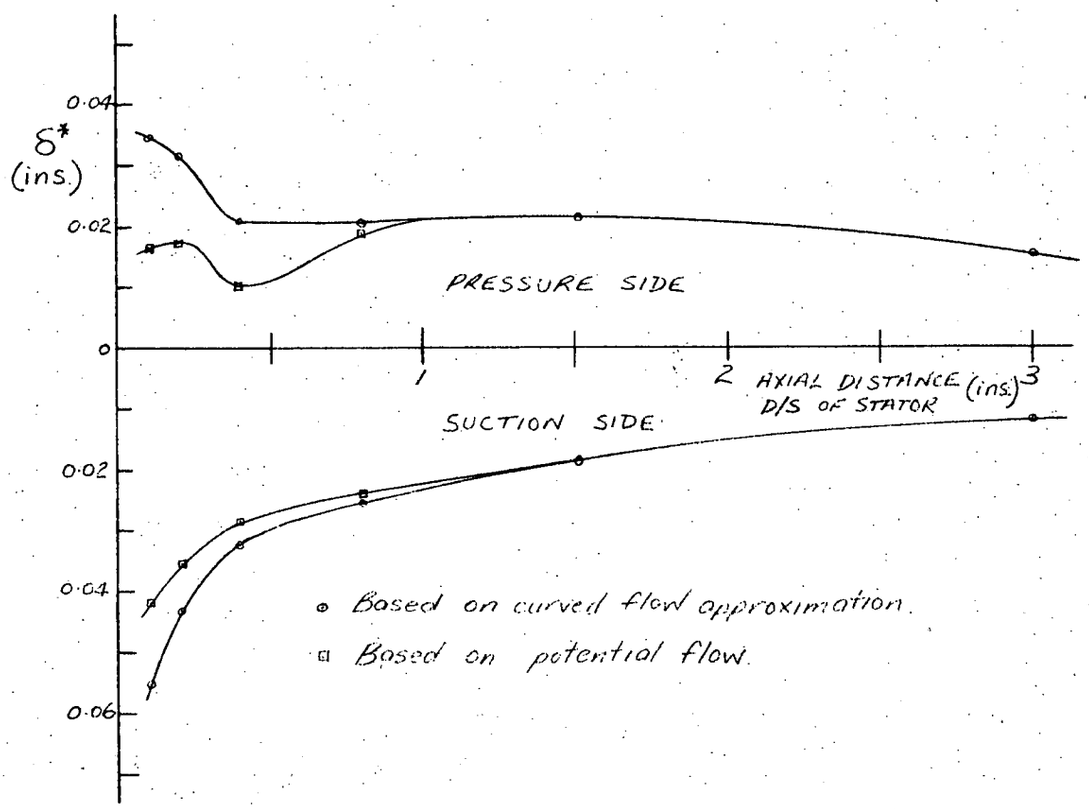

FIG. 5.18 STATOR WAKE DISPLACEMENT THICKNESS

A second approximate set of δ^* values was determined in a similar way, but using Q values obtained from the Wilkinson model potential flow velocity distributions. This was done only to introduce the general effect of a significant and varying "potential flow" velocity defect, which is not obtained (in the case of the stator wake) using the above method of extrapolating the measured free stream distributions. For convenience, the potential flow curves were superimposed on the measured curves by aligning the positions of minimum velocity. In the other direction the two mean velocities were aligned. The situation was then as sketched in Fig. 5.19. The values of δ^* for each side of the wake were determined by applying Eq. (5.1) between the wake centre and the points A. (The numerical integration therefore included a small section on each side where $1-q/Q$ was negative.)

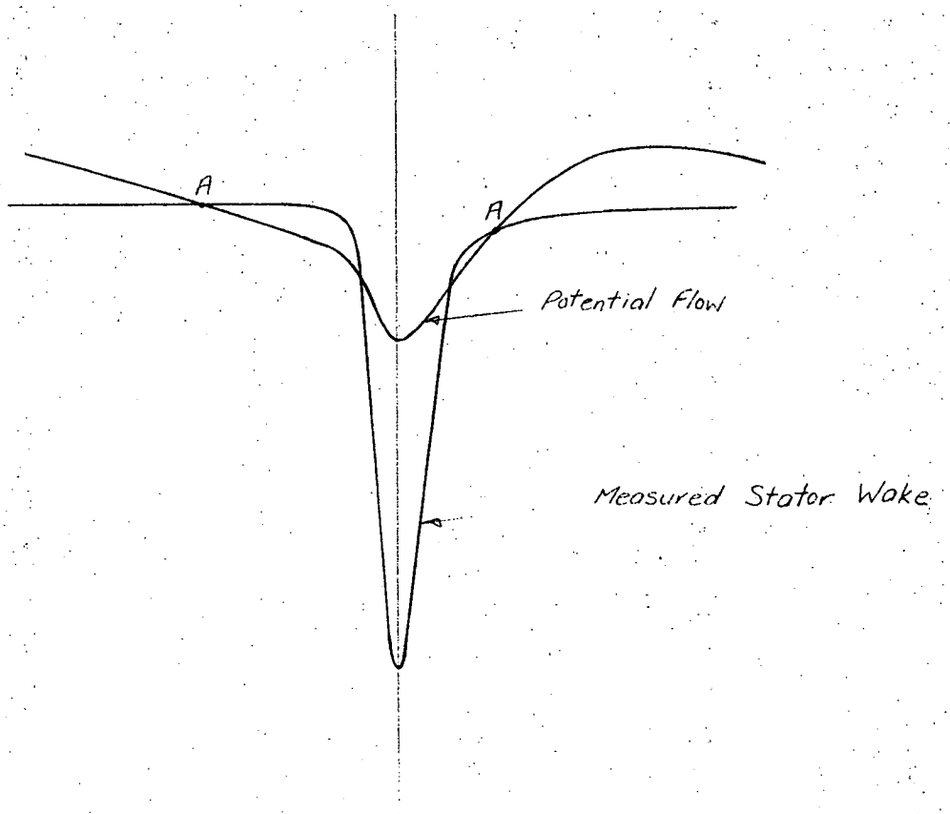

FIG. 5.19

The author does not suggest that this is possibly a suitable definition of the wake displacement thickness. It is intended only to give approximate values of a δ^* based on the idea of a flow deficiency with respect to the "potential flow" velocity distribution. The values of the displacement thickness calculated by the second method are also shown in Fig. 5.18.

An approximate effective rotor blade shape was constructed using

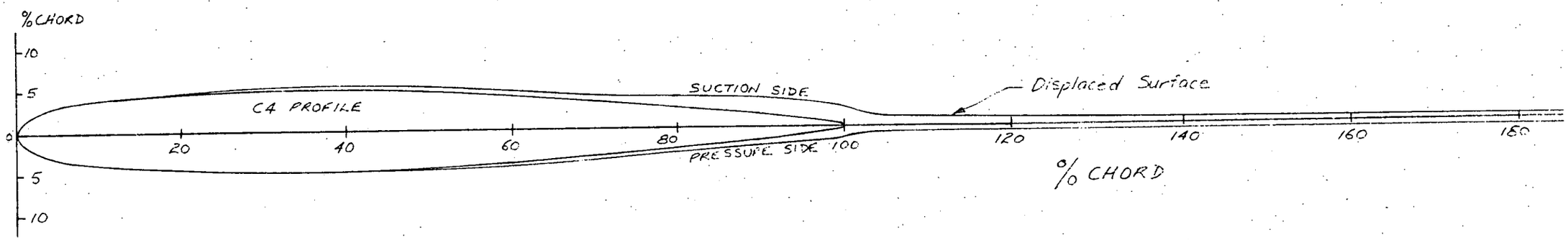

FIG. 5.20 EFFECTIVE ROTOR BLADE SHAPE
(NEGLECTING CAMBER)

1. Wake δ^* values corresponding to the second method of calculation above, but making the approximation of a constant pressure side δ^* of 0.02 ins. for all axial positions.

and 2. Boundary layer δ^* values obtained from a theoretical prediction of the stator blade boundary layer development computed by Oliver (Ref. 13).

The displaced surface near the trailing edge was obtained by a smooth interpolation between the boundary layer δ^* values and the initial wake δ^* values. The effective blade shape construction, after removing camber and wake angle, is shown in Fig. 5.20.

5.7.2 Revised Vortex-Source Model

The previous vortex-source model programme was revised to include m wake thickness sources situated at the mid-points of m equal segments on a straight line, one chord-length long, extending from the trailing edge of the rotor blade at the measured stator wake angle of 21.8 deg. (See Fig. 5.8). For ease of calculation, the slightly curved section of the measured wake centre-line near the T.E. was neglected. The revised geometry for one rotor blade is shown in Fig. 5.21.

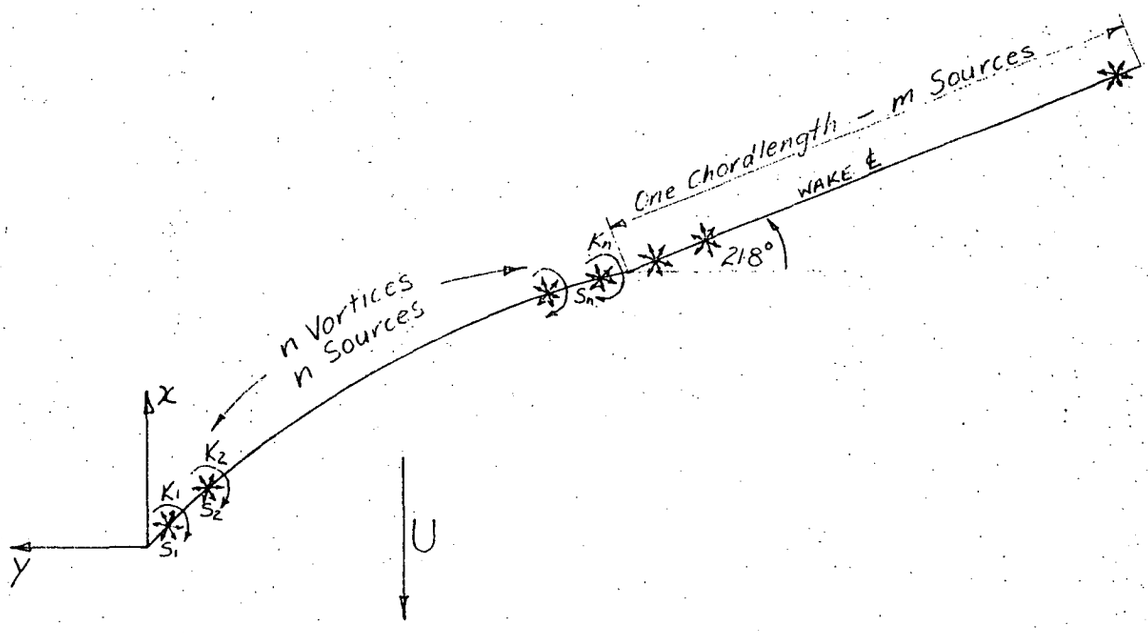

FIG. 5.21 REVISED MODEL OF ROTOR BLADE

New values of the source strength S for the n camber-line and m wake sources were calculated using average thickness gradients estimated from the effective blade shape construction of Fig. 5.20. As the displaced surface was different for each side, the expression

for the source strength became

$$\sigma(\xi) = Q_T\left(\frac{dz}{d\xi}\right)_{\text{pressure}} + Q_T\left(\frac{dz}{d\xi}\right)_{\text{suction}} \qquad \ldots\ldots(5.5)$$

(cf. Eq. 3.9)

Clearly, with the wake displacement thickness tending towards the momentum thickness with increasing distance from the trailing edge, the profile closing condition expressed in Eq. (3.10) was not applicable. (The decay of the effective thickness was such that the contribution of sinks further downstream than about half a chord's length was almost negligible.)

To correctly model the effective blade shape, the sources should, strictly speaking, have been located at positions midway between the two displaced surfaces and not on the blade and wake centre-lines. In the interests of geometrical simplicity, this technicality was ignored.

5.7.3 Comparison Between Original and Revised Model Velocity Distributions

The revised programme was used to compute absolute velocity distributions for the same axial positions downstream of the rotor as considered previously. (Care was taken to ensure that none of the wake source discontinuities corresponded to any of these axial positions.) The absolute velocities were determined, as before, from Eq. 3.14, except that there were now additional source components due to the wake. The circulation values for each vortex were the same as for the original vortex-source model programme, i.e. those obtained from the measured relative velocity distributions.

Figs. 5.22 and 5.23 show comparisons between absolute velocity distributions calculated from the wake model and the original vortex-source model distributions 0.20 ins. and 0.40 ins. downstream of the rotor. The wake model computation was carried out with 30 sources (and vortices) along the camber-line and 30 sources along the wake segment.

The wake model velocity distributions are only meaningful outside the actual wake regions, as in this kind of consideration, the displaced surface representing the wake is treated as forming part of an effective blade profile. The model is designed only to indicate the effect of the wake on the flow outside it.

Apart from an overall increase in the mean velocity of about 0.8%, the allowance for the extra effective thickness due to the boundary layer and wake has the effect of increasing the downstream velocity defect and shifting the positions of maximum defect closer to the wake. For the axial position 0.20 ins. downstream, the increase in velocity defect is over 60% and there is a distinct "valley" similar in shape to the measured wake profile (see Fig. 4.2). This is a result of the rapid decrease in effective thickness in the region of the blade T.E.

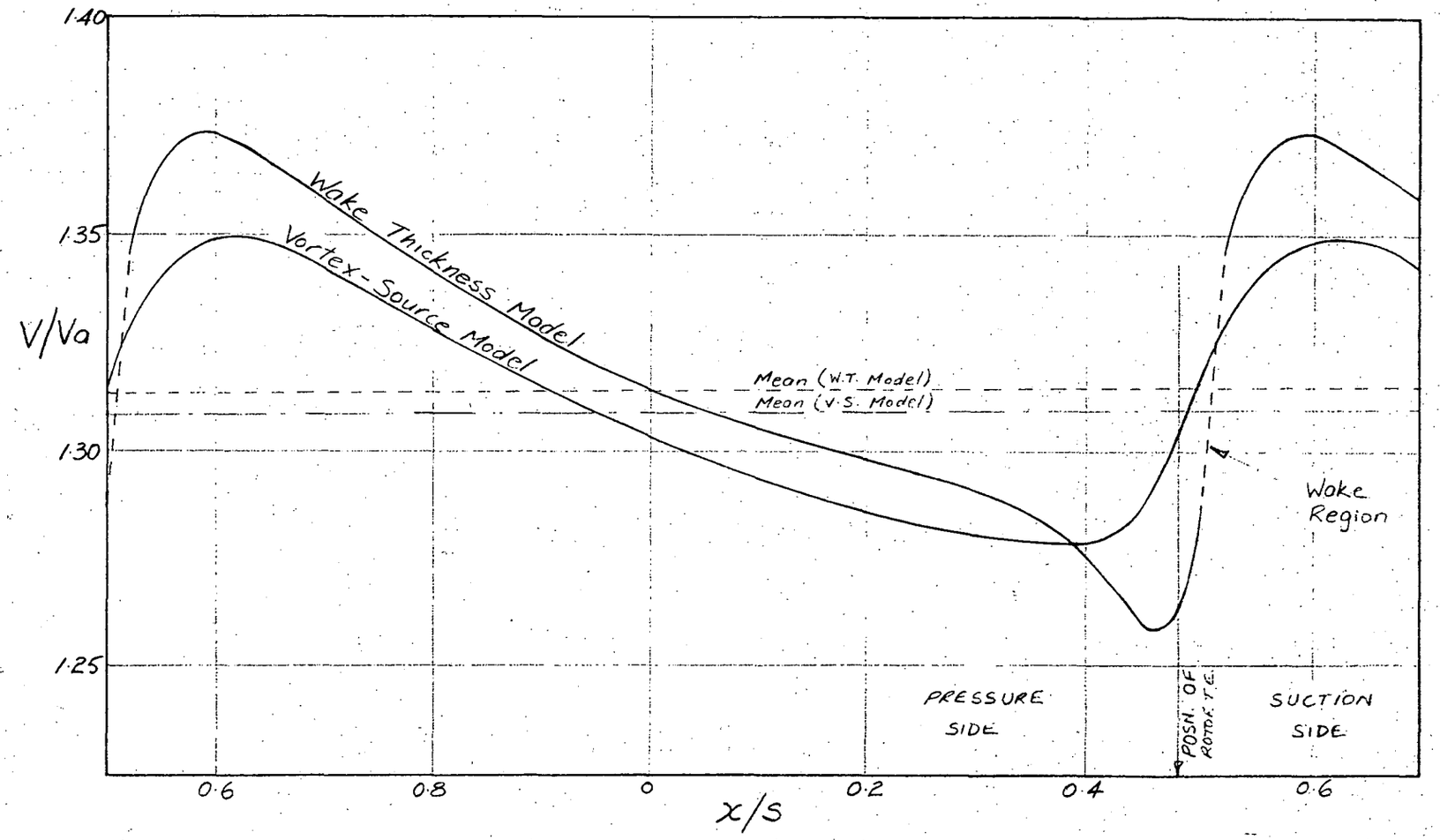

FIG. 5.22 COMPARISON BETWEEN ORIGINAL AND REVISED MODEL VELOCITY DISTRIBUTIONS 0.20 INS. (6.7%C) DOWNSTREAM OF THE ROTOR

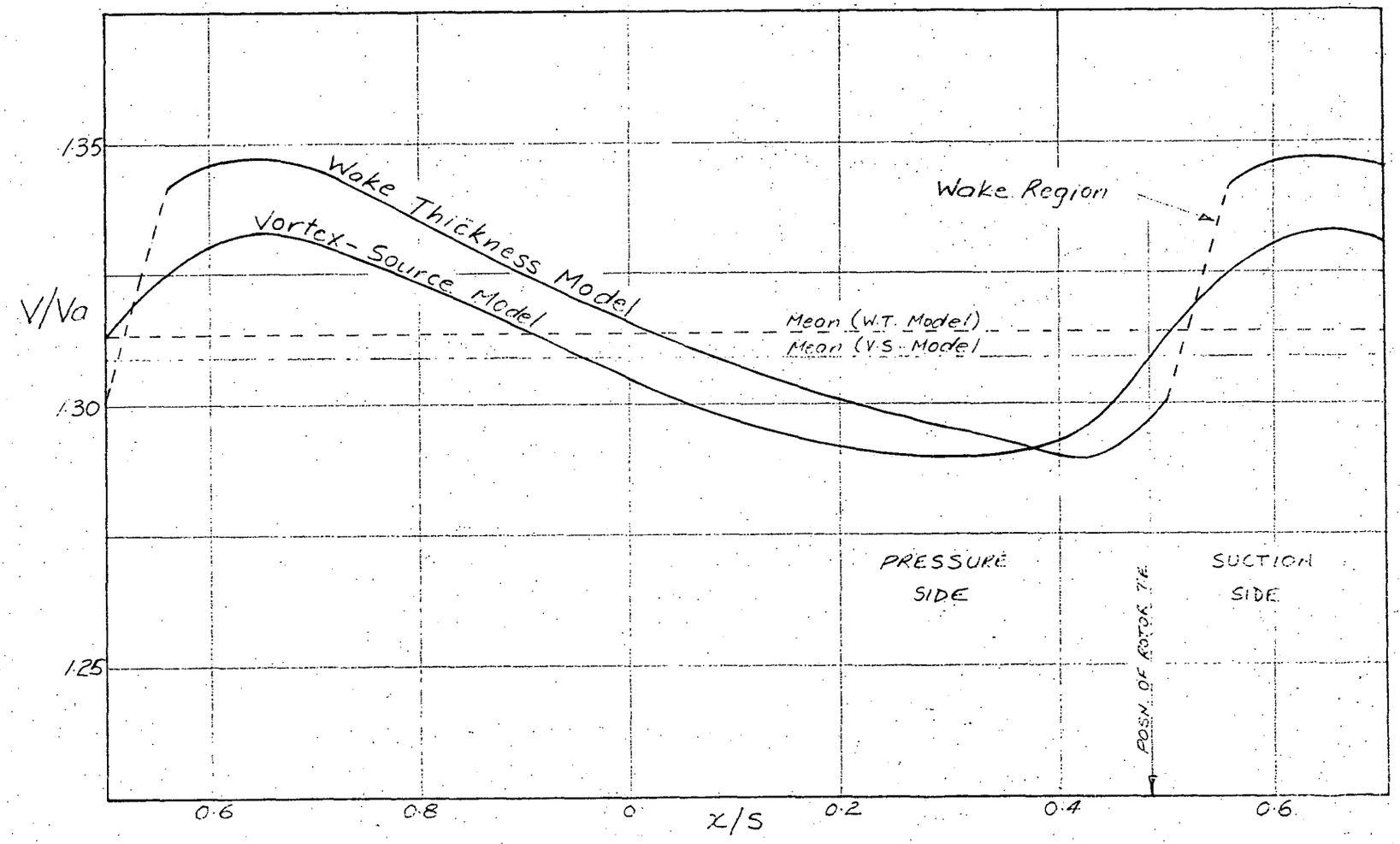

FIG. 5.23 COMPARISON BETWEEN ORIGINAL AND REVISED MODEL VELOCITY DISTRIBUTIONS 0.40 INS. (13.3%C) DOWNSTREAM OF THE ROTOR

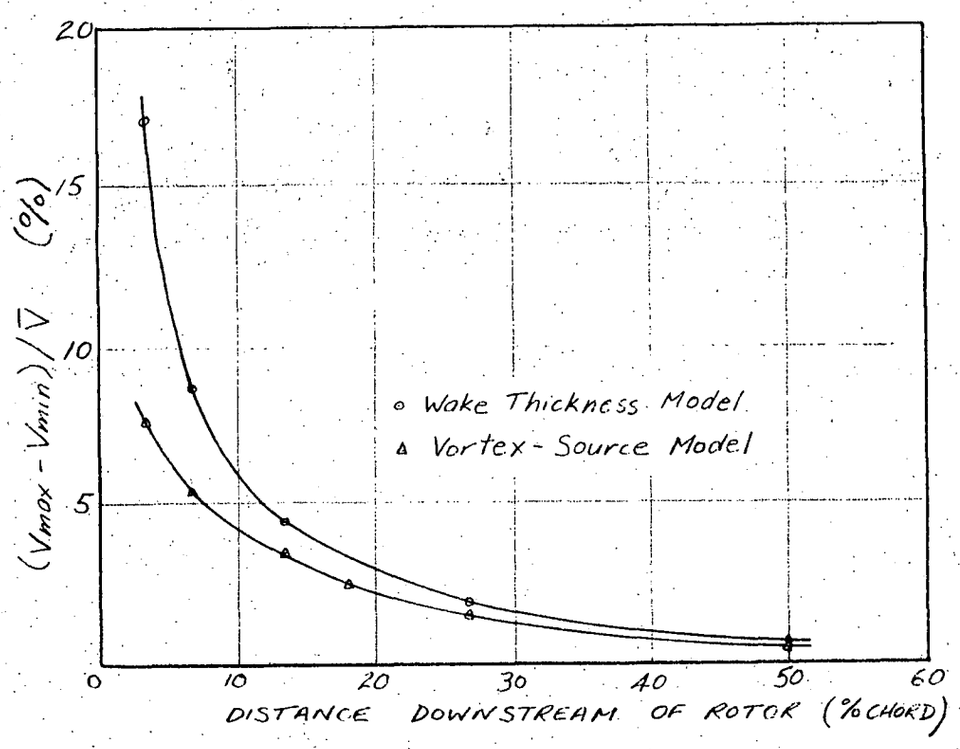

FIG. 5.24 CHANGE IN VELOCITY DEFECT

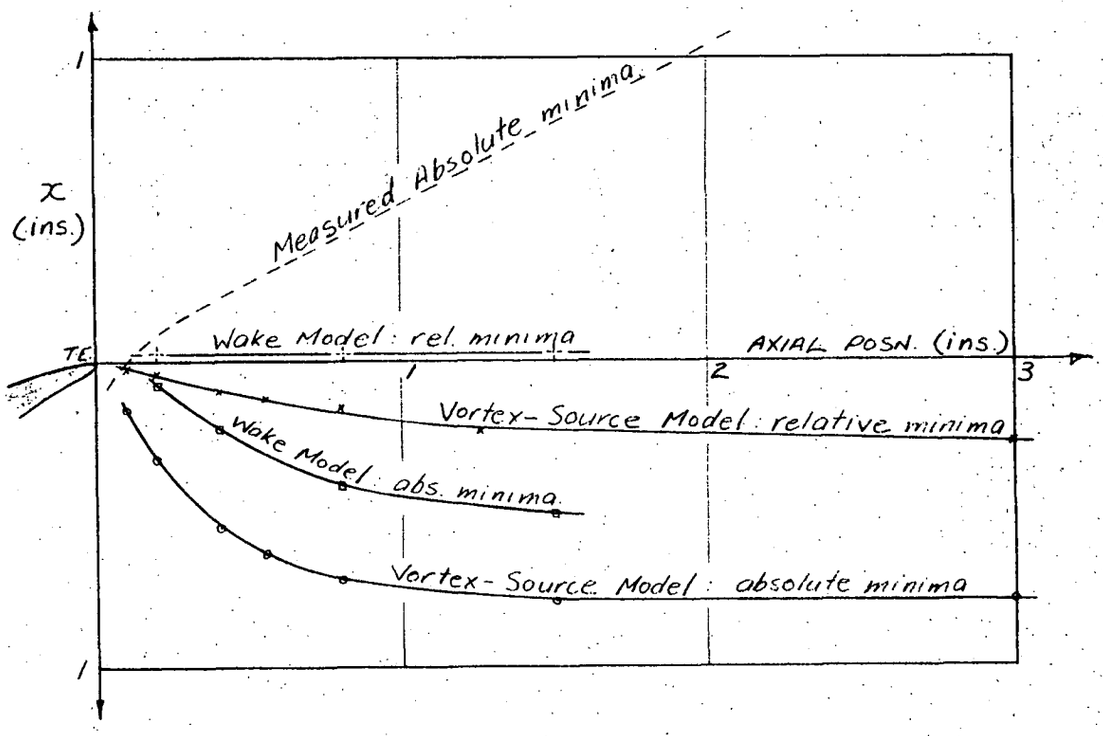

FIG. 5.25 CHANGES IN LOCI OF VELOCITY MINIMA

The increase in velocity defect resulting from the allowance for boundary layer and wake effects is illustrated in the defect decay curves of Fig. 5.24.

Fig. 5.25 shows the change in position of the loci of both the absolute and relative velocity minima. It is observed that the effect of accounting for the boundary layer and wake thickness effect is to shift both loci considerably closer to the position of the relative stagnation streamline - particularly for the relative velocity minima. This is indicative of the likely effect of the presence of the wake on the actual "potential flow" velocity distribution downstream of the rotor (and stator). With the additional effect of the vorticity in the wake (neglected in the thickness model) it is possible that the true "potential flow" relative velocity minima do, in fact, lie very close to the line of maximum relative wake defect (which is expected to correspond closely to the stagnation streamline.)

The model of the effective blade shape developed above is only approximate. As explained above, the thickness sources should really be located on the centre-line of the equivalent blade profile and not on the original blade and wake centre-lines. The boundary layer δ^* values were theoretical estimates only, and the wake δ^* values were also, of necessity, approximate, as it was not possible to formulate a satisfactory definition of the displacement thickness for a blade wake.

CHAPTER 6

COMPRESSOR NOISE INVESTIGATION

6.1 Introduction

As part of the overall study of unsteady flow in the Vortex Wind Tunnel, the author carried out a brief investigation of the compressor noise generated as a result of blade row interaction effects. Initially, the main object was to examine the change in the measured noise spectrum in the vicinity of the working section, when the axial clearance between the I.G.V. and rotor rows was changed from the usual 3.55 ins. (1.18C) to 1.55 ins. (0.52C). The author later decided to take further measurements to investigate possible variations in the generated noise with different relative peripheral settings of the I.G.V. and stator rows. The results of this later study were extremely interesting and indicated a very simple technique for considerably reducing the noise generated in any axial flow machine.

6.2 Measurements

The noise measurements were carried out with a Rohde & Schwarz sound level meter used in conjunction with a Muirhead wave analyser. The microphone was aligned radially on the horizontal diameter of the tunnel, about 6 ins. from the middle of the intake screens (Fig. 6.1).

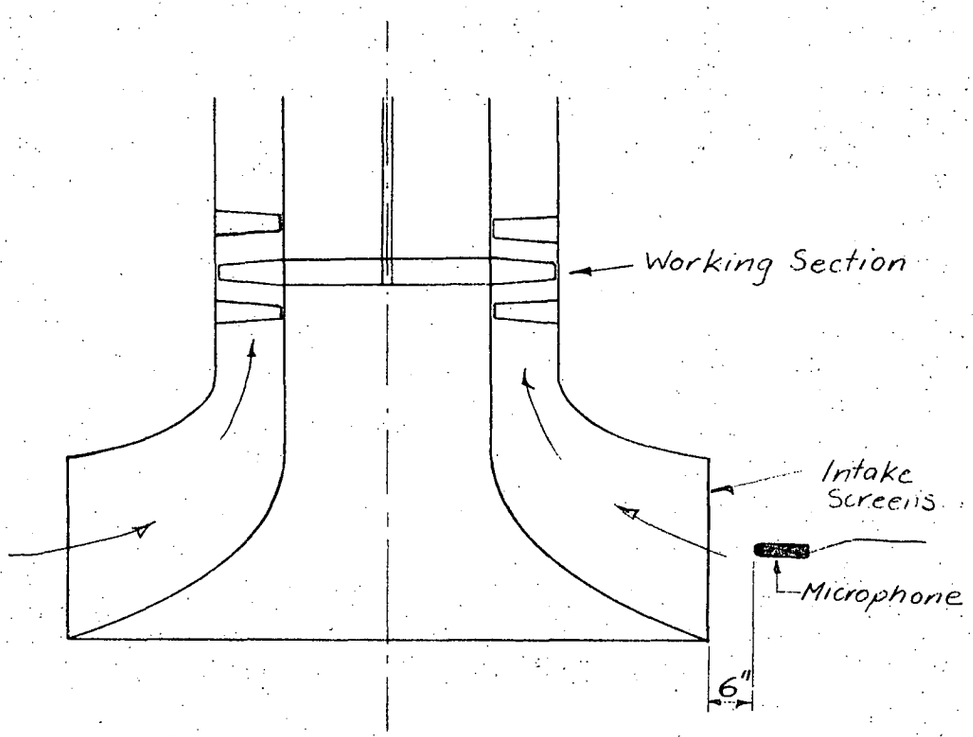

FIG. 6.1 NOISE LEVEL TEST POSITION

The instruments were used to measure the overall sound pressure level in decibels (dB) and the third octave bandwidth frequency response at the test position, with the compressor operating at 500 r.p.m., for:

1. the usual I.G.V./rotor clearance of 3.55 ins. (1.18C)
2. an I.G.V./rotor clearance of 1.55 ins. (0.52C)

The rotor/stator clearance was the same in both cases - about 3.6 ins. Some measurements were also taken for a compressor speed of 750 r.p.m.

6.3 Results and Discussion

6.3.1 Sound Pressure Levels

The sound pressure readings (representing the overall noise level) for the two different I.G.V./rotor spacings are summarized in the following table. For readers not familiar with the logarithmic decibel scale, it may be of help when examining the results to note that:

(1) a difference of 1 dB means a factor of 1.12;
(2) a difference of 6 dB means a factor of 2;
(3) a difference of 20 dB means a factor of 10.

TABLE 6.1
Sound Pressure Readings (dB)

I.G.V./ROTOR SPACING (ins.)	AMBIENT NOISE	WARD-LEONARD CONTROL ONLY[1].	500 R.P.M.	750 R.P.M.
3.55	65	80	85.0	97.5
1.55	65	80	93.8	101.0

At 500 r.p.m. there is an increase in the overall sound pressure level of 8.8 dB with the 2 in. reduction in the I.G.V./rotor spacing. The sound pressure levels quoted above for operation at 500 r.p.m. and 750 r.p.m. include the small level of ambient noise and the noise due to the Ward-Leonard control. However, the logarithmic scale is deceiving, and it can be shown that, except in the case of the small 85.0 dB total, the contribution of these other noise sources to the measured sound pressure level is negligible - i.e. the actual sound pressure levels generated by the compressor itself are almost the same as the values of the total levels. A rough calculation, based on the summation of pure tones, indicated that in the case of the 85.0 dB sound pressure level for 3.55 ins. row clearance and 500 r.p.m., the noise level due to the compressor alone would not be more than 2 dB less than the total level.

1. The Ward-Leonard speed control was situated about 10 ft. beyond the D.C. motor at the far end of the tunnel.

Hence, at 500 r.p.m., there is an increase of the order of 10 dB in the overall sound pressure level generated by the compressor with the reduction of just over one half in the I.G.V./rotor spacing. This represents an increase in the noise level at the measuring point by a factor of about 3 and must be attributed largely to blade row interaction effects. The results of Sections 3.3 and 4.5 suggest that the "potential flow" interaction effects between the I.G.V. and rotor rows will still be almost negligible at 1.55 in. row clearance. It would therefore appear that the very large increase in generated noise is due mainly to the greater interaction effect of the I.G.V. wakes with the downstream rows. The results also indicate that wake interaction effects are a very significant, if not perhaps the most significant, factor in the generation of noise in axial flow machines.

At 750 r.p.m., the relative increase in the sound pressure level with the reduced I.G.V./rotor spacing is considerably less than that at 500 r.p.m.; the 3.5 dB change represents an increase by a factor of only 1.5. It is interesting to note, in the light of the above discussion, that the I.G.V. (and other) wakes are thinner at this higher speed. However, it is possible that, at 750 r.p.m., the noise generated as a result of I.G.V. wake interaction effects is a lower proportion of the total noise produced by the compressor.

6.3.2 Frequency Response Curves

Fig. 6.2 shows the measured third octave bandwidth frequency response at the test station for the two different I.G.V./rotor spacings for the compressor speed of 500 r.p.m.[1]

The most significant feature is the very large amplitude peak at the band frequency of 320 Hz. for 1.55 ins. I.G.V./rotor clearance, which is virtually non-existent in the case of the larger clearance. This band frequency corresponds to the rotor blade passing frequency (b.p.f.), 308 Hz. at 500 r.p.m.,[2] and the peak clearly represents increased noise due to blade row interaction effects associated with the rotor movement - as deduced from the overall sound pressure level measurements in the previous discussion. As indicated above, the main mechanisms of noise generation are likely to be associated with:

1. the passage of the rotor blades through the I.G.V. wakes; and
2. the passage of the rotor wakes over the stator blades.

At 94 dB the peak amplitude, corresponding to the noise

---

1. The points in Fig. 6.2 are plotted for the band centre frequencies.
2. The actual single frequency corresponding to the peak was determined using the wave analyser and was found to be the same as the calculated rotor b.p.f., i.e. 308 Hz.

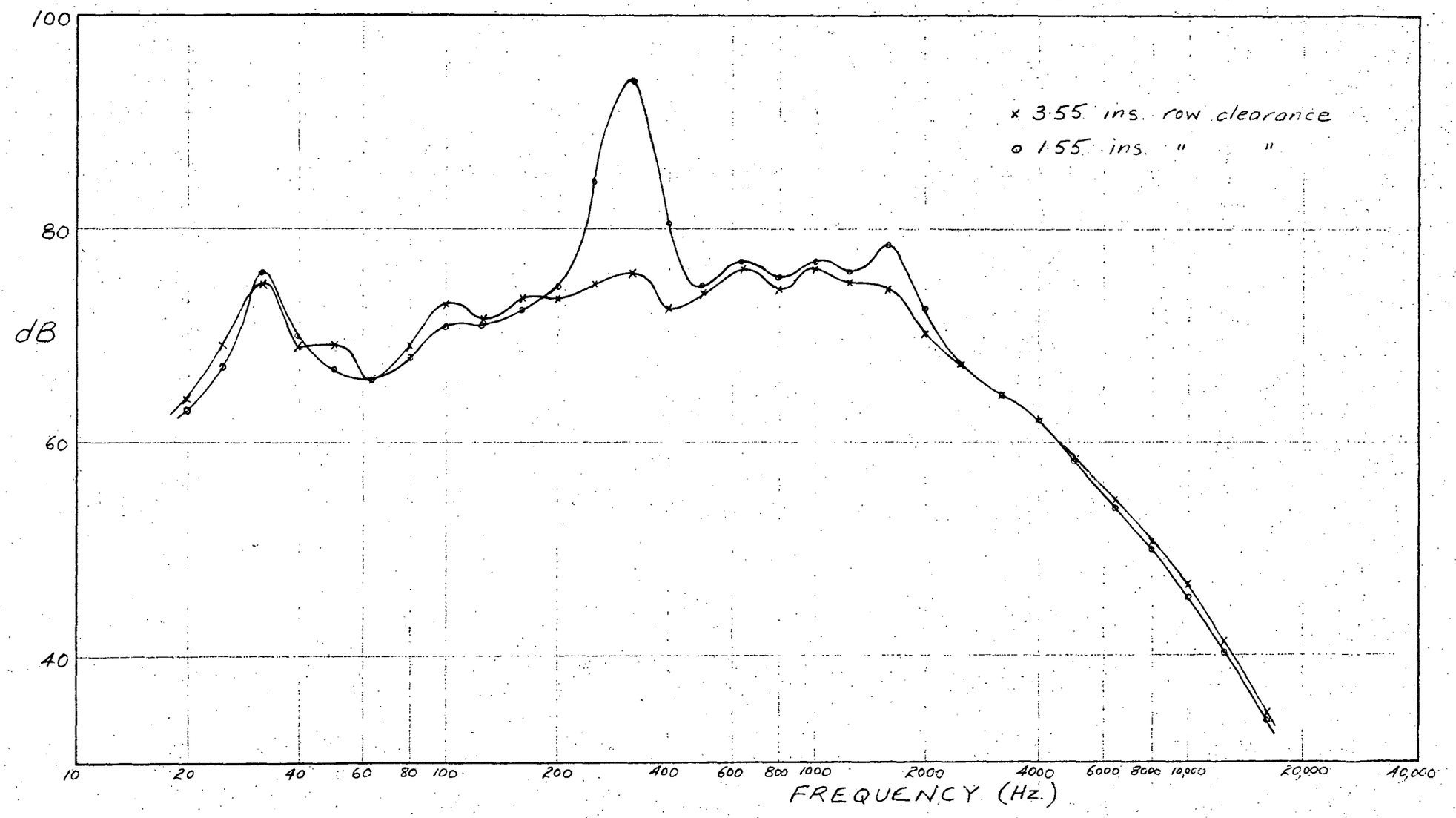

FIG. 6.2 THIRD OCTAVE BANDWIDTH FREQUENCY RESPONSE

generated by blade row interaction effects, represents almost 10 times the level at any other frequencies outside the general region of the peak for the 1.55 in. row clearance, and also about 10 times the level corresponding to the rotor b.p.f. for 3.55 ins. row clearance. The lack of a prominent peak at the rotor b.p.f. for the row clearance of 3.55 ins. indicates that interaction effects due to the rotor movement are apparently no more significant than other noise generating effects for this row spacing.

Other noticeable features of the frequency response curves of Fig. 6.2 are the secondary peaks at band frequencies of 620 Hz, 1000 Hz. and 1600 Hz. These correspond to higher harmonics of the rotor b.p.f. The relatively large peak at the band frequency of 32 Hz. was due to background noise generated by machinery in an adjoining laboratory.

6.4 Effect of the I.G.V./Stator Peripheral Relationship on Noise Generated

A further series of measurements was performed to investigate the effect, if any, of different peripheral relationships between the I.G.V. and stator rows on the noise generated by the compressor.

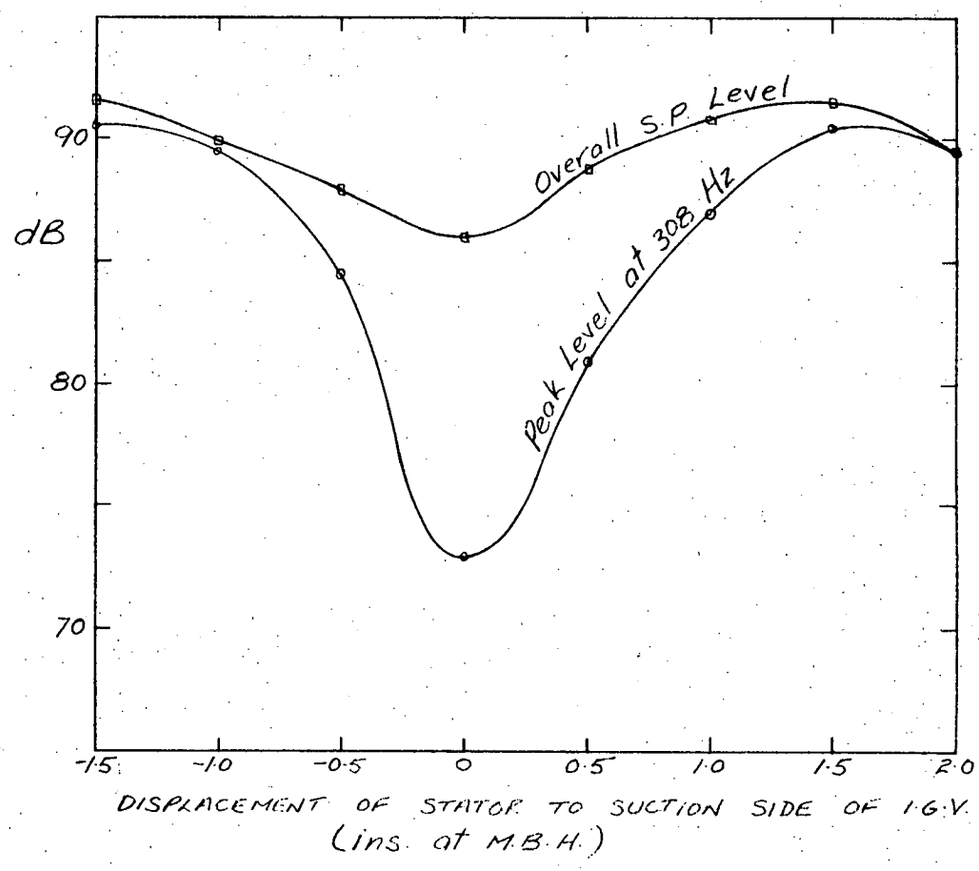

FIG. 6.3 VARIATION OF SOUND PRESSURE LEVEL WITH I.G.V./STATOR PERIPHERAL RELATIONSHIP

Fig. 6.3 shows plots of:

1. the overall sound pressure level,

and 2. the sound level at the peak frequency of 308 Hz.

recorded at the test point for different relative positions of the I.G.V. and stator rows at a compressor speed of 500 r.p.m. The displacements are quoted in inches at mid blade height and the zero corresponds to each stator blade centre situated axially downstream of a guide vane centre.

The curves of Fig. 6.3 indicate that the noise generated by the compressor varies considerably, depending on the peripheral position of the stator blades relative to the I.G.V. wake segments. The variation of 17.5 dB in the 308 Hz peak level represents a change between the two extreme positions by a factor of 7.5, and shows that interaction effects associated with the rotor movement are involved.

It is possible that the effect is due to a considerable reduction in the noise generated by the interaction between the rotor wakes and the stator when the stator blades are immersed in the I.G.V. wake avenues. This could be explained by the reduction in the rotor wake velocity defect which occurs within the I.G.V. wake avenue, as observed in the I.G.V. wake traverse of Fig. 4.6 (see Section 4.4).

The results presented above represent the situation at one particular test station only. At any given position in the room the measured noise levels and the changes produced by altering the positional relationships between the blade rows are determined by the standing wave pattern set up, and will therefore vary from point to point. Hence the actual magnitudes of noise levels quoted above are of limited significance.

Nevertheless, the curves of Fig. 6.3 do suggest that the overall noise generated by the compressor varies significantly with changing relative peripheral positions of the I.G.V. and stator rows and that there is some optimum positional relationship between the two for which the overall noise generated is a minimum. It would also seem that the rotor wake/stator interaction is the main mechanism of noise generation in the compressor.

In view of the above results, it is very likely that the large measured increase in noise produced by the 2 in. reduction in the I.G.V./rotor spacing shown in Table 6.1, was due in part to the corresponding change in the peripheral position of the stator relative to the I.G.V. wake avenues and not just to the general increase in the magnitude of I.G.V. wake effects at the positions of the downstream rows.

Clearly, a more detailed investigation of the noise level changes described above is required. However, it does appear likely that by

suitably adjusting the relative peripheral settings of the stationary blade rows in any axial flow machine, it is possible to significantly reduce the level of noise generated by blade row interaction effects.

CHAPTER 7

CONCLUSIONS

"Potential Flow" Unsteadiness

Hot wire measurements upstream of the rotor have shown that the movement of the rotor blades causes large variations in velocity with time. For the flow conditions adopted for the investigations the absolute velocity defect 0.03 chord-lengths upstream was nearly half the mean velocity. Some variation was still evident 0.7 chord-lengths upstream. It was not possible to measure directly the "potential flow" velocity variation downstream of the rotor because of the presence of the rotor wakes. However, a consideration of measurements and potential flow model calculations has indicated that "potential flow" absolute velocity defects downstream of the rotor are only about 20% of the defects for corresponding positions upstream. This implies that "potential flow" interaction effects on a blade row due to the presence of an upstream row will be insignificant compared with the effects of a downstream row (provided there are no great differences in the row spacings). Further measurement of the "potential flow" unsteadiness for a wide range of rotor blade shapes and settings and flow conditions is required before these aspects can be considered sensibly in a design situation. (Potential flow calculations discussed in Section 3.5.3 have shown that a small change in incidence is likely to considerably alter the measured velocity defect upstream of the rotor).

The measured "potential flow" velocity distributions upstream of the rotor were considered as instantaneous velocity - distance profiles and compared with a potential flow mapping model of the flow through a cascade of thick aerofoils developed by Frith (Ref. 12) and Oliver (Ref. 13). There was a good agreement in both shape and dimensions between the measured and calculated distributions, with differences of only 5-6% between the measured and calculated defects. This was particularly encouraging considering that the mapping model necessitated the use of an approximate blade shape and neglected boundary layer and wake effects.

A simple potential flow model based on a thin aerofoil approximation of the rotor blades has been developed by the author. Initially each blade was replaced by a row of thirty vortices distributed along the camber-line, with circulation values calculated from measured blade surface velocity distributions. This proved to be an inadequate model of the real flow and gave predicted values of the upstream velocity defect of only about half the measured ones. When allowance was made for the rotor blade thickness by adding a row of sources along the camber-line, the predicted upstream velocity distributions showed excellent agreement

with the measurements - even better than for the mapping model. There also appeared to be good agreement between the vortex-source model and measured velocity distributions downstream of the rotor for the region outside the rotor wakes.

The development of the vortex-source model has shown that the "potential flow" velocity defect upstream of the rotor can be thought of as consisting of two separable components - one due to a circulation effect and one due to a blade thickness effect. For the particular flow conditions considered, the circulation and thickness components each contributed approximately 50% to the overall defect. However, it is likely that different flow conditions and other settings of blades with the same thickness would produce different results. Clearly, further measurement is required, but it would appear that the magnitude of "potential flow" unsteadiness can be considerably reduced by decreasing the blade thickness as much as other design considerations will allow.

The mapping model and vortex-source model predictions of the "potential flow" velocity distribution downstream of the rotor differed significantly, in contrast to the excellent agreement upstream. There were differences of 10-15% in the predicted velocity defects. This has been attributed to differences between the two models in the flow conditions in the region of the blade trailing edge, e.g., blade shape and position of the rear stagnation point. All three models used in this thesis - Frith mapping, vortex-source and Wilkinson - were based on different assumptions as regards the position of the rear stagnation point. The mapping model incorporated the Kutta-Joukowski condition which fixes the rear stagnation point at the trailing edge. The vortex-source model was based on measured blade velocity distributions and the effective rear stagnation point position for this model should therefore have been approximately the same as for the real flow conditions. In the Wilkinson model the position of the rear stagnation point is determined by equating the vortex strengths at the corresponding discontinuities on the suction and pressure surfaces nearest the trailing edge. Until more detailed investigations are carried out to ascertain the true situation regarding the position of the rear stagnation point in unsteady flow, it is not possible to say which of the above models is likely to give the best approximation of the real flow. The vortex-source and Wilkinson models are more versatile than the Frith mapping model in that they can readily be extended to take into account boundary layers and wakes and also three dimensional effects.

The Rotor Wake

The hot wire measurements performed downstream of the rotor have shown that the "potential flow" and rotor wake absolute velocity

variations add in such a way as to produce a pronounced velocity peak on the suction side of the wake at positions near the rotor trailing edge. The measured absolute rotor wake defect was only about 12% of the mean velocity and approximately constant with axial position from the trailing edge to 0.5 chord-lengths downstream. This was, at first, surprising in view of the large and rapidly changing relative wake velocity defects observed in measurements near the T.E. of stationary blade rows. However, an examination of the velocity diagram indicated that results similar to those measured could be expected in the absolute flow. The locus of the absolute wake velocity minima corresponded to the expected relative rotor wake centreline, i.e. the stagnation streamline, up to a position 0.08 chord-lengths from the rotor, but tapered off to the pressure side and away from the trailing edge closer to the rotor.

Traverses through the I.G.V. Wake

Hot wire traverses through the I.G.V. wake both upstream and downstream of the rotor have been presented. The I.G.V. wake was evident as turbulent fluctuations superimposed on the mean velocity-time curve due to the rotor movement. The non-uniform distribution of the wake turbulence over traces detected by hot wires situated near the edges of the I.G.V. wake, both upstream and downstream of the rotor, has shown that the motion of the rotor apparently causes an oscillatory variation in the position of the I.G.V. wake. This needs to be examined in more detail.

The I.G.V. wake traverse revealed that there was no change in the "potential flow" velocity variation upstream of a rotor blade and hence apparently no change in blade circulation as it passed through the I.G.V. wake. It has been suggested that the passage of the blade through the wake may be associated with changes in the position of the rear stagnation point, but that these occur too quickly for corresponding changes in the circulation to eventuate and the latter settles on some mean value. General doubts regarding the applicability of the Kutta-Joukowski condition in unsteady flow have been raised.

Unlike the situation upstream, the mean velocity-time distribution downstream of the rotor varied significantly with position in the I.G.V. wake avenue. There was a considerable drop in the measured velocity defect - possibly as much as 50% - detected by a hot wire situated near the centre of the wake avenue. The observed changes may have been due to a variation in the general flow pattern around the rotor blade, such as movement of the rear stagnation point, which noticeably affected the flow downstream of the rotor, and not upstream. (Flow model calculations have shown that the "potential flow" downstream of a cascade blade is likely to be extremely sensitive to the conditions at the trailing edge.) Alternatively, the changes in the

velocity profile may have been the result of local interaction between the I.G.V. and rotor wakes at the measuring position to produce a smaller rotor wake defect - this could possibly be accounted for by the change in flow angle across the I.G.V. wake which would allow the same relative wake velocity defect to correspond to varying absolute defects. Some information on the variation in flow angle across a blade wake is required before this possible explanation can be investigated further.

The clearance of over one chord-length between the I.G.V. and rotor rows was unusually large. It is possible that, for smaller row spacings, there may be observable changes in the upstream velocity distribution due to changes in the flow pattern around the rotor blade on passage through the I.G.V. wake. The traverses both upstream and downstream of the rotor should be repeated for the smallest possible I.G.V./rotor spacing.

Velocity Distribution Downstream of the Stator

Measurements of the velocity distribution downstream of the stator have shown that the stator wake apparently creates a free stream velocity gradient which, near the trailing edge, adds to the "potential flow" distribution to give almost uniform velocity outside the wake. The gradient can be thought of as being induced by a net total vorticity in the wake. Surprisingly, the phenomenon is not evident in measurements of the I.G.V. wake, although dissimilar wake behaviour can be expected because of the difference in flow conditions for the two rows. A more thorough experimental investigation of the effect of the blade wakes on the flow outside them is warranted.

The velocity distribution downstream of the stator has been found to vary, depending on the relative peripheral settings of the I.G.V. and stator rows. The results of the noise study presented in Chapter 6 suggest that this may be due to the change in the effect the rotor wakes have on the flow around the stator blades when the I.G.V. and rotor wakes interact. Unfortunately, the main evidence of the change in the velocity distribution consists of measurements performed with a Conrad three hole pressure probe by Johnston and Lockhart (Ref. 20). More accurate and detailed measurement with a hot wire probe should prove valuable.

Rotor Wake Model

It has been shown that considerable difficulty arises in attempting to define a displacement thickness δ^* for a blade wake in the same way as for a boundary layer, particularly in the region close to the trailing edge. Here the wake is unsymmetrical, with the velocity outside the wake usually different for each side. There is a large "potential flow" velocity defect in the vicinity of the wake (10-20% of the wake defect) and the potential flow velocity distribution is, itself, likely to be significantly affected by

the presence of the wake. Approximate displacement thickness values for the I.G.V. and stator wakes have been calculated by extrapolating the nearly linear free stream velocity distributions on each side to the centre of the wake. δ^* values for each side of the wake were then determined in the same way as for a boundary layer, except that the potential flow velocity distribution was taken as varying linearly. This method was based on a vortex flow approximation of the curved flow outside the viscous region.

The pronounced effects of accounting for blade thickness in the development of the thin aerofoil model, particularly the large shift in the position of minimum velocity, prompted the author to extend the vortex-source model just to take into account the effective thickness of the rotor blade boundary layer and wake. The relative rotor wake was assumed to be the same as the measured stator wake. The revised model gave large increases in the defect of the absolute "potential flow" velocity distributions downstream of the rotor, e.g. a 60% increase 0.067 chord-lengths downstream. There was also a further significant shift in the positions of the loci of both the absolute and relative "potential flow" velocity minima towards the relative stagnation streamline. It is expected that the true relative minima (if, indeed, it is possible to consider separate "potential flow" and wake components of the velocity distribution) lie very close to the stagnation streamline (and relative wake centreline). The revised vortex-source model was not intended as a practical wake model, but was used only to investigate the effect of the wake on the "potential flow" velocity distribution. The two vortex sheet model suggested by Oliver (Ref. 22) is a more realistic wake model and should prove invaluable in examining many of the unsteady flow problems discussed in this thesis, for example, wake - wake and wake - boundary layer interaction.

Noise Investigation

The results of a brief investigation of the compressor noise generated by blade row interaction effects have proven most interesting. Measurements of the sound pressure level at a test station near the compressor intake screens have shown that there are large variations in the generated noise, depending on the relative peripheral positions of the I.G.V. and stator blades. At the test station, the change in level between extreme values at the rotor blade passing frequency (b.p.f.) was 17.5 dB, representing a change by a factor of 7.5. It was suggested that the effect may be the result of a considerable reduction in the noise generated by the interaction between the rotor wakes and the stator when the stator blades are immersed in the I.G.V. wake avenues - explained by the observed reduction in the rotor wake velocity defect which occurs within the I.G.V. wake avenue.

The effect of reducing the clearance between the I.G.V. and rotor rows from 1.18 chord-lengths to 0.52 chord-lengths (for a fixed I.G.V./stator configuration) was to increase the overall sound pressure level at the test station by a factor of 3 (10 dB). Frequency response curves showed that this was due almost entirely to a very large change in the component corresponding to the rotor b.p.f. The latter increased from 75 dB to 95 dB - a change by a factor of 10. The peak represented increased noise generated by

1. the passage of the rotor blades through the I.G.V. wakes

and 2. the passage of the rotor wakes over the stator blades.

The results suggest that these are likely to be the main mechanisms of noise generation in an axial flow compressor. Insufficient measurements were taken to determine how much of the increase in noise level with the reduced I.G.V./rotor spacing was due to the general increase in I.G.V. wake effects in the region of the downstream rows and how much was due to an effective change in the I.G.V./stator peripheral relationship.

The noise level measurements need to be repeated in greater detail and for many different test positions so that a more realistic assessment of the magnitude of sound level changes can be made. Nevertheless, it does appear that the noise generated by interaction effects in any axial flow machine can be greatly reduced by suitably adjusting the relative peripheral settings of its stationary blade rows. It is recommended that this research be extended to a wide variety of axial flow machines and, in particular, to high speed machines, such as gas turbines used in aircraft propulsion.

APPENDIX A

MAJOR DIMENSIONS OF THE VORTEX WIND TUNNEL

	I.G.V.	Rotor	Stator
No. of Blades	38	37	38
Core Diameter	27"	27"	27"
Shell Diameter	45"	45"	45"
S/C at Mid Blade Height	0.99	1.02	0.99
Hub Stagger	17.2°	4.2°	37.2°
Mid Blade Stagger	13.9°	29.5°	29.5°
Tip Stagger	11.25°	42.15°	25.1°
Hub Camber	34.40°	52.5°	32.9°
Mid Blade Camber	27.8°	31.1°	31.1°
Tip Camber	24.25°	19.1°	29.4°

APPENDIX B

METHOD FOR GENERATING THICK, CAMBERED AEROFOILS IN CASCADE USING A CLOSED MAPPING FUNCTION - FRITH (REF. 12)

A closed mapping function is used to transform the unit circle in the ζ or circle plane into a cascade of thick cambered aerofoils in the z or cascade plane.

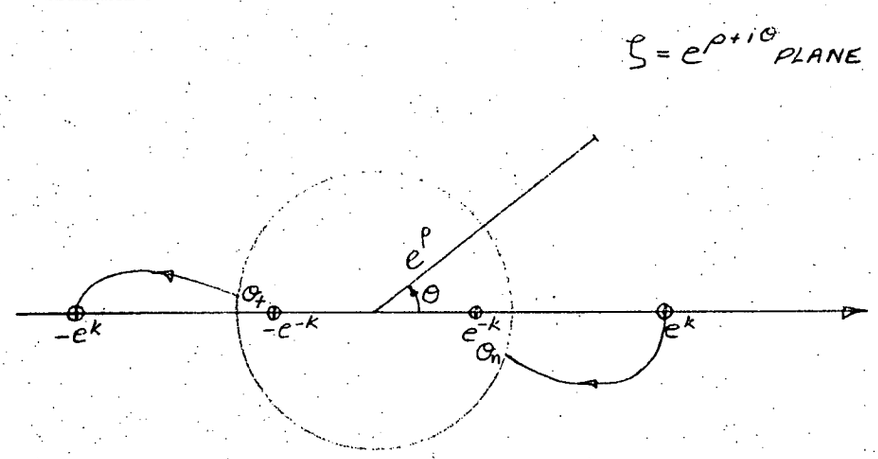

THE CIRCLE PLANE

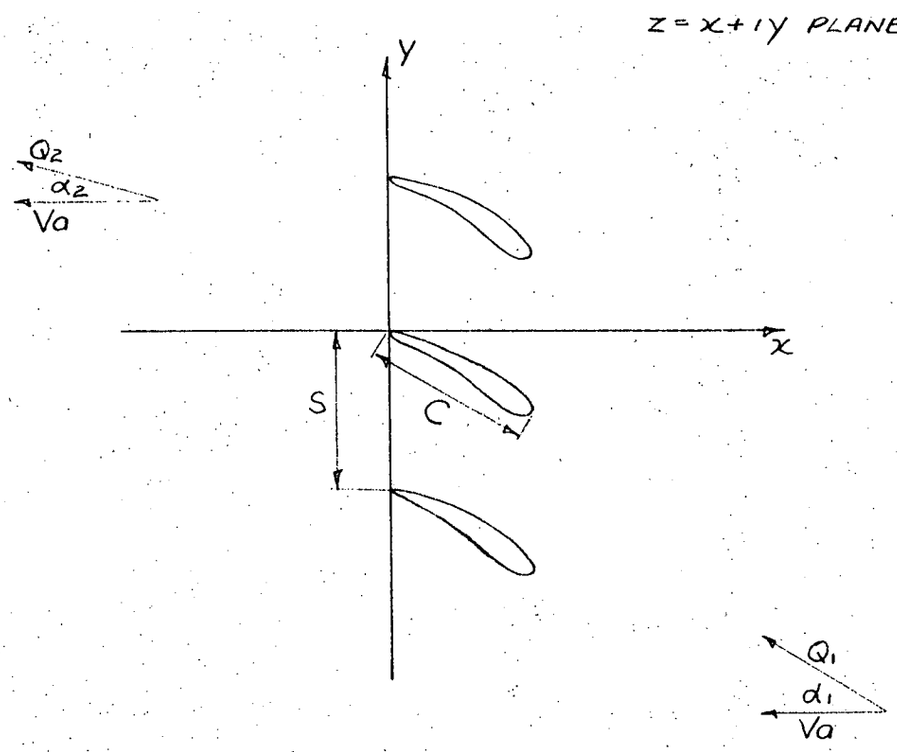

THE CASCADE PLANE

The complex potential flow in the ζ plane having the unit circle as a streamline is given by

$$F(\zeta) = \phi + i\psi = \frac{sVa}{2\pi}\left[\ln\frac{(\zeta-e^{k})(\zeta-e^{-k})}{(\zeta+e^{k})(\zeta+e^{-k})} + i\left\{\tan\alpha_1 \ln\frac{(\zeta-e^{k})}{(\zeta-e^{-k})} - \tan\alpha_2 \ln\frac{(\zeta+e^{k})}{(\zeta+e^{-k})}\right\}\right]$$

where s is the spacing of the cascade, Va the axial velocity and α_1, α_2 are the air inlet and outlet angles respectively. k is a parameter specifying the location of the complex sources and sinks on the real axis in the circle plane. It is related to the solidity and stagger of the cascade.

The conformal mapping function that maps the circle into the cascade plane takes the form

$$\frac{dz}{d\zeta} = \frac{se^{-k}}{\pi} h(\zeta)g(\zeta)$$

where $h(\zeta) = \dfrac{\zeta^2(e^{-2k}-e^{2k})}{(\zeta^2-e^{2k})(\zeta^2-e^{-2k})}$

and $g(\zeta)$ is an analytical function chosen so that it is regular in the domain $|\zeta| \geqslant 1$ and has a number of zeros on the real axis inside the unit circle. The complex sources in the cascade plane corresponding to these zeros define the aerofoil shape. Frith employs three sources, this being the least number required to generate a thick, cambered aerofoil. The use of a greater number of sources would give more control of the blade surface shape.

The method provides a limited amount of flexibility in its present form, there being effectively six parameters that ultimately define the aerofoil shape - k, r_n, α_1, r_t, α_2 and i. r_n and r_t are the radii of the leading and trailing edges respectively and i is the air incidence angle.

The values used by Oliver to model the rotor in the Vortex Wind Tunnel were

k = 0.3300	r_n = 0.0600	α_1 = 0.7405
i = 0.0500	r_t = 0.0200	α_2 = 0.4328

NOTATION

C	Chord length.
d	Distance of outer vortex sheet from wake centre in wake model.
E	Voltage.
h	Specific enthalpy.
h_o	Stagnation enthalpy.
H	$= \delta^*/\theta$ Boundary layer shape factor.
i	$= \sqrt{-1}$
K	Circulation (clockwise positive).
m	No. of sources used to model wake thickness.
n	No. of vortices along camberline used to model blade circulation.
p	Pressure.
q,Q	Relative flow velocity.
Qm	Vector mean velocity.
Qu	x component of relative flow velocity.
Qu_m	x component of vector mean velocity.
Q_T	Transport velocity.
r	Radius of curvature.
Ra	Hot wire resistance at ambient air temperature.
Rw	Operating hot wire resistance.
s	Blade spacing.
S	Source strength.
t	Time.
T	Air Temperature.
u,v	x,y component of flow velocity variation.
U	Rotor blade velocity.
V	Absolute flow velocity.
$\bar{V}$	Average absolute flow velocity over time τ.
Va	Axial velocity.
Va_m	Mean axial velocity through rotor.
V_{RMS}	RMS value of absolute velocity fluctuations.
W	Velocity potential.
x,y	Positional co-ordinates (peripheral, axial).
z	2z = profile thickness (z also used as a complex no.)
α	Thermal coefficient of resistivity.
α_1	Relative rotor inlet flow angle.

α_2	Relative rotor outlet flow angle.
δ^*	Boundary layer and wake displacement thickness.
θ	Boundary layer and wake momentum thickness.
ξ	Distance along chord and streamline.
ρ	Density.
$\sigma(\xi)$	Source strength per unit length of chord.
τ	Time for rotor to move a distance equal to one blade spacing.
ϕ	Flow coefficient Va/U.
ψ	Pressure coefficient $\Delta p/\frac{1}{2}\rho U^2$.

REFERENCES

1. Dean, R.C. — "On the Necessity of Unsteady Flow in Fluid Machines". Trans. A.S.M.E., Vol. 81, Series D, No. 1, March, 1959, pp. 24-29.

2. Horlock, J.H. — "Unsteady Flow in Turbomachines". Proc. Third Aust. Conference on Hydraulics and Fluid Mechanics, 1968, pp. 221-227.

3. Whitehead, D.S. — "Aerodynamic Aspects of Blade Vibration". Proc. Instn. Mech. Engrs., Vol. 180, Pt. 3 (i), 1965-6, pp. 49-60.

4. Yeh, H. — "An Actuator Disc Analysis of Inlet Distortion and Rotating Stall in Axial Flow Turbomachines". Jour. Aerospace Sciences, Vol. 26, No. 11, November, 1959, pp. 739-753.

5. Rizk, W. and Seymour, D.M. — "Investigations into the Failure of Gas Circulators and Circuit Components at Hinkley Point Nuclear Power Station". Proc. Instn. Mech. Engrs., Vol. 179, Pt. 1, 1964-65, pp. 627-673.

6. Von Karman, T. and Sears, W.R. — "Airfoil Theory for Non-Uniform Motion". Jour. Aeronautical Sciences, Vol. 5, No. 10, August, 1938, pp. 379-390.

7. Smith, L.H . Jr. — "Wake Dispersion in Turbomachines". Trans. A.S.M.E., Vol. 88, Series D, No. 3, September, 1966, pp. 688-690.

8. Parker, R. — "Pressure Fluctuations due to Interaction between Blade Rows in Axial Flow Compressors". Proc. Instn. Mech. Engrs., Vol. 183, Pt. 1, 1968-69, pp. 153-160.

9. Oliver, A.R. — "Comparison between Sand Cast and Machined Blades in the Vortex Wind Tunnel". Aust. Dept. of Supply, A.R.L. Report ME 103, September, 1961.

10. Hinze, J.O. — "Turbulence - An Introduction to its Mechanism and Theory". McGraw-Hill Book Company, 1959, Chap. 2.

11. King, L.V. — "Convection of Heat from Small Cylinders and a Stream of Fluid". Phil. Trans. Royal Soc., Vol. 214, 1914.

12. Frith, D.A. — "A Method for Generating Thick, Cambered Aerofoils in Cascade using a Closed Mapping Function". Aust. Dept. of Supply, A.R.L. Report M.E. 121, April, 1968.

13. Oliver, A.R. — Unpublished Data. University of Tasmania, 1970.

14. Boxhall, P.J. and Nilsson, U.E. — Unpublished Data. University of Tasmania, 1968.

15. Parker, R. — "Calculation of Flow through Cascades of Blades having Relative Motion and the Generation of Alternating Pressures and Forces due to Interaction Effects". Proc. Instn. Mech. Engrs., Vol. 182, Pt. 1, No. 11, 1967-68, pp. 229-240.

16. Csanady, G.T. — "Theory of Turbomachines". McGraw-Hill Book Company, 1964, Chap. 6.

17. Preston, J.H. — "The Non-Steady Irrotational Flow of an Inviscid Incompressible Fluid, with Special Reference to Changes in Total Pressure Through Flow Machines". Aeronautical Quarterly, Vol. 12, Pt. 4, November, 1961, pp. 343-360.

18. Wilkinson, D.H. — "A Numerical Solution of the Analysis and Design Problems for the Flow Past One or More Aerofoils or Cascades". U.K. Ministry of Technology, Aeronautical Research Council, R & M No. 3545, April, 1967.

19. Lockhart, R.C. — Unpublished Data. University of Tasmania, 1971.

20. Johnston, I.T. and Lockhart, R.C. — Unpublished Data. University of Tasmania, 1970.

21. Lighthill, M.J. — "On Displacement Thickness". Jour. Fluid Mechanics, Vol. 4, Pt. 4, August, 1958, pp. 383-392.

22. Oliver, A.R. — "Definition of Wakes by Vortex Sheets". Proc. Fourth Aust. Conference on Hydraulics and Fluid Mechanics, 1971, pp. 19-26.

23. Johnston, I.T. — Unpublished Data. University of Tasmania, 1971.